NTNU
Det skapende universitet

Konvertering av silica nanostrukturer med metallothermisk reduksjon.

Sigurd Sørensen

Materialteknologi
Innlevert: mars 2016
Hovedveileder: Gabriella Tranell, IMTE
Medveileder: Ivar Andre Ødegård, IMT

Norges teknisk-naturvitenskapelige universitet
Institutt for materialteknologi

Preface

This Master thesis was written during the autumn and winter of 2015/16 at the Norwegian University of Science and Technology (NTNU) in Trondheim.

I wish to convey my gratitude to Professor Gabriella Tranell for her patience, guidance, and support throughout the process of my work with this thesis. I also with to convey my gratitude to Ivar Andre Ødegård for all the aid he has provided, both in practical matters and laboratory work, and as a person who gives feedback on ideas and problem-solving. My thanks also go out to Ragnhild Sæterli for her help and experience during the TEM investigation, and Randi Holmestad for making that possible, as well as Kristin Høydalsvik for her help with the XRD investigation.

Sigurd Sørensen

Trondheim March 6th 2016

Sammendrag

Produksjon av fornybar energi ved bruk av silisiumbaserte solceller er en viktig del av vår innsats for å redusere utslippet av klimagasser og få bukt med en av vår tids største utfordringer; global oppvarming. For å gjøre overgangen fra avhengighet av fossile brennstoffer til et mer bærekraftig, fornybart energigrunnlag, er forbedring av dagens solceller essensielt.

Diatomfrustuler er et materiale med spesielle optiske egenskaper. Frustuler er et silisiumoksid skall som alger lager, og er formet med en slik struktur at de fungerer som optiske krystaller som fokuserer lys og hjelper algene å gjøre fotosyntese. Dersom vi er i stand til å gjenskape den samme strukturen som frustulene har i andre materialer, vil det kunne gi oss muligheten til å bruke naturens egne triks til å gjøre våre solceller mer effektive.

Denne oppgaven omhandler konvertering av frustuler fra arten *Cosinodiscus Centralis* fra silisiumoksid til silisiumkarbid gjennom en metalloterm reduksjon med magnesiumgass i inert atmosfære med tillegg av forskjellige former for karbon. For å se på effekten av struktur på prosessen ble det også gjort forsøk der frustuler ble byttet ut med skiver av silikaglass. De reagerte frustulene og glasset ble så undersøkt med røntgendiffraksjon for å finne ut hvilke stoffer som var blitt dannet. De reagerte frustulene ble og undersøkt med scanning electron microscope (SEM) for å vurdere i hvor stor grad strukturen overlevde prosessen.

For å vurdere fremtidig brukbarhet av tunneling electron microsope (TEM) for karakterisering av frustuler ble det og gjennomført en utforskende undersøkelse der frustuler fra et tidligere prosjekt ble benyttet.

Prosessen glasskivene og frustulene gjennomgikk innebar oppvarming til 800^{o}C i en lufttett reaktor. Reaktoren ble stående på den temperaturen i en time før den ble avkjølt i romtemperatur. Hver reaktor inneholdt enten glass eller frustuler skylt i destillert vann og etanol, i tillegg til magnesium pulver. Hver prøve ble også tilsatt enten ingen ekstra karbon, karbon i form a grafittpulver, eller karbon i form av vegetabilsk olje (raps). Etter varmebehandling ble prøvene skylt i en 10/40/50 vol% blanding av saltsyre (HCl), etanol, og vann, og deretter med destillert vann.

Det ble funnet at prøvene som inneholdt frustuler og hadde blitt tilsatt olje viste klare tegn til å ha dannet silisiumkarbid under prosessen. Det ble også funnet at det ble dannet en film på overflaten av frustulene som beskyttet den underliggende strukturen og førte til at den ble bevart gjennom prosessen. Ingen av prøvene med skiver av glass viste tegn til å ha dannet silisiumkarbid under prosessen. Prøvene uten tilsatt karbon eller tilsatt karbon i form av grafittpulver viste heller ingen tegn til å ha dannet silisiumkarbid under prosessen.

Under TEM undersøkelsen ble flere verktøy testet. Dette inkluderte diffraksjon, high resolution scanning tunneling electron microscopy (HRSTEM), mørkefeltsmikroskopi, og gjennomtrengende energi-dispersive X-ray spectroscopy (EDS). Det ble funnet at flere av disse, spesielt EDS og mørkefeltsmikroskopi, virket lovende nok til at en mer grundig undersøkelse med TEM kan anbefales for fremtidige studier innenfor konvertering av frustuler.

Summary

The production of renewable energy by silicon based solar cells is an important part of our efforts to reduce the emissions of greenhouse gases and tackle the greatest challenge of our day; global warming. To make the transition from dependence upon fossil fuels, to a more sustainable, renewable energy base, the improvement of silicon based solar cells is essential.

Diatom frustules is a material with special optical properties. Frustules are a silica shell made by algae. They are formed with a peculiar structure that makes them act as photonic crystals and focus light for the algae to use for photosynthesis. If we were able to recreate this same structure in other materials, we might be able to use nature's own tools to make solar cells more efficient.

This thesis is about the conversion of frustules from the species *Cosinodiscus Centralis* from silicon oxide into silicon carbide by way of the metallothermic reduction using magnesium gas in an inert atmosphere with different forms of carbon added. To investigate the effect that the structure of the frustules had on the process samples were also made where the silica frustule was replaced by silica glass. The reacted samples of frustules and glass was investigated using X-ray diffraction (XRD) to see what compounds were created during the process. The reacted frustules were investigated using scanning electron microscopy (SEM) to see how well their special structure survived the conversion process.

To evaluate the use of tunneling electron microscopy (TEM) for future studies of frustules, an exploratory TEM investigation was also conducted.

Samples were placed in an air tight reactor and paced in an oven at 800^{o}C. The reactor was left there for one hour before it was cooled in room temperature. Each sample contained either glass or frustules washed in distilled water and ethanol, and magnesium powder. In addition, each sample was added either no additional carbon, carbon in the form of graphite powder, or carbon in the form of food oil (rapeseed). After heat treatment, the samples were washed in a 10/40/50 % solution of hydrochloric acid (HCl), ethanol, and water, and then in distilled water.

It was found that the samples containing frustules and added food oil showed clear signs of having formed silicon carbide during the process. It was also found that during the process, a film had formed on the surface of the frustules that protected the underlying structure and made it survive the through the conversion process. None of the samples containing glass showed any signs of having formed silicon carbide during the process. The samples that were either added no carbon, or added carbon in the form of graphite powder showed no sign of having formed silicon carbide during the process.

During the exploratory TEM investigation several of its tool were tested. This included diffraction, high resolution scanning tunneling electron microscopy (HRSTEM), dark field microscopy, and penetrating energy-dispersive X-ray spectroscopy (EDS). It was found that several of these, in particular EDS and dark field microscopy, were promising enough for a more in-depth investigation of converted frustules in the future is recommended.

Contents

1 Introduction

1.1 Background

Biomimetics is the concept of using nature to do the hard labor of science, so that humans do not have to [(1)]. From airplanes with wings to Velcro, nature made it first, and we merely followed in its footsteps. To counteract the consequences of centuries of fossil fuel use, we are now obliged to harness energy from the sun. To avoid further tapping natures reserves of stored solar energy, it is only sensible to cheat and look at some of the solutions evolution has come up with over the course of millions of years. Harnessing light is, after all, the basis for photosynthesis, and in the ceaseless competition for survival and procreation, nature has surely had some inventive ideas along the way.

Diatoms are a common type of algae found in waters all around the world. Their characteristic feature is their shell, the so-called frustule, that surrounds the biomass. In certain species of diatoms, these frustules have evolved to focus and trap light and act as a photonic crystal[(2)]. If we are able to replicate or reproduce this highly structured architecture, we could apply this to increase solar cell efficiency. Conversion of frustules from its original silica into silicon carbide mean we have more tools available to utilize them, for instance by coating them with graphene using epitaxial growth on the Silicon carbide surface[(3)], creating a good basis to make a supercapacitor; an electronic device with the charge capacity of a battery, but the speed of a capacitor[(4-7)].

Much work has been done throughout the world on using silica frustules as templates for other materilals. Since the summer of 2014 experiments on using magnesium as an instigator for a metallothermic reaction to create silicon carbide from the silica of diatom frustules of algae, has been going on internally at the *Department of Materials Science and Engineering* at NTNU. This work was based on the work done by I. A. Ødegård, who showed that it is possible to create diatom frustule replicas in silicon nitride using metallothermic reduction with magnesium. The internal reseach had mixed results, but the general consensus of the scientist involved was a cautious optimism for the feasibility of conversion, particularly with the addition of extra carbon to the reaction.

1.2 Aim of work

In this master thesis, we will attempt to answer the following: Firstly, is metallothermic reduction using magnesium gas and added carbon a possible process for converting nanostructured silica into silicon carbide? Secondly, to what degree does it preserve the nano-structure of the frustules? And finally, is TEM a useful instrument to detect whether, and to what degree, silica frustules have been converted to silicon carbide?

A sample of frustules having undergone the same metallothermic process during previous, internal research and exhibiting clear signs of the presence of silicon carbide during XRD analysis was used for transmission electron microscopy (TEM) analysis. This was done to examine to what degree TEM analysis is a useful tool for looking at conversion of the silica nanostructure into silicon carbide and which parts of, if any, are converted at a higher rate than other.

2.3 Conversion of diatoms

The experiments performed in this thesis attempts to take aspects of earlier experiments performed on similar materials. Key features in our attempt (low temperature, reserving structure, using magnesium) have all been seen in earlier results, but they have not come together in one experiment.

Several other Silicon carbide structures have been made from organic compounds. Magnesium vapour has been used before to reduce frustules to Silicon while keeping its original morphology. Bao et al. managed to make silicon replicas of *Aulacoseira* diatoms through metallothermic reduction at 650˚C and retain a high surface area (>500 m^2g^{-1}) and a significant amount of micropores (<20 Å). This was done by spreading frustules evenly within a steel boat to form a 0.2-mm-deep powder bed. The frustule-bearing steel vessel, together with magnesium granules was placed within a steel ampule that was then welded shut. [(8)] Petrack et al. managed to do the same with *Mallomonas caudate* and *Synura petersenii* at 900˚C. They did it using a custom made tube reactor out of heat resistant steel. The 18 cm long tube reactor contained a rack with a large reservoir at each end, containing 3g magnesium, and 12 smaller wells spaced out between them, containing samples. The tube reactor was warmed up to 900˚C over 4 hours, and kept there for 5 hours before cooled to room temperature. Lastly, the samples were carefully dissolved in 17% aqueous HCl to remove magnesium oxide. [(9)]

Several formations of silicon carbide particles have been created from organic matter earlier, though normally at much higher temperatures. SiC particles have been made from raw rice husks as long back as 1998. [(10)] Sheets of SiC for tubular heat exchangers have been made from rolled cotton fabric by Amirthan et al. There the SiC was made through the use of liquid Si at 1600˚C. In their experiment, cotton fabric was rolled several times around a mould and submerged in a phenolic resin alcohol solution. The roll was cured at 130˚C before the core was removed and heated at 1100˚C for two hours in a N_2 atmosphere. Liquid silicon was added to the porous carbon form in a vacuum graphite furnace at 1600˚C under Ar atmosphere, and held for another two hours. This created a dense tube of SiC able to hold gas. [(11)] Carbon tubes containing SiC has been made from sugar bagasse, fibrous material left after sugar has been extracted from sugar canes. The bagasse fibre was heated to 1800-2400˚C in Ar atmosphere and created SiC inside the tubes from Si absorbed from the soil. [(12)]

SiC from diatom frustules has been made by Simonenko et al. “Biosilica” grade diatomite powder was used as a silicon bearing component and Phenolic powdery binder was used as a polymeric source of carbon. The diatomite powder and the phenolic polymer was mixed to create a stoichiometric blend and pressed into cylindrical shapes. The cylinders underwent reaction at 1400˚C for 4 h in dynamic vacuum. The grinding and mixing that the frustules underwent in preparation for the process meant that the frustules did not retain any of its original shape and architecture. [(13)]

Shi et al. has shown that it is possible to create SiC from an ordered hierarchical macro-mesporous SiO_2/C precursor by metallothermic reduction at low temperatures. In their study, the SiO_2/C-precursor was made from copolymer and polystyrene spheres and held a 71 wt% SiO_2 29 wt% C blend. It was mixed with magnesium turnings and heated to 700˚C for 12 h. The resulting product was washed in a 2M HCl solution to remove traces of Mg_2Si and MgO. Their report states that the proximity and even distribution of SiO_2 and C in the precursor makes the intermediate Si able to react directly with the carbon instead of going through the CO phase of the normal carbothermic process for SiC from SiO_2 [(14)]

In 2014 Ødegård et al. showed that it is possible to reproduce the architecture of the diatom frustules in silicon nitride through magnesium reduction at 800˚C. In their experiments, it was

determined through EDS, XRD, and Raman analysis that the nano-architecture could be preserved reasonably well through a conversion of the material it was built up of. Much of the methods and techniques used in this project is based upon the work done in that publication. [15]

We can see from the work that has been done earlier that many of the aspects of what we are trying to do in this experiment has been done before, though not exactly what we are doing here. Silicon carbide has been made from organic compounds, but not from frustules. [10, 11] It is shown that SiC can be made directly from SiO_2 in the presence of carbon and a reduction agent. [14] Magnesium has been used to reduce diatoms, but into elemental silicon, not carbide. [8, 9] Silicon carbide has been made from diatom frustules, but at different temperatures and using a different source of carbon. [13] Finally the architecture is observed to be preserved through a similar reaction under similar condition. [15] We see all the different aspects of our experiment has been done in some form in earlier works.

2 Theory

2.1 Diatoms

Diatoms are single celled algae surrounded by two porous silica shells, called frustules. The particular architecture of the frustules is made up of highly ordered pores that penetrate the shell. Since the diatoms get their energy from photosynthesis, it is believed that these pores are efficient light harvesting structures. [16]

There are currently over 200 000 different species of phytoplankton and they can be found in nearly every aquatic habitat. Most are autotrophic, meaning they produce their own nutrients from CO_2 by photo- or chemosynthesis to produce organic carbon. Diatoms are thought to produce ~40% of all organic carbon in the ocean each year. [17, 18]

The silica frustules consist of two identically shaped, but differently sized, overlapping halves named thecae. Each theca consists of a valve and a side wall called a cingulum. Where the cingulum of the upper and lower thecae overlap is called a girdle band. The algae make the silica in the frustules from orthosilicic acid through a process called biomineralization. [19]

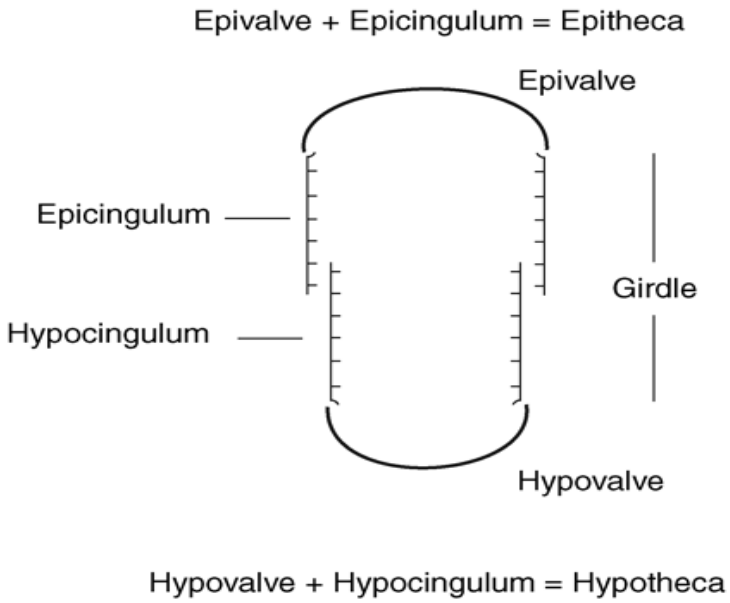

FIGURE 1.

Schematic explanation of how a frustule is built up. (1)

The porosity of the frustules comes from the 3 dimensional structure consisting of foramen, cribellum, cribrum, and areola. The Cribellum is the smallest feature. It is the small dimples covering the series of holes that is the cribrum. The cribrum, again covers the underlying areola.

The valves have a diameter of 100-300 µm. The largest of the layers in the frustule, the areola, has a thickness of 1000 nm and holes with a diameter of 1.3 µm. The layer above the areola, the cribrum has a thickness of 300 nm and its holes are having a diameter of 250 nm. The cribellum, the thinnest layer, has a thickness of only 50 nm and holes also of 50 nm. [20, 21]

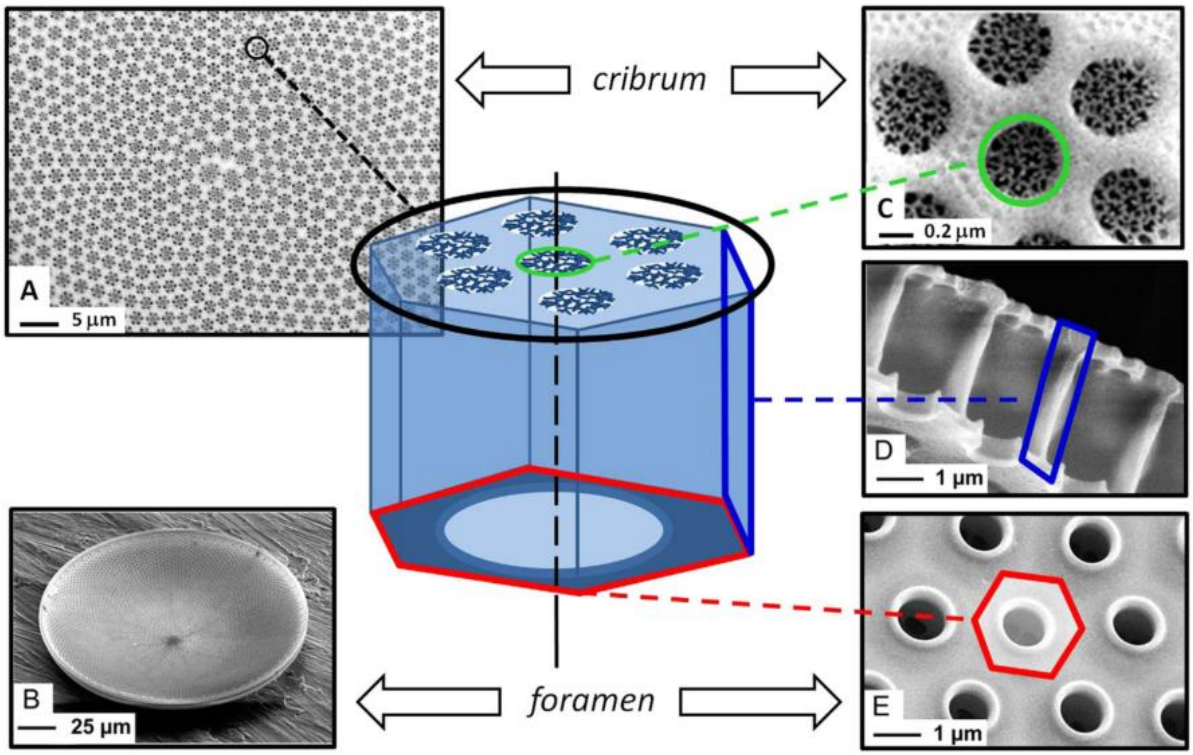

FIGURE 2 GENERAL SCHEME OF *COSINODISCUS CENTRALIS* FRUSTULE AND SEM IMAGES OF CRIBRUM (A, C) FORAMEN (B, E), AND THE SIDE-WALLS OF THE AREOLA (D) [22]

Diatom frustules makes possible a high degree of homogeneity on both nano- and micrometer scales. The great number of diatom also makes for a large variation in size and shapes of the frustules.[23]

Diatoms are already used as a filtering agent in industry through the use of diatomaceous earth where the large surface area are attributed to its good filtering abilities.[24, 25]

The scattering that occurs when light enter the pores of the frustules are thought to cause light to travel a longer distance within the material, thus increase absorption. [26] Exploiting this effect for photovoltaic cells could be very desirable.

2.2 Optical Properties

The optical properties of diatom frustules are well established. In 2004 Fuhrman et.al[2] showed that, along the same lines as the colour of butterfly wings[27] or the anti-reflective properties of the eyes of some moths[28], the frustules of the algae *Coscinodiscus Granii* exhibited extraordinary optical properties because of its structure, which was hypothesized as aiding the algae in photosynthesis. In 2007 De Stefano et.al.[29] showed the same properties in *Coscinodiscus Walesii*. Their research showed that the areola of the frustule was able to scatter incoming light so as to focus it to a high intensity at a point 100 µm behind the surface of the valve, corresponding to a position in the middle of the frustule.

The light focusing properties of *Cosinodiscus Centralis* were shown both experimentally and by computer simulation by Romann et.al in 2015 [30]. By using bidimensional hyperspectral mapping measurements the researchers were able to directly visualize the light distribution after transmission through diatom frustules. They found that for *Cosinodiscus Centralis*, an area of high light intensity was formed 50-170 µm beyond the frustule valve. This phenomenon was persistent and unchanged for different curvatures of the valve, and was not consistent with what one would expect from a conventional lens-induced convergence. It was therefore concluded that the phenomenon is likely caused by the porous nanostructure.

2.3 Silicon Carbide

Normally, silicon carbide (SiC) is produced through a process called the Acheson process, after its inventor Edward Goodrich Acheson in 1896. The process works by sending a current through a graphite core submerged in a reaction mixture consisting of silica sand and carbon. The current heats up the graphite to a temperature above 1500˚C and allows the process to take place, producing Silicon carbide and giving off Carbon monoxide. The result is a hollow cylinder of SiC with graphite at its interior and partially reacted charge at its exterior. The salt in the mixture is added to the charge mixture to remove iron and other contaminations and the Graphite cylinder needs to be continually vented lest the furnace explodes from the carbon monoxide that is produced. The reaction of SiC from silica and carbon is written as

$$SiO_2 + 3C \rightarrow SiC + 2CO \quad (1)$$

Though in reality the process goes through several steps, including gaseous steps whose diffusion slows it down. Those reactions are:

$$C + SiO_2 \rightarrow SiO_{(g)} + CO_{(g)} \quad (2)$$

$$SiO_2 + CO_{(g)} \rightarrow SiO_{(g)} + CO_{2\,(g)} \quad (3)$$

$$C + CO_{2\,(g)} \rightarrow 2CO_{(g)} \quad (3)$$

$$2C + SiO_{(g)} \rightarrow SiC + CO_{(g)} \quad (4)$$

All these gas phases of the process would also make it incapale of preserving any detailed morphology from the starting material to the product. [31, 32]

2.4 Traditional Use

Silicon carbide is one of the hardest materials known. With a hardness of 2800 kg/mm^2 and a compressive strength of 3900 MPa [33] it is often used as an abrasive for grinding, cutting, and drilling. Sinterability and good mechanical properties makes it a choice material for components that needs to be resistant to wear and tear, especially at high temperatures. [34] For instance it is used as break discs in car wheels. It has good heat resistance and is used to make heat exchangers, linings in furnaces and engines, and as valves.

FIGURE 3 SIC USED AS ABRASIVES

Its electrical properties causes it to be used in electronic equipment. It is used as a varisistor, an electronical device that changes its resistance as a function of the applied voltage. It can do this by having a high electrical resistance below a certain voltage which is reduced when that voltage is overstepped. It is a semiconductor with a bandgap of 2.36 eV and can be used to create diodes and MOSFETs, though they need a very high degree of purity and low amount of defects to function efficiently. The first LEDs were made out of SiC, though it is no longer used for lights because of its indirect bandgap. [34]

2.5 Metallothermic reactions

Metallothermic reactions are a type of reaction where a substance is reduced through the oxidation of a metal. The most famous of these reactions are the termite reaction where iron oxide is reduced to iron as aluminium is oxidised. highly exothermic reaction, capable of melting any iron in its vicinity.

$$Fe_2O_{3(s)} + 2Al_{(s)} \rightarrow 2Fe_{(s)} + Al_2O_{3(s)} \quad (5)$$

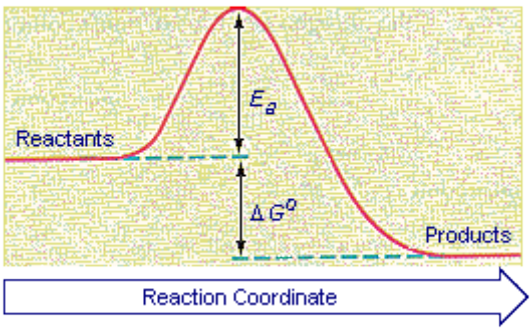

FIGURE 4 ACTIVATION ENERGY

Metallothermic reaction usually requires a very high initial temperature to get going. The thermite reaction, for instance, is normally ignited by burning a magnesium wire. This is because the activation energy of the reaction is very high. Activation energy is a measure of how much energy two atoms colliding need to react. [35]

2.6 Bragg's Law

A concept used in several analysis techniques is Bragg's Law. It explains how and why a beam of electromagnetic radiation will reflect off a crystal only at certain angles.

$$2d \sin\theta = n\lambda \tag{6}$$

In the formula, λ is the wavelength of the incoming light, *d* is the distance between atomic planes in a crystal, *n* is any positive integer (1, 2, 3 …), and θ is the angle between the crystal plane and the incoming beam. This formula describes the case of a reflection in a crystal.

When light, in this case in an X-ray frequency, hits a crystal it interacts with the atoms in the crystal. Each atom hit by the X-ray sends it back out in all directions. When this happens, each atom is acting as a new source of the reflection. These new waves will interfere with each other causing constructing and destructing interference. Because of the regularity of crystals, it can occur that all the new waves reflected off the atoms creates constructive interference.

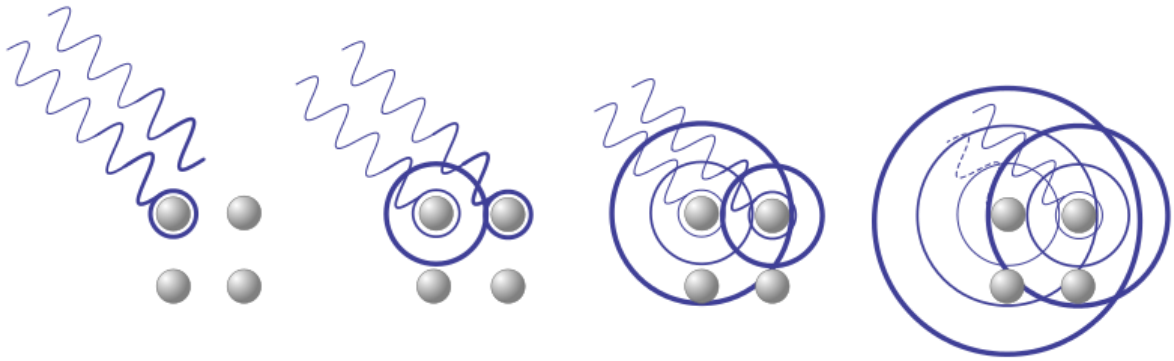

FIGURE 5 X-RAYS INTERACTING WITH ATOMS IN A CRYSTAL. THE WAVEFRONTS CREATE CONSTRUCTIVE INTERFERENCE IN CERTAIN DIRECTIONS. [36]

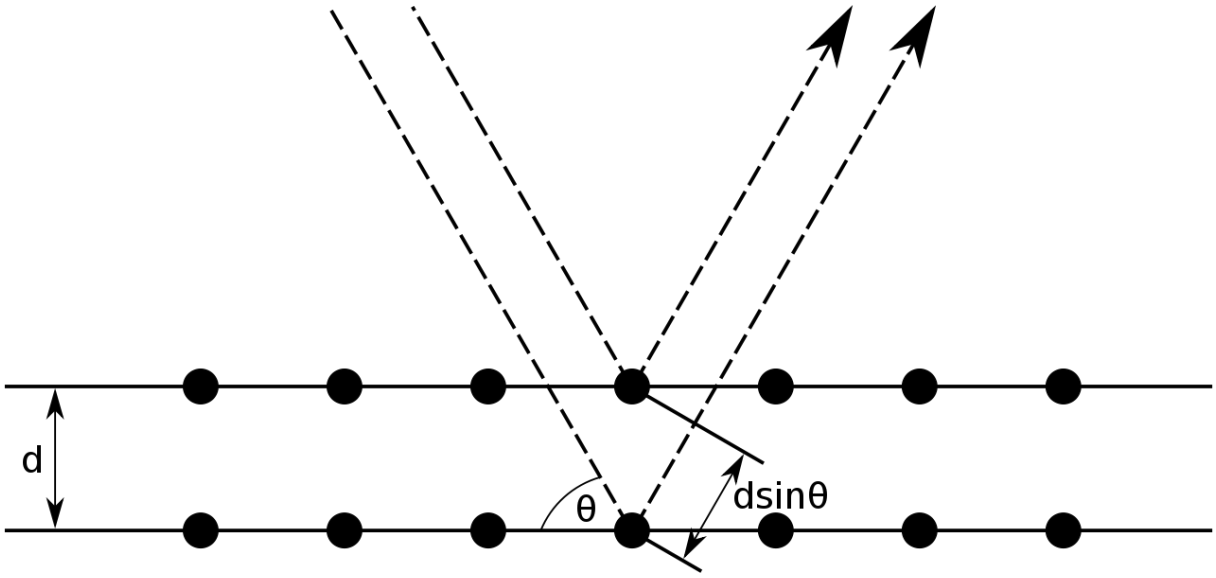

FIGURE 6 ILLUSTRATION OF BRAGG'S LAW

These angles are determined by the difference in traveling distance of the two x-rays. Imagine two incoming rays hitting the first and second atomic layers and bounce off in a random direction.

The two rays will travel two different distances. If that difference in distance is equal to any number of whole wavelengths, the waves will match up and have constructive interference. We use this effect in both X-ray diffraction and in Transmission Electron Microscope Imaging.[37]

2.7 Analysis Tools

2.7.1 TEM

A Transmission Electron Microscope is a device that fires electrons at high energies through a thin sample. Along the way, the electron interacts with the atoms of the sample and produce effects that can be interpreted, and used to glean several properties of the sample.

Most TEMs are built for accelerations between 100 and 300 kV. A higher acceleration of the electrons means that the electrons are able to penetrate through thicker samples and gives higher resolutions; at 100 kV the maximum penetration is around 200 nm, at 200 kV it is 1000 nm. The high acceleration voltage gives the electrons a significantly smaller wavelength than visible light and is able to make pictures with resolution down towards 0.1 nm.

The TEM instrument is somewhat similar to a scanning electron microscope. At the top, it has an electron gun that emits electrons either by charging some kind of filament, or for a more coherent beam, creating a potential gradient large enough to pull free and accelerate electrons. This is called a field emission gun. The electrons are focused down on to the specimen sample through a series of lenses and apertures. The sample itself sits at the end of a sample holder rod, extended through the specimen port,and sealed in vacuum to prevent contamination and scattering by molecules in the air.[37]

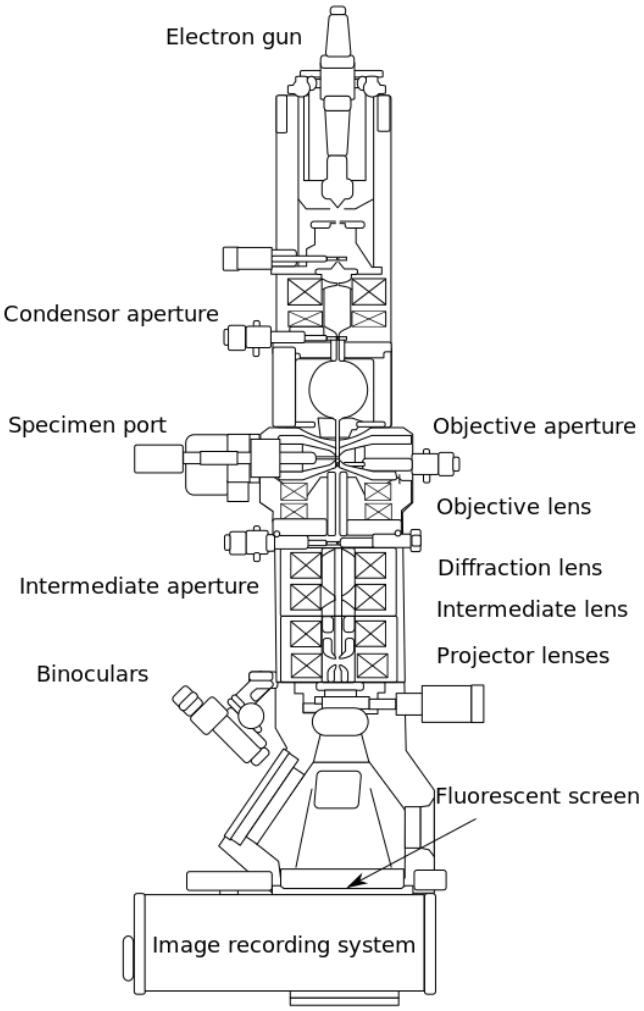

FIGURE 7 SCHEMATIC OF A TRANSMISSION ELECTRON MICROSCOPE

A TEM can be operated in several modes to get different kinds of results. The modes of operation utilized in this assignment is described below.

2.7.2 STEM

STEM stands for *Scanning Tunnelling Electron Microscopy* and makes the function of the TEM closer to a normal SEM. An electron beam “scans” the sample by moving quickly back and forth. The difference is that while in a SEM, the electrons bounce off the surface of the sample and creates a picture, the STEM mode creates the picture from the electrons piercing through the sample. Areas of the sample where the electron beam may penetrate unimpeded by much mass appear bright in the image projected onto the fluorescent screen, while areas with high density will appear darker.[37]

2.7.3 Diffraction

By focusing on the back focal plane, we can get an image of the diffraction pattern made as the electrons travel through the sample. This pattern is made by inelastic scattering of the monochromatic electron beam. Given the regularity of the wavelength of the electron and the regularity of the positions of atoms in a crystalline structure, the electrons will scatter according to Bragg's law. When this scattering is projected onto a fluorescent surface it will create a pattern of dots where the constructive interference of the diffraction adds up. We can use the pattern to identify different crystalline structures in the sample we are imaging.

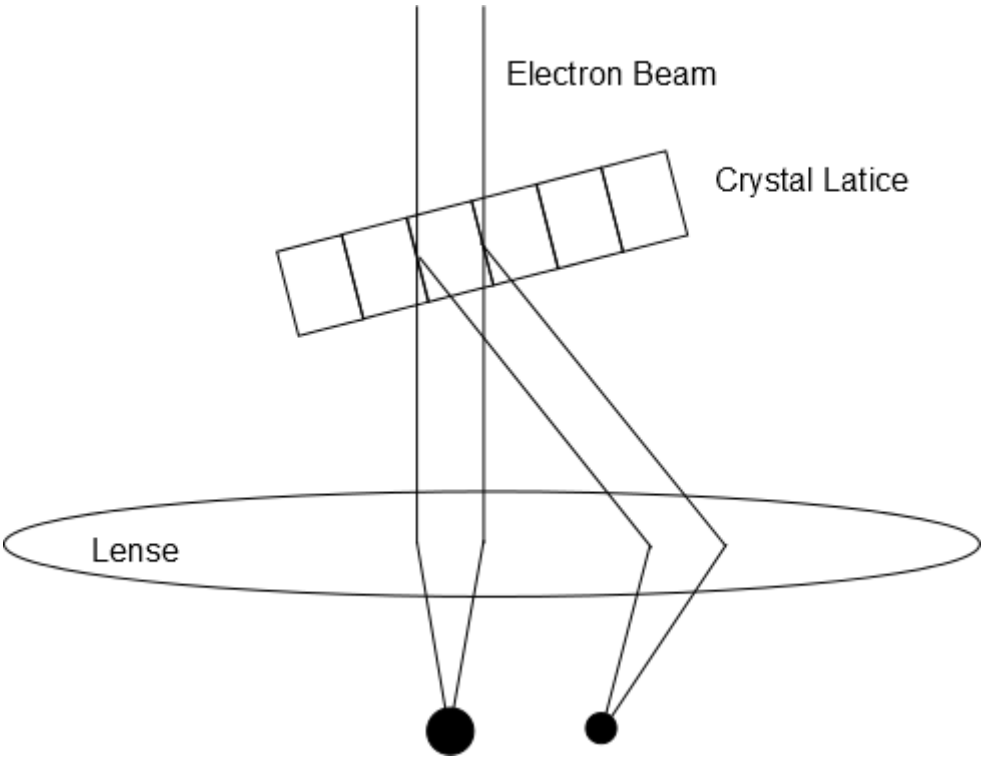

FIGURE 8 AN ELECTRON BEAM INTERACTS WITH THE CRYSTAL LATTICE AND CREATES A DIFFRACTION PATTERN ACCORDING TO BRAGG'S LAW.

The angle between the incoming electron beam and the crystal lattice is the θ in Bragg's Equation. Using Bragg's Equation and the wavelength of an electron beam we can calculate the aroximate magnitude of this angle. In the following example we imagine a using an electron beam with an energy of 200 keV (λ=0.00251 nm) to find the first order of reflection of the (111)-planes of an aluminium crystal (a=0.404 nm).

$$2 \times \frac{0.404\ nm}{\sqrt{1^2 + 1^2 + 1^2}} \times \sin\theta = 0.00251\ nm \tag{7}$$

This gives us θ=0.3°. This means that because of the very small wavelength of the electron beam, a diffraction pattern is created at very small angles, and though the chance of the beam traveling through the sample without scattering is small, to get lower orders of diffraction nodes (i.e. 1, -1, 2, -2) the sample needs to be oriented in a way that the crystal lattice is neat parallel with the electron beam. [37]

2.7.3.1 Interpreting Diffraction images

Diffraction Images from TEM analysis appear as a series of dots on a black background with a large, bright spot in the center. These points are the pattern that the electron beam makes after being diffracted and scattered while traveling through the sample.

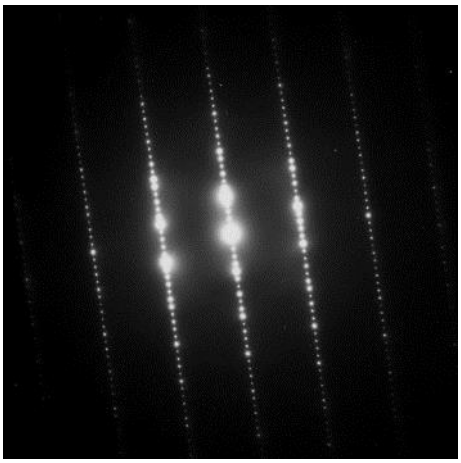

FIGURE 9 AN EXAMPLE IF A TEM DIFFRACTOGRAM [38]

This is a picture of a highly ordered and symmetric crystal where one could do indexing of the reflexes to find what kind of crystal is pictured. Given the near-amorphous nature and probable partial conversion of our samples, this is probably not how our results will appear. Our results will more likely look like a series of reflection points in circles around the center. Their distance from the center corresponds to the inverse of the distance between the atoms in the structure. This means that indexing the points to find a matching crystal structure is impossible. If we have a measuring rod in the image, or in a reference image of the same magnification, this is easily done. Having that, one only needs to count the pixels from the center to the reflection of interest and see how long that is in inverse distance. This gives the distance between the miller planes.

$$d_{hkl} = \frac{1}{d_{diffractogam}} \tag{8}$$

To identify which material we are looking at, the measured plane distances must then be cross referenced with known plane distances of expected materials.

One additional piece of information used to identify materials from diffraction patterns is the angles between the diffraction nodes. By knowing the symmetry of the crystal structure containing the planes making the diffraction nodes, we also know which angles the different planes have relative to each other in the crystal. These angles appear in the diffractogram.

This will likely not be relevant for this thesis, though, because we will be looking at amorphous and nano-crystalline materials. This makes for much less organized diffraction results. An example of this is seen in figure 10. As we can see, the diffraction nodes appear more like circles, and it is impossible to find the angle between any different node.[37]

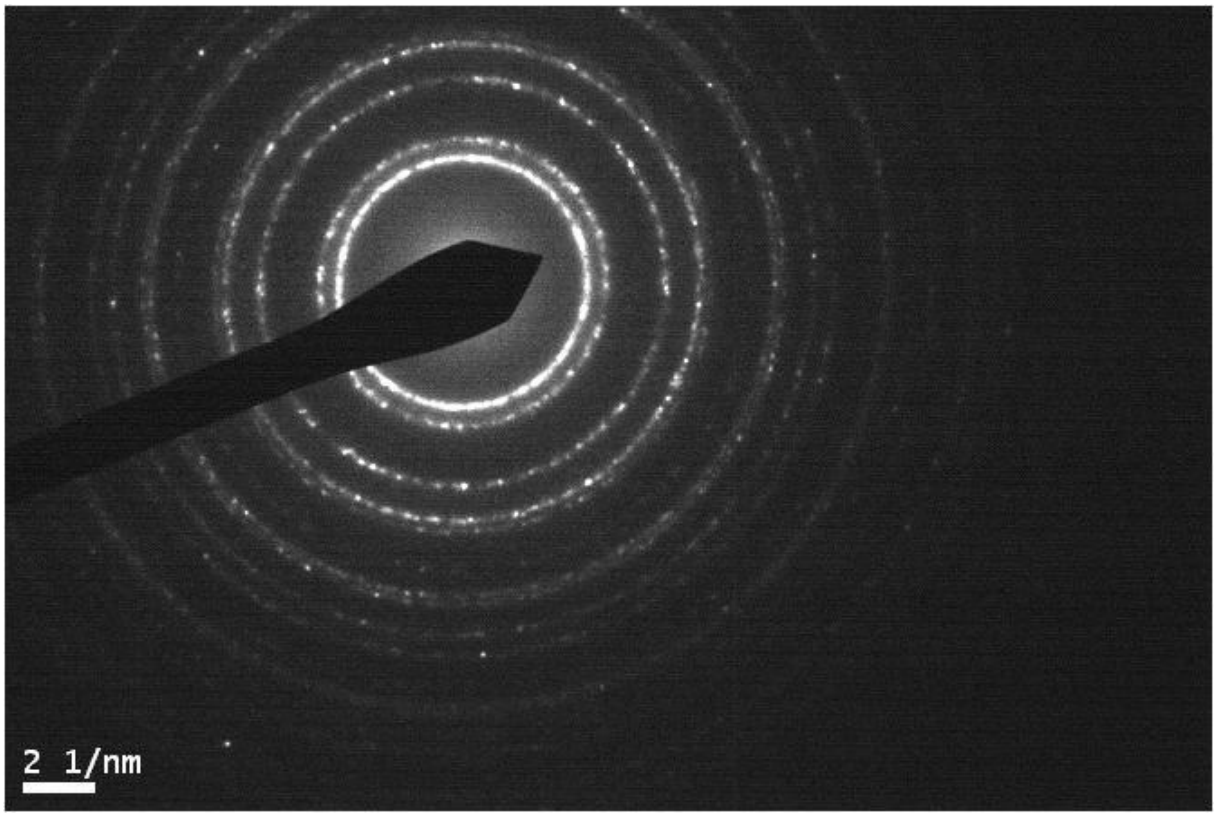

FIGURE 10 AMORHOUS TEM DIFFRACTION EXAMPLE [39]

2.7.4 Dark Field

Dark Field imaging is a method of combining the diffraction mode imaging with the normal STEM function to look for specific crystals in a sample. In a normal STEM, the image is produced from the electrons traveling straight though the sample corresponding to the zero node of diffraction in the diffraction image. The intermediate aperture in the microscope blocks out the diverging beams, making all areas creating a diffraction darker. To create a dark field image, the opening in the aperture is moved so that the diffracted electrons pass through. This reverses the image, making the all the parts of the sample where the beam may pass though unobstructed appear dark while the parts of the sample that caused diffraction appears bright. This by itself is handy in that it gets easier to spot small artefacts in an image, but what makes it extra useful for the purposes of this investigation is at we can use the diffraction mode to choose which diffraction node to center our aperture on. Since the different nodes are created by different crystals in the sample, we can effectively choose which material to highlight in the image. [37]

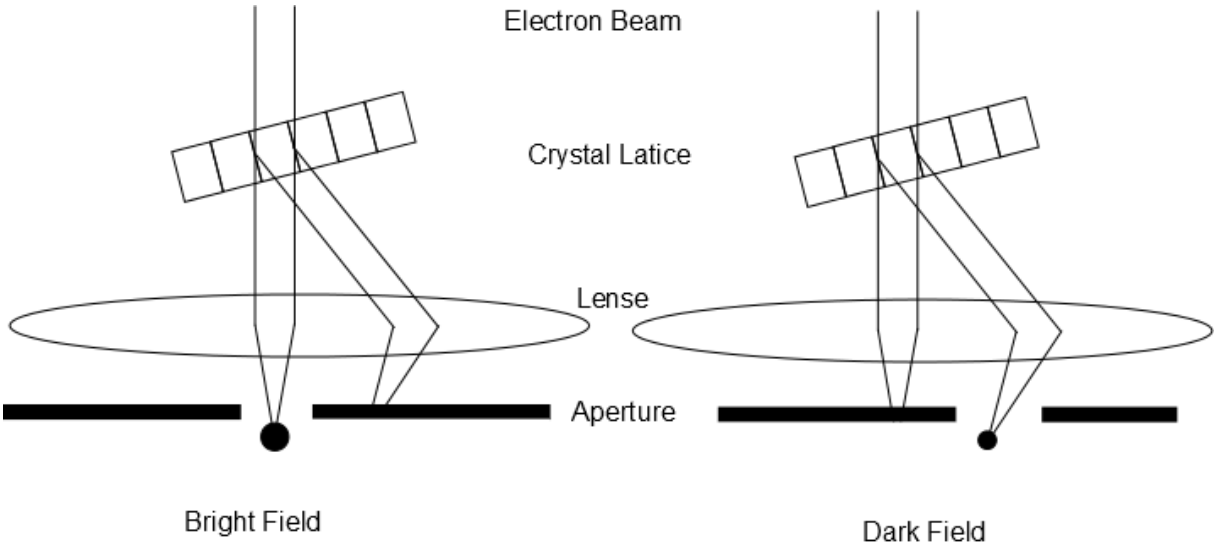

FIGURE 11 THE DIFFERENCE IN APERTURE POSITION BETWEEN NORMAL, BRIGHT FIELD (LEFT) AND DARK FIELD (RIGHT)

2.7.5 EDS

EDS is an initialization for Energy-dispersive X-ray spectroscopy. It is a method for elemental analysis and chemical characterization. By using X-rays to excite the electrons of an atom to a higher energy state, we can look at the energy that is released during relaxation to tell which element is present in a sample. When using EDS in a TEM it has the advantage of being penetrating.[40] That is, instead of only getting a reading of the surface of your sample, it gives a result for the entire depth of the point you are probing. In addition, it is quick enough to be able to create a mapping, showing elemental composition in an area. Using these two properties together we can use an EDS mapping to see whether some parts of the frustule reacts more, and therefore contains more carbon, than other parts of the frustule. Since the density of silicon shown by an EDS mapping is the general thickness of the sample at each point, if the distribution of carbon shown is uniform with the distribution of silicon, then the uptake of carbon is uniform. If some parts of the frustule react more than others, we should see a disparity between the two.

2.7.6 XRD

X-Ray Diffraction is an analysis technique that uses X-rays and Bragg's law of diffraction to determine the distance between atomic planes in a crystalline material. It is a very useful tool to determine, not just the elemental composition of a material, but also what kinds of crystal it is.

Bragg's law states that constructive interference in a material will occur when the difference in distance travelled by two photons hitting two different atomic layers in a material is some whole number of waves. At all other distance differences, the reflection will only amount to noise. By looking at which angles an incoming x-ray beam creates a diffraction, we are able to calculate the distance between atomic planes using Bragg's Law.

Each compound has a "fingerprint" of different plane distances caused by its crystal structure. When a diffractogram of a sample is made, we are able to use which elements we know to be present to search a database for a "match" to all the compounds that can create the peaks observed in the results.

Because the results gained from XRD is based on the crystallography of the sample, amorphous and highly polycrystalline samples will not get as clear result as a regular, monocrystalline material will. This causes noise in the signal, resulting in diffractogram that is more difficult to read and interpret. (41)

2.8 Rapeseed oil

One of the substances used in this thesis for adding carbon to the reaction is a commercially available food oil. The oil used is a Rapeseed oil available from a local grocer.

According to the information on the package, this oil consists of 100% fats, of which 7% is saturated fats and 93% is unsaturated fats. Of these unsaturated fats 70% is mono-unsaturated and 30% in poly-unsaturated.

Fats are organic molecules consisting of three fatty acids connected to a triglyceride. Fatty acids are long chains of hydrocarbons. Triglyceride is a molecule with the chemical formula of $C_3H_5O_3$ where each of the oxygen atoms connect the triglyceride to the fatty acids. The structure of fat is shown in Figure 12

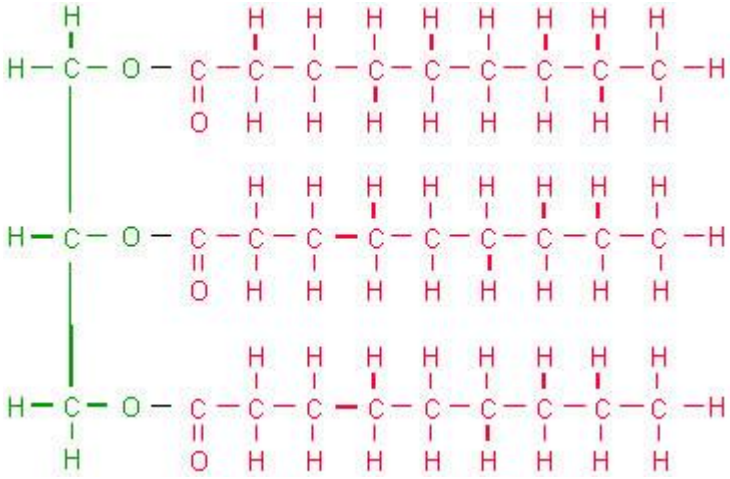

FIGURE 12 CHEMICAL STRUCTURE OF A FAT.

Fats are divided in to saturated and unsaturated fats. In a saturated fat, the bonds in the carbon chains of the fatty acids are all single bonds. In unsaturated fats, one (mono-unsaturated) or more (poly-unsaturated) of the carbon-to-carbon bonds are double bonds. Carbon atoms with double bonds are unable to support as many hydrogen atoms as carbon atoms with only single bonds. The difference between saturated and unsaturated is illustrated in figure 13

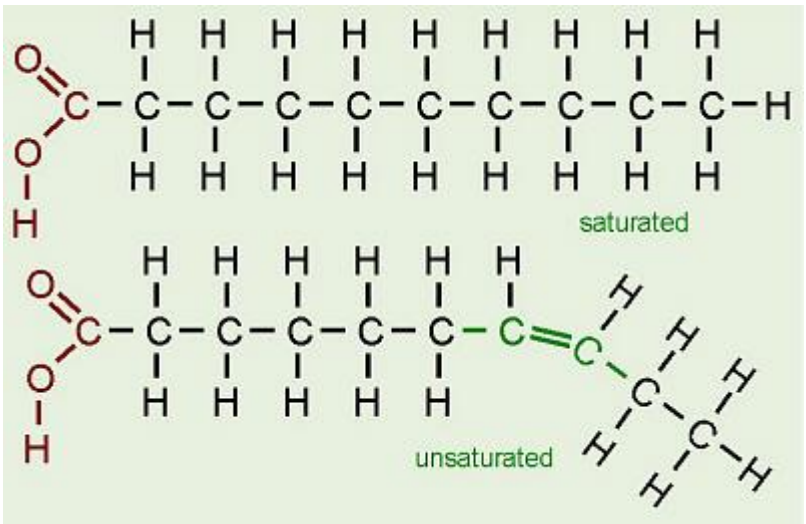

FIGURE 13 DIFFERENCE BETWEEN SATURATED, AND UNSATURATED FATTY ACIDS [42]

Because the oil used is generally mono-unsaturated, we approximate the chemical formula for the oil to be $C_XH_{2X}O_6$.

When organic compounds are heated, they undergo pyrolysis. Pyrolysis is the same process used to turn wood into charcoal. It is a process where the organic compound releases hydrogen and methane gasses, leaving carbon.

Much research is done on the pyrolysis of vegetable oils for the purpose of making biofuels, but finding data relevant for our use, at the correct temperature and in an inert atmosphere, has proven difficult.

The best overview found is presented in table 1.

TABLE 1 PYROLYSIS PRODUCTS FROM RAPESEED OIL (43)

Components	**Molar % at 800°C**
C_1-C_4 cut	45,1
C_5-C_9 cut	12,6
C_{10}-C_{14} cut	1,0
C_{15}-C_{18} cut	0,2
Aromatics	11,6
Esters	7,7
CO	3,8
CO_2	1,6
Coke	3,1
Other Products	13,3
H_2	4,6

The largest portion, C_1-C_4, is a group of components consisting of CH_4, C_2H_4, C_2H_6, C_3H_6, C_3H_8, C_4H_8, C_4H_{10}, and traces of acetylene.

One flaw in this information is that this is for pyrolysis done in the presence of oxygen. As our reaction happens in inert atmosphere, this does not necessarily reflect our components accurately. In lieu of better information it will have to suffice.

As we see in table 1 and illustrated further in figure 14, the pyrolysis of vegetable oils results in a lot of different organic components, including adding a not insignificant amount of hydrogen.

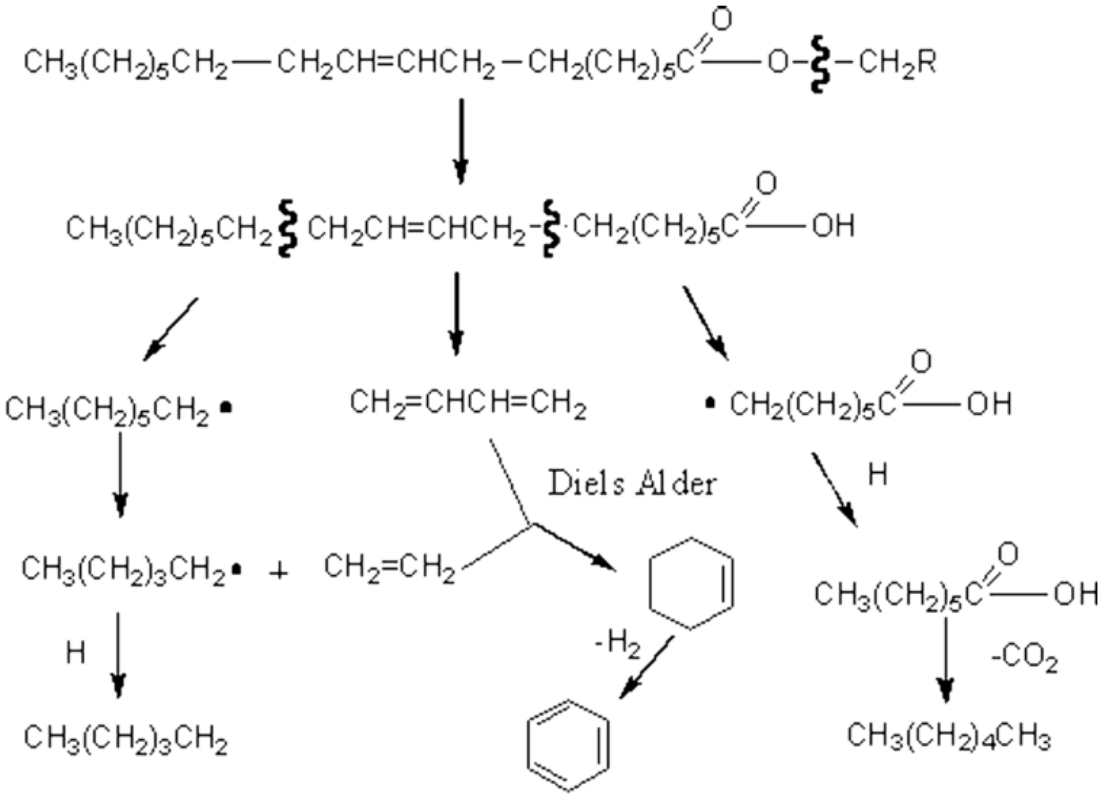

FIGURE 14 SIMPLE MECHANISM OF THE PYROLYSIS OF VEGETABLE OIL. (44)

No reliable data has been found on how these compounds react with magnesium gas and polycrystalline (or amorphous) silica.

3 Experimental

3.1 Experimental Matrix

In this thesis, samples of frustules are subjected to a metallothermic process involving magnesium gas and carbon. The processed frustules are then subjected to analysis through XRD to determine whether any silicon carbide was formed. The samples were also subjected to SEM imaging to determine whether the nano-structure of the frustules survived the process.

As a simpler replacement to silica frustules, sheets of fused silica glass was exposed to the same process and analysed through XRD. The goal of this was to get a better understanding of the process by looking at which compounds was formed when using a simpler silica material that was lacking the large surface area and possible organic residue of the frustules.

We are attempting to create SiC from the SiO_2 in the frustules by a metallothermic process using Magnesium gas as reductant in an Argon atmosphere. This chapter will go thoroughly go through the process as it was performed, first on the frustules, then on the glass replacement samples.

TABLE 2 SAMPLES CONTAINING FRUSTULES

Sample Name	Additives	Additional notes
1 – Plain	None	
2 – Powder	Carbon Powder	
3 – Oil1	Oil	Nearly all sample lost.
4 – Oil2	Oil	
5 – Oil3	Oil	

Originally, only four different samples were planned. One with no added carbon, one with added carbon as nano-graphite powder, and two samples with carbon added as oil. It was decided to make two samples with added oil due to previous experiences during internal research having shown that even with equal preparation, the two samples might give different results during XRD analysis. Experiences during the sample preparation then lead to almost all if sample 3-Oil1 to be lost, and had to be redone. Luckily, enough sample material was salvaged from sample 3-Oil1 to use in analysis.

The amount of samples planned for and made were reduced by the amount of frustules available.

3.1 Sample materials

The algae are gathered by zooplankton-sheet in the Trondheimsfjord in the months of March and April, and consist mainly of the species *coscinodiscus centralis* with the addition of a few other undetermined species. Since they are gathered from nature it is impossible to know the exact conditions under which they are grown.

Using plankton sheet as a filter, frozen samples of *cosinodiscus* algae are first washed with de-ionized water to thaw. The algae are then washed in laboratory grade ethanol to dissolve organic fats and materials. To get a thorough wash, this step is repeated three times. After the ethanol the algae are then again washed with de-ionized water to remove any remaining water soluble impurities.

Due to the fact that some of the frustules from the same batch had been used during previous experiments, the washed frustules had been stored for 15 months in plastic vials identical to the one used during filtration prior to being used for the rest of the experiments.

The amount of frustules used per sample varied depending upon how much material was available, but the aimed for amount around 3 mg per sample.

FIGURE 15 SIEVE MADE USING PLANKTON SHEET AND A CUT-OFF PLASTIC VIAL.

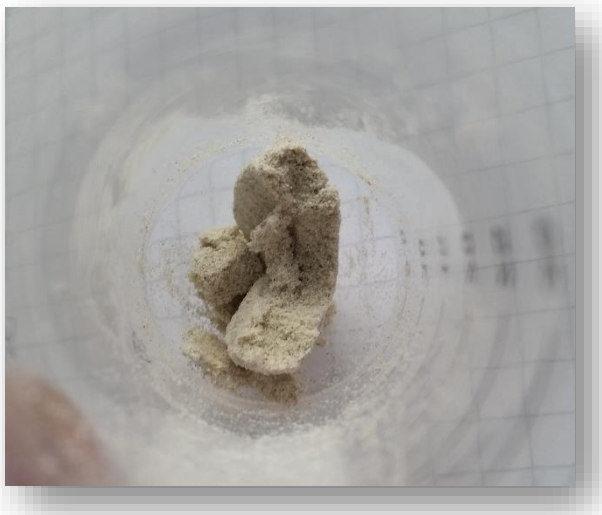

FIGURE 16 WASHED, UNREACTED FRUSTULES.

3.2 Adding carbon

Two different carbon additives was used in the experiments. One was nano-sized graphite powder, the other was a cheap commercially available plant-oil used in food and cooking. They were added to the process as carbon sources to contribute to the carbon left over from the pre-process preparation. This was done in the hope that adding more carbon to the process would result in a higher amount of silicon carbide created. Two different sources of carbon were chosen to see whether the use of non-organic graphite was a viable option even though, it being in a solid form, had much less contact area than the liquid bound carbon of the organic oil. The oil was chosen by the virtue of being cheap, available, and on the presumption that it was somewhat analogous to the oil- and fat-bound carbon left over in the algae organic matter.

The graphite powder was added to the sample by mixing it thoroughly in with the frustules before loading the reactor.

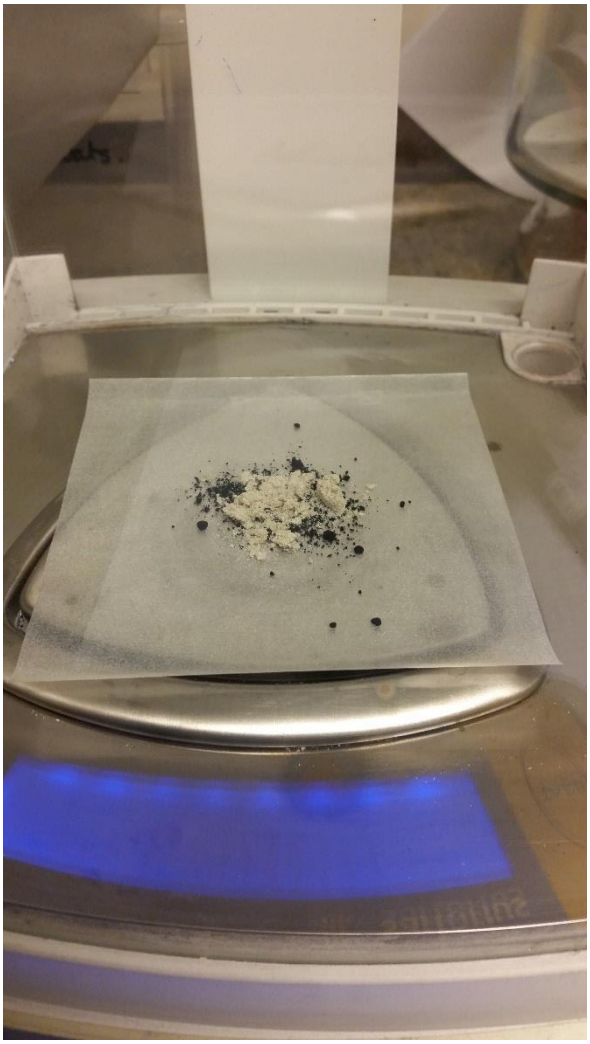

FIGURE 17 FRUSTULES AND CARBON POWDER

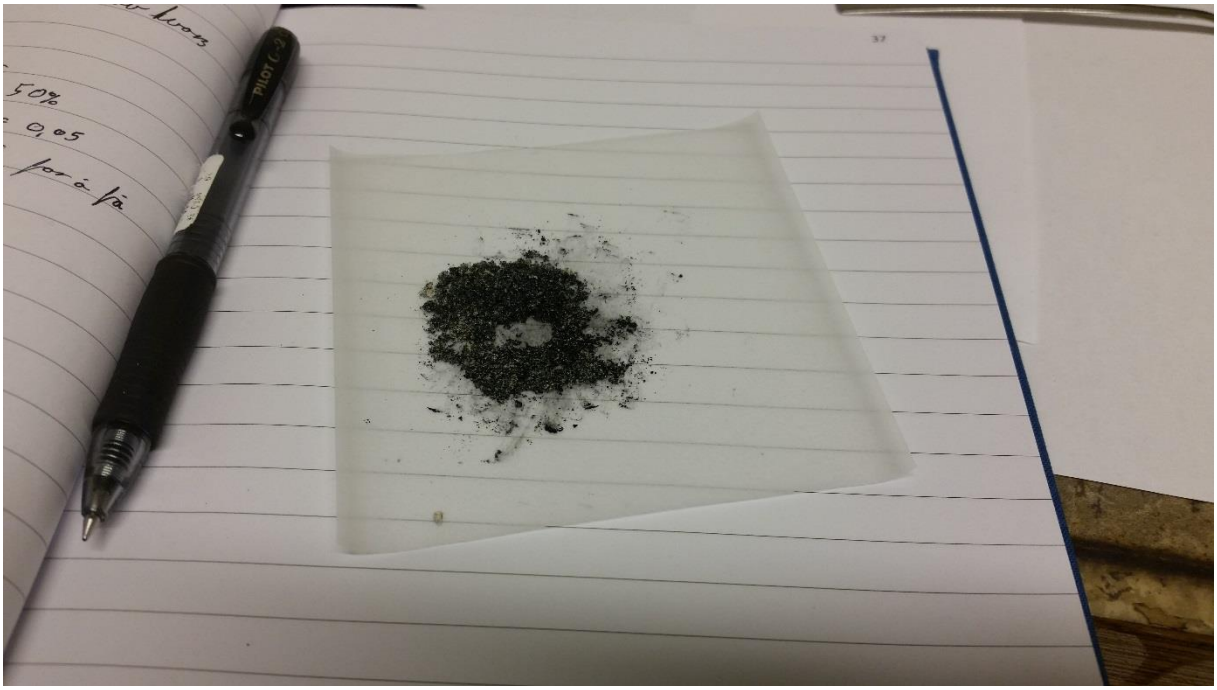

FIGURE 18 FRUSTULES AND CARBON POWDER AFTER MIXING

The oil was added to the sample by filtering it through the frustules, using the steel mesh as a sieve. Some stirring was also required to get the oil to coat the frustules properly instead of them merely floating on top of the oil.

Both the powder and the oil was added in excess to encourage the carbide forming reaction as much as possible. This means that the specific and relative amounts of the raw materials are not relevant

3.3 Heat treatment

Before heat treatment, the sample is placed on a steel mesh that allows the magnesium gas to have access to the frustules. The mesh with the frustules is then placed within a custom-built stainless steel reactor together with 0.2 g Mg powder, and a small roll of stainless steel sheet to act as a spacer and separate the magnesium powder from the sample. All this is done in an inert argon atmosphere both to prevent the combustion of magnesium, but also to avoid any oxygen being present during the heat treatment and interfering with the reaction. The reactors are closed firmly to prevent any gas exchange.

The loaded reactor is placed in a muffle furnace, pre heated to 800^{o}C and left there for 60 min before it is take out and cooled in room temperature until it is cool enough to easily handle.

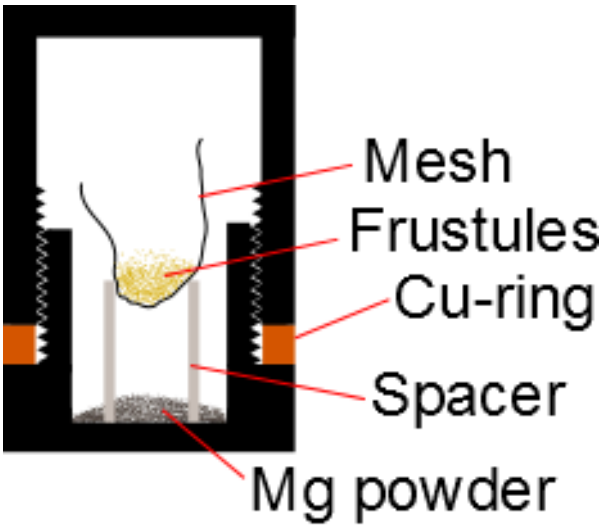

FIGURE 19 REACTOR SCHEMATICS

FIGURE 20 REACTOR USED IN EXPERIMENTS

3.4 Post-Treatment

After the heat treatment, the samples are washed, rinsed, and filtered in a solution of 50/40/10 vol% water, ethanol, and hydrochloric acid. The sample is then washed thoroughly three times to remove any magnesium that might have condensed on the sample during cooling.

After washing with the acidic solution, the samples are washed using distilled water, and then lab-grade ethanol before set to dry at 90^{o}C for 40 min to remove any remnant of the filtering.

3.5 XRD Analysis

For the XRD analysis, the machine used was a Bruker D8 Advance DaVinci Diffractometer.

The settings used was 10-75^{o} 120 minutes with a variable slit.

The software used was DIFFRAC.EVA V4.1.

When searching the database for compounds matching the peaks found, the search was limited to elements we suspect are present based on the reaction process and the sample material. The included elements be fund in the table below.

TABLE 3 ELEMENTS INCLUDED IN SEARCH FOR MATCHING PEAKS

Included Elements
Si
C
Mg
N
O
Cl
Fe

The inclusion of silicon, carbon, magnesium, and oxygen in the search is self-evident. Nitrogen is added in the search because a leak in the reactor would cause nitrides to form. Chlorine is added to detect possible leftovers from the cleaning using HCl. Iron is added to the search to detect possible interaction with the steel mesh.

When the search is done, several hundred possible matches are found, especially when the sample is amorphous and the signal may be weak and noisy. The possible matches must then be looked through manually, and the most reasonable matches are highlighted.

3.6 Glass Replacements

To examine what effect the porosity and structure of the frustules have on the viability of the reaction, the same process was performed on sheets of silica glass. The silica glass was chosen for its availability and because its chemical composition is the same as the algae frustules. The silica glass has a completely different structure, being a glass and thus completely amorphous, and lack the porosity of the frustules it has a much lower surface area on which the reaction may take place. From this one can expect that the process will take place at a lesser degree, but hopefully be easier to detect on a flat surface.

The glass replacements underwent the exact same procedure as the frustules concerning preparation and treatment. Like the frustules, different forms carbon additives were used for easy comparison.

TABLE 4 SAMPLES OF GLASS REPLACEMENTS DONE

Sample	**Preparation**
Glass 0	Blank, unprocessed
Glass 1	Processed, no carbon added
Glass 2	Processed, added carbon powder
Glass 3	Processed, added oil

3.7 TEM Experiment

A TEM investigation was reformed on a sample named B3-2. This sample had gone through the process described above, and was a leftover from earlier experiments. The sample had showed clear signs of the presence of SiC in an XRD analysis as shown by figure 21

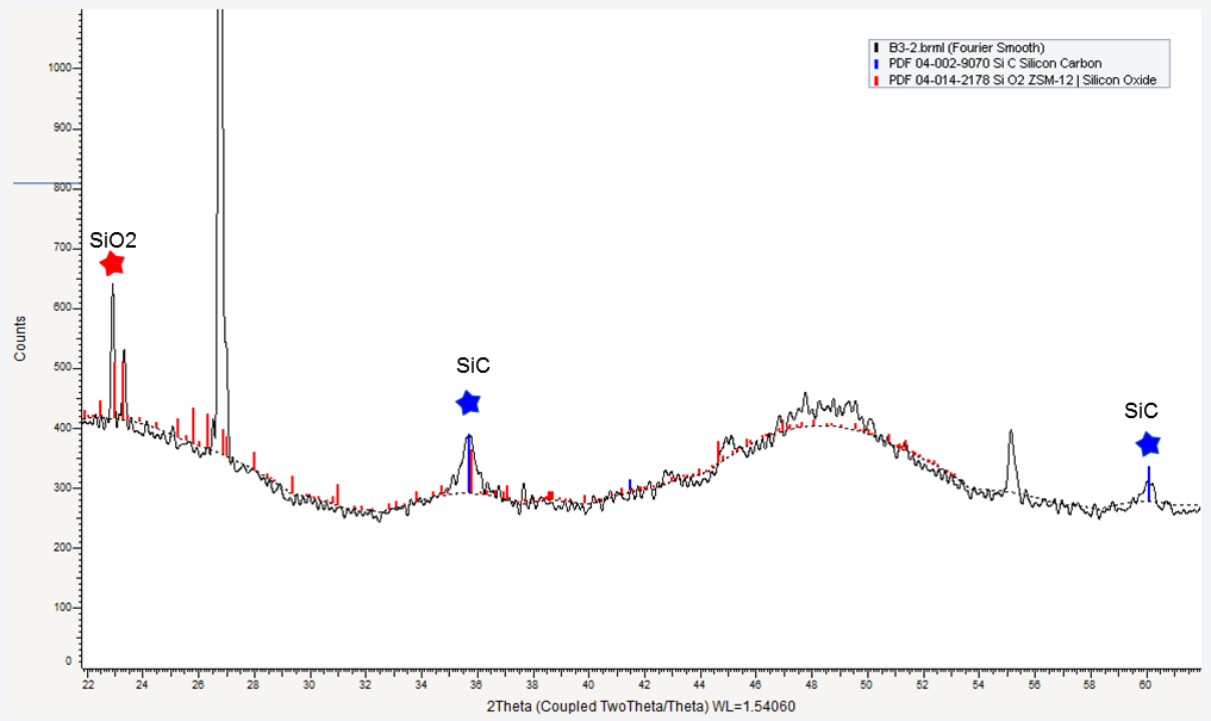

FIGURE 21 SAMPLE USED FOR TEM EXPERIMENTS. SHOWS CLEAR PRESENCE OF SIC.

Though we ideally should have used one of the samples created for this thesis so that the sample used was representative for the rest of the samples discussed in this thesis, this was impossible due to scheduling considering when the TEM investigation could take place. The sample that was used was chosen for being the one with the clearest signs of the presence of silicon carbide.

Four samples were created; two on an SiO-grid and two on an C-grid, as well as two crushed in a mortar and two not crushed by mortar. This was done to determine the best way of preparing the sample. Usually, extensive preparation is required for TEM samples in order to make them thin enough to let the electron beam pass through, but given the porous nature of the frustules, this was deemed unnecessary. Half the samples were crushed to see whether that was a necessary step to get pieces of frustule small enough to look at in the TEM microscope. After the samples are crushed (or not crushed) they are placed on a sample holder consisting of a grid of either a carbon film, or a SiO film. The carbon film is the one usually used, but the SiO film was also tested in the suspicion that, it being close to the mostly SiO_2 nature of the frustule sample, would have an easier time getting the tiny fragments of sample to stick to it properly and not bounce off from electrical forces. There was also the possibility that the carbon film would interfere with the results in an analysis that was looking for signs of carbon.

During the investigation, only sample 1 was actually used for imaging.

TABLE 5 SAMPLES CREATED FOR TEM ANALYSIS

Sample	Grid	Crushing
1	Carbon	Mortar
2	Carbon	None
3	SiO	Mortar
4	SiO	None

4 Results

4.1 XRD Results

4.1.1 Frustules

Coming out of the reaction, metallic bubbles was found on the inside of the reaction chamber. This is in all likelihood magnesium condensed out of gas as the reactors cooled. Magnesium was also found still in powdered form at the bottom of the reactor. This shows that during the reaction the amount of magnesium gas in the reactor was at saturation.

In the samples where carbon was added in the form of oil (3, 4, and 5 in table 2) the steel mesh used to contain the frustules during the reaction while allowing the magnesium gas access was found to have undergone corrosion during the reaction and had become very brittle, falling apart at the slightest disturbance, leaving large holes. This caused much of the sample material to fall away and becoming unusable as it mixed with the magnesium powder remaining at the bottom of the reactor. This may also have caused fragments of the steel mesh to become mixed in with the frustules and showing up as iron oxide in the XRD diffractographs for those samples.

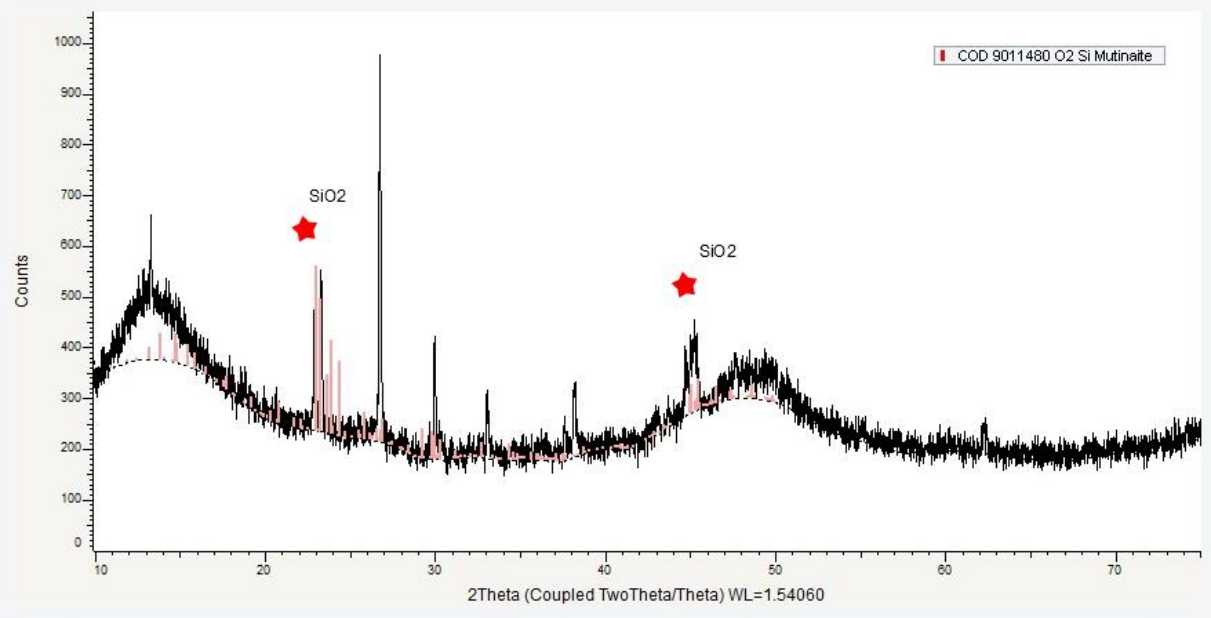

FIGURE 22 XRD RESULTS FOR SAMPLE 1-PLAIN

The results from sample 1-Plain show only the presence of silica tagged, though we see several other peaks that the system has not matched to any compounds.

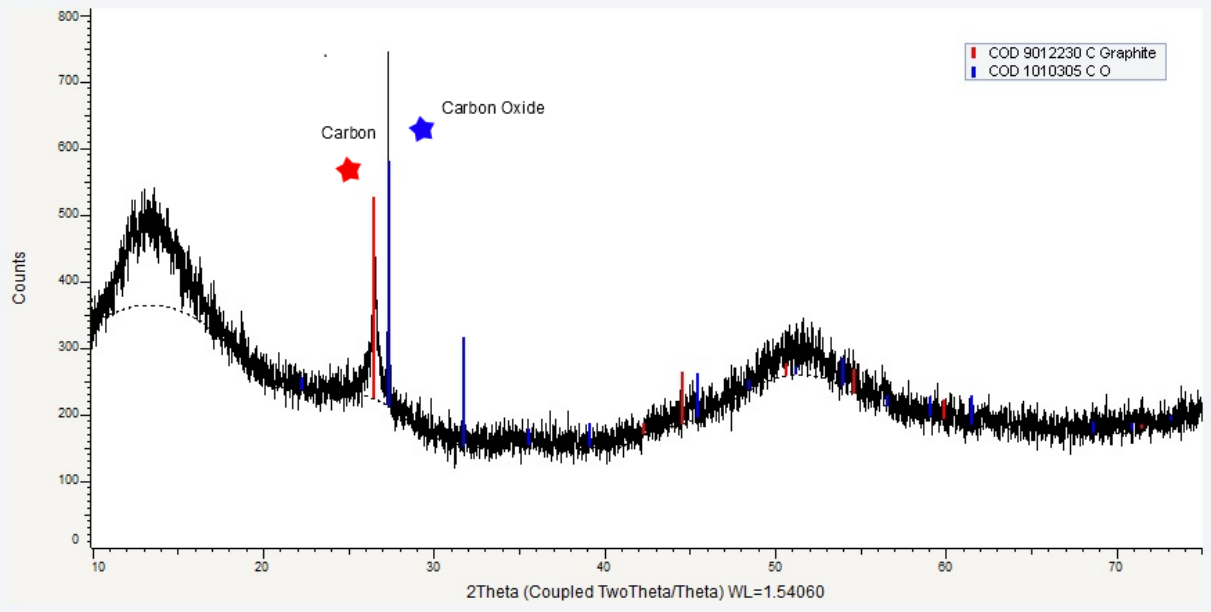

FIGURE 23 XRD RESULTS FOR SAMPLE 2-POWDER

Looking at sample 2-Powder, shown in figure 23, we see only the presence of carbon and a carbon-oxide compound. We see no presence of silica or silicon carbide in the results.

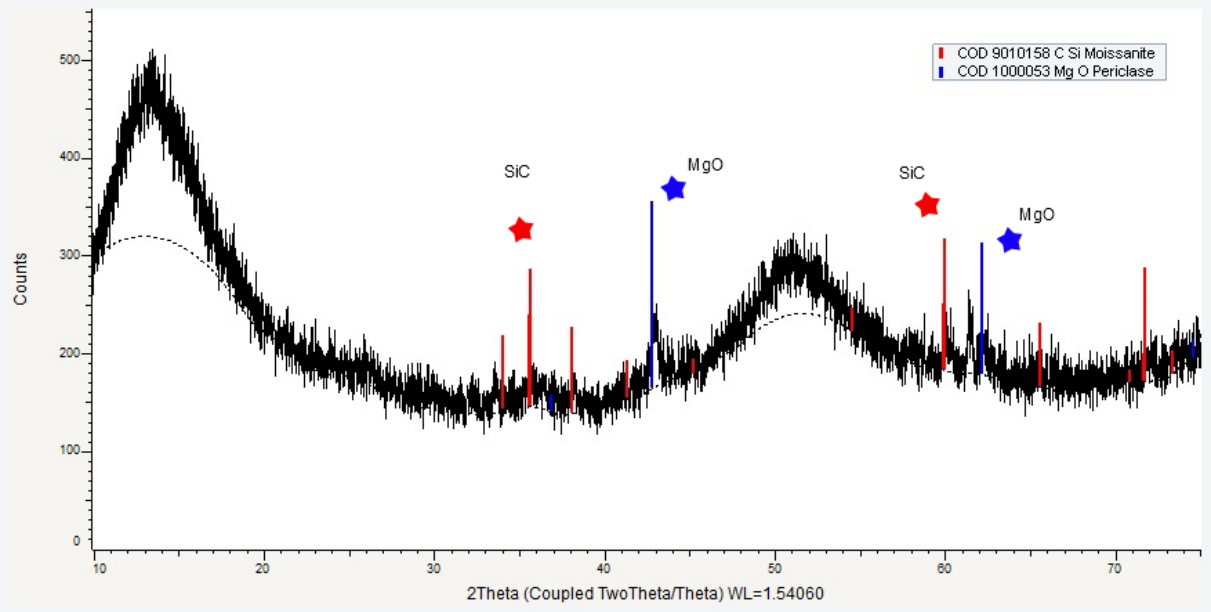

FIGURE 24 XRD RESULTS FOR SAMPLE 3-OIL1

In the diffraction results for sample 3-Oil1 we can see signs of the presence of silicon carbide and magnesium oxide. The results show no sign of either the silicon oxide, or the carbon found in other samples.

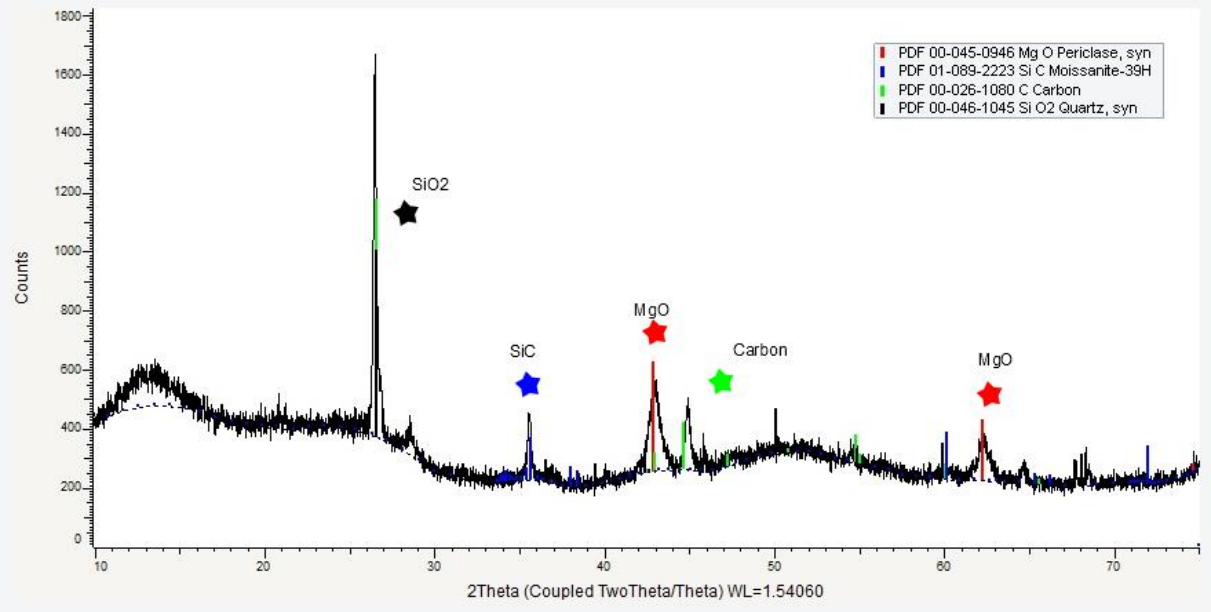

FIGURE 25 XRD RESULTS FOR SAMPLE 4-OIL2

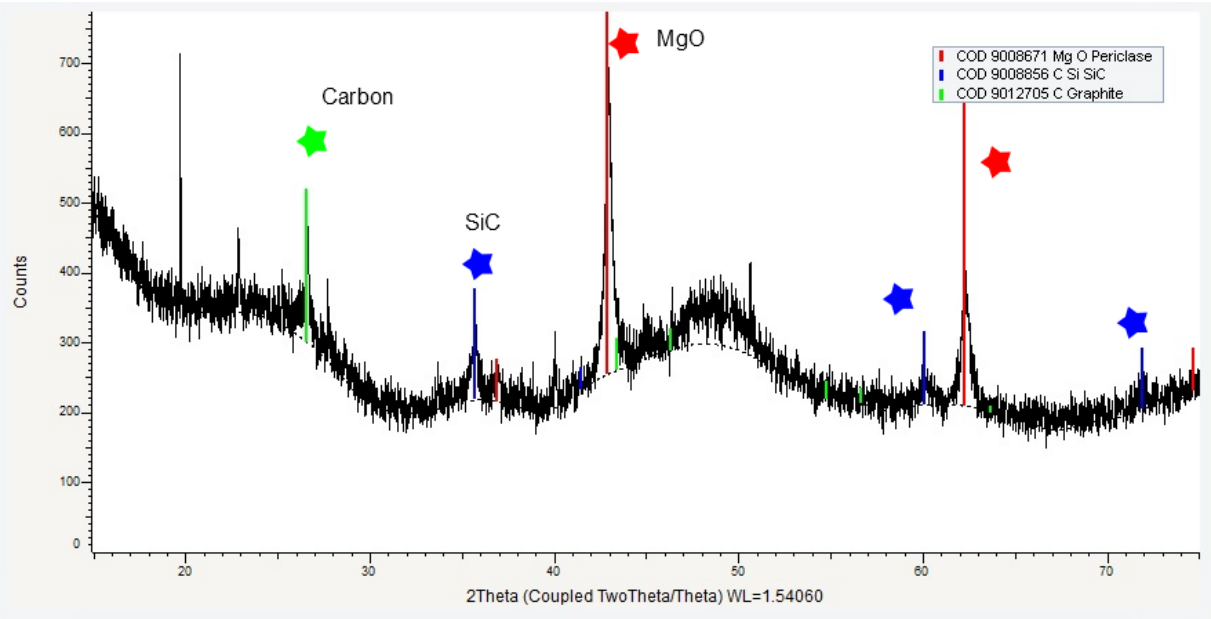

FIGURE 26 XRD RESULTS FOR SAMPLE 5-OIL3

In the XRD results for sample 5-Oil3 and sample 4-Oil2, we see again a clear silicon carbide signal. In both, the peak at 2Theta=36^{o} is an unambiguous indicator of the presence of silicon carbide. In addition, we have possible peaks at 2Theta=60^{o} and 2Theta=72^{o} that fit with the same carbide presence.

We also see the same peaks at 2Theta=43^{o} and 2Theta=62^{o}, showing the presence of magnesium oxide, as we saw in sample 4-Oil2. The search found no match for silicon oxide in this sample, but that may because it is again overlapping with the carbon peak tagged at 2Theta=28^{o}, like we saw in 4-Oil2.

4.1.2 Glass Replacements

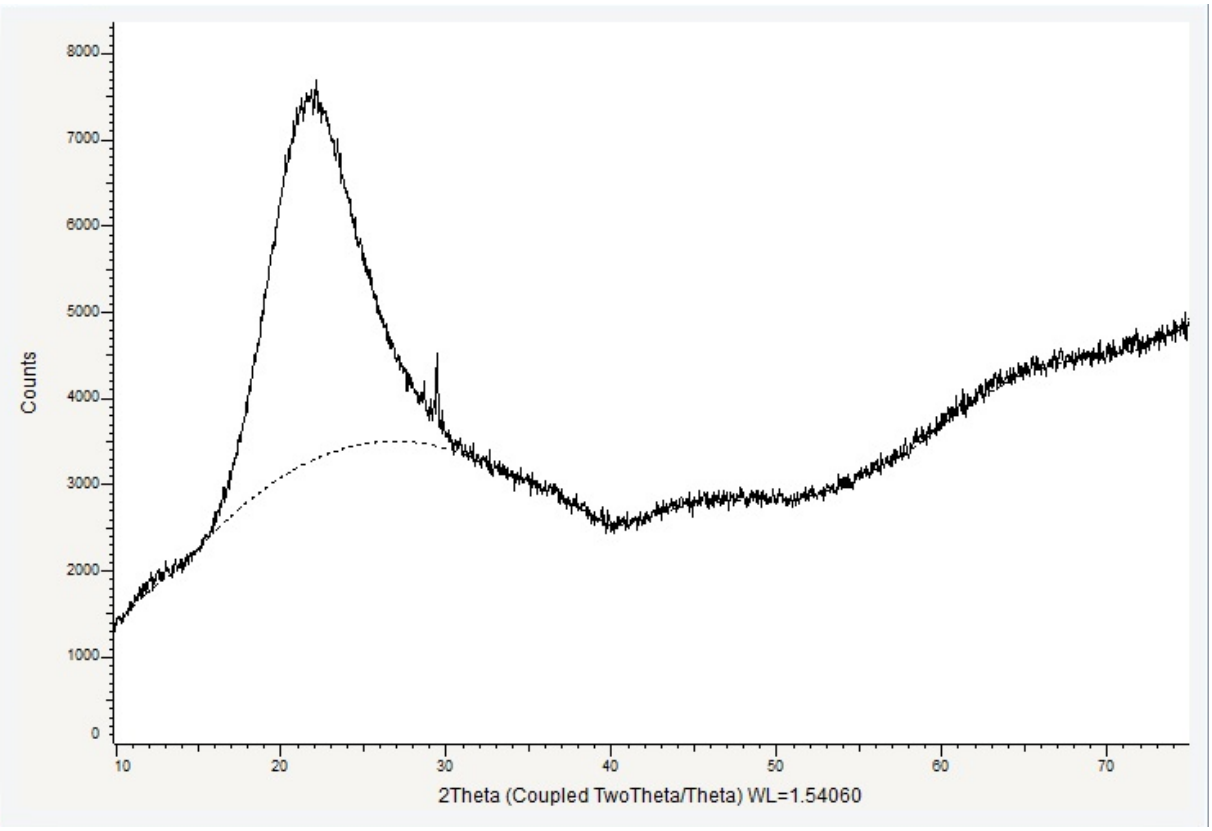

FIGURE 27 XRD RESULTS FOR THE SAMPLE GLASS 0

The sample Glass 0, which was a control sample that did not undergo the process. The results, shown in figure 27, show no signal. This is expected for an amorphous material such as glass.

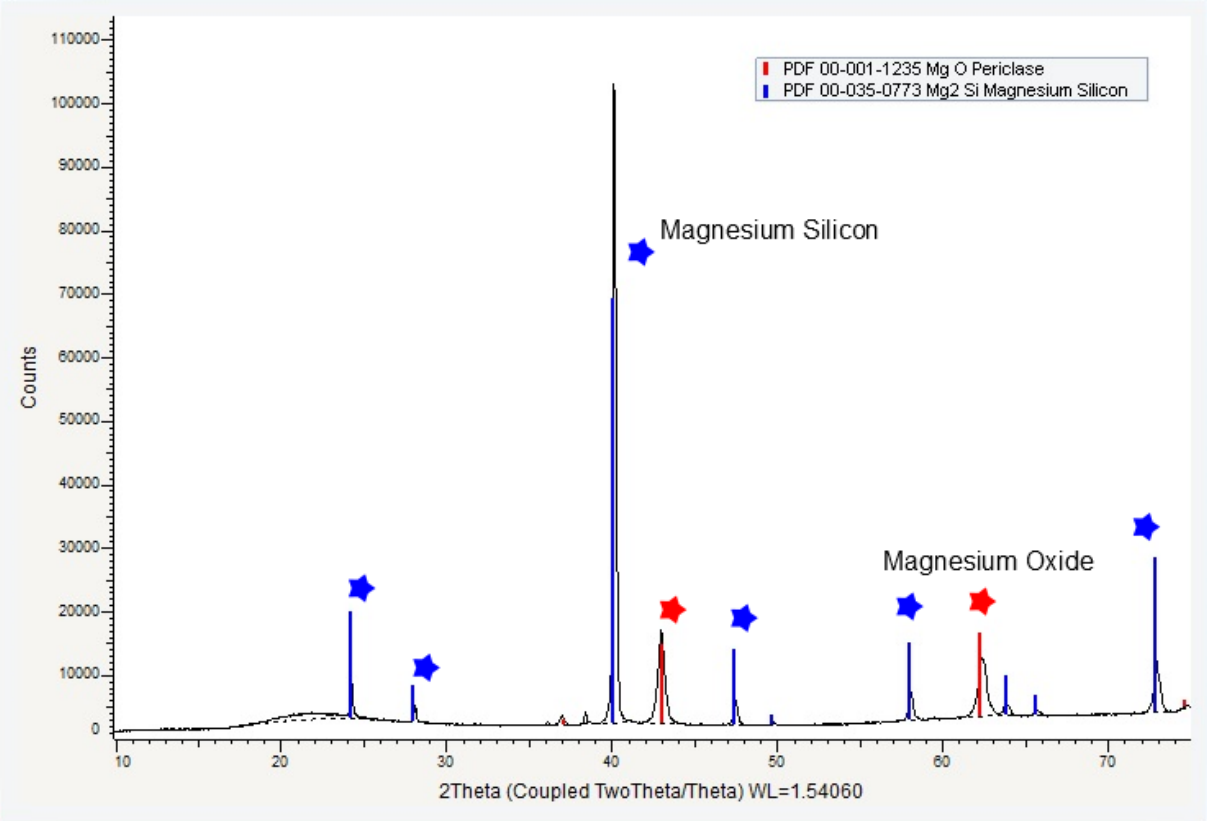

FIGURE 28 XRD RESULTS FOR SAMPLE GLASS 1 WHICH UNDERWENT THE PROCESS, BUT WAS NOT ADDED ANY CARBON.

In the XRD results from sample Glass1 we see the presence of magnesium oxide as well as a magnesium-silicon mixture. This shows that the magnesium gas has reacted with the glass surface.

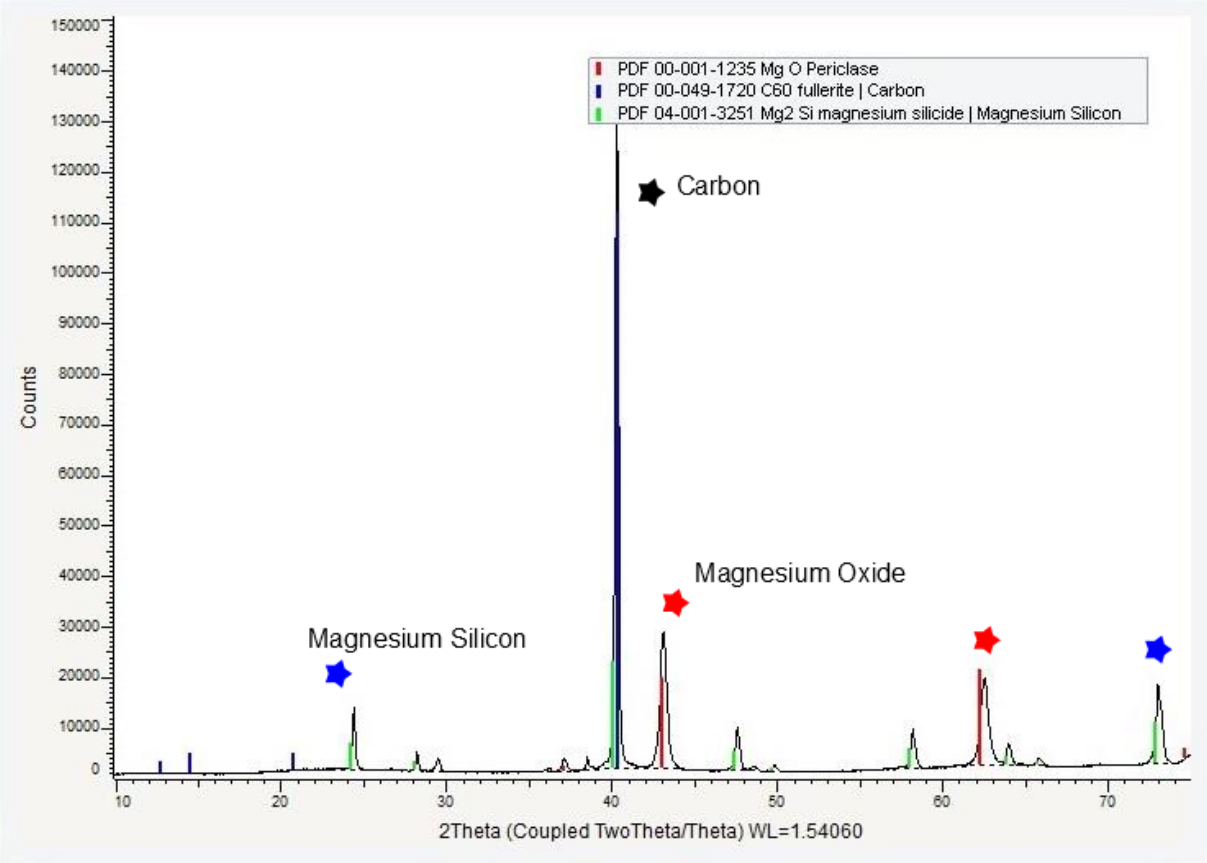

FIGURE 29 XRD RESULTS FOR SAMPLE GLASS 2 WHICH WAS ADDED CARBON IN POWDERED FORM.

The XRD results from samples Glass 2 show the sample as sample Glass1, but with the added presence of carbon. We see no sign of the presence of silicon carbide.

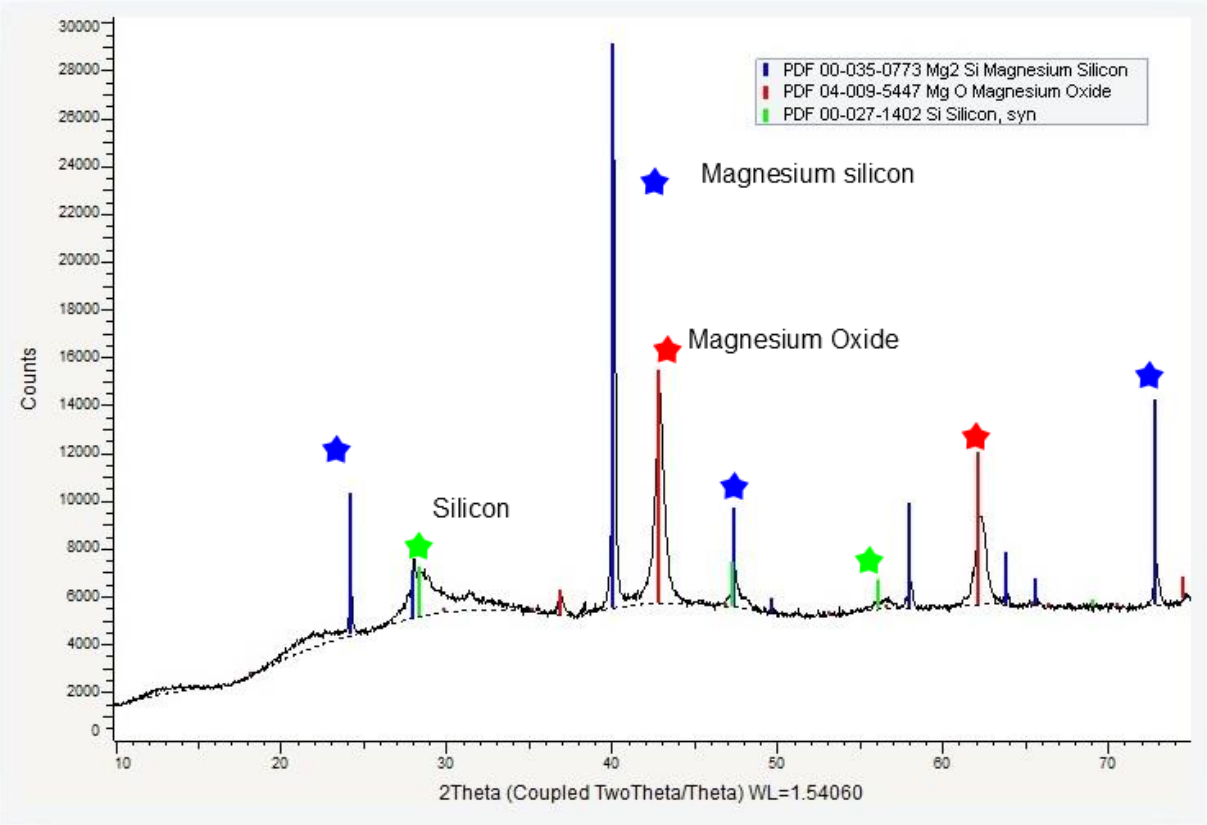

FIGURE 30 XRD RESULTS FROM SAMPLE GLASS 3 WHICH WAS ADDED CARBON IN THE FORM OF OIL.

The XRD results from sample Glass 3 show much the same components as the previous sample, but with no tagged carbon and the addition of elemental silicon that we have not seen in the previous samples.

4.2 SEM Results

Frustules from each sample (1-Plain, 2-Powder, 3-Oil1, 4-Oil2, 5-Oil3) was placed on carbon tape for SEM imaging. There are three categories of image per sample.

Firstly, an overview image was taken. This is to assess the general condition of the sample i.e. are the frustules mostly crushed or intact, and how much other, non-frustule, material is in the sample. This "other" material is generally a mix of organic matter left over from the process, or storage, small bits a pieces of frustules that have broken and stuck together, and, for the case sample 2-Powder, remaining carbon powder that survived cleaning.

Secondly, a mostly intact frustule is found and imaged. This is to see the general look of the frustules in the sample and what effect the process has had on the frustule as a whole.

Lastly, interesting details are imaged. This includes looking closely at the cribrum and areola of the frustule, and what damages may have occurred to them, as well as any other details found interesting.

4.2.1 Before-Pictures

To get a source of comparison and see what changes the process can make in the structure of the frustules, we must first look at some images taken before the heat treatment.

All the images are distorted by charge build up in the sample. This is because the silica the frustules are made of are poor conductors of electricity. This causes what appears as shadows and bright spots in the image.

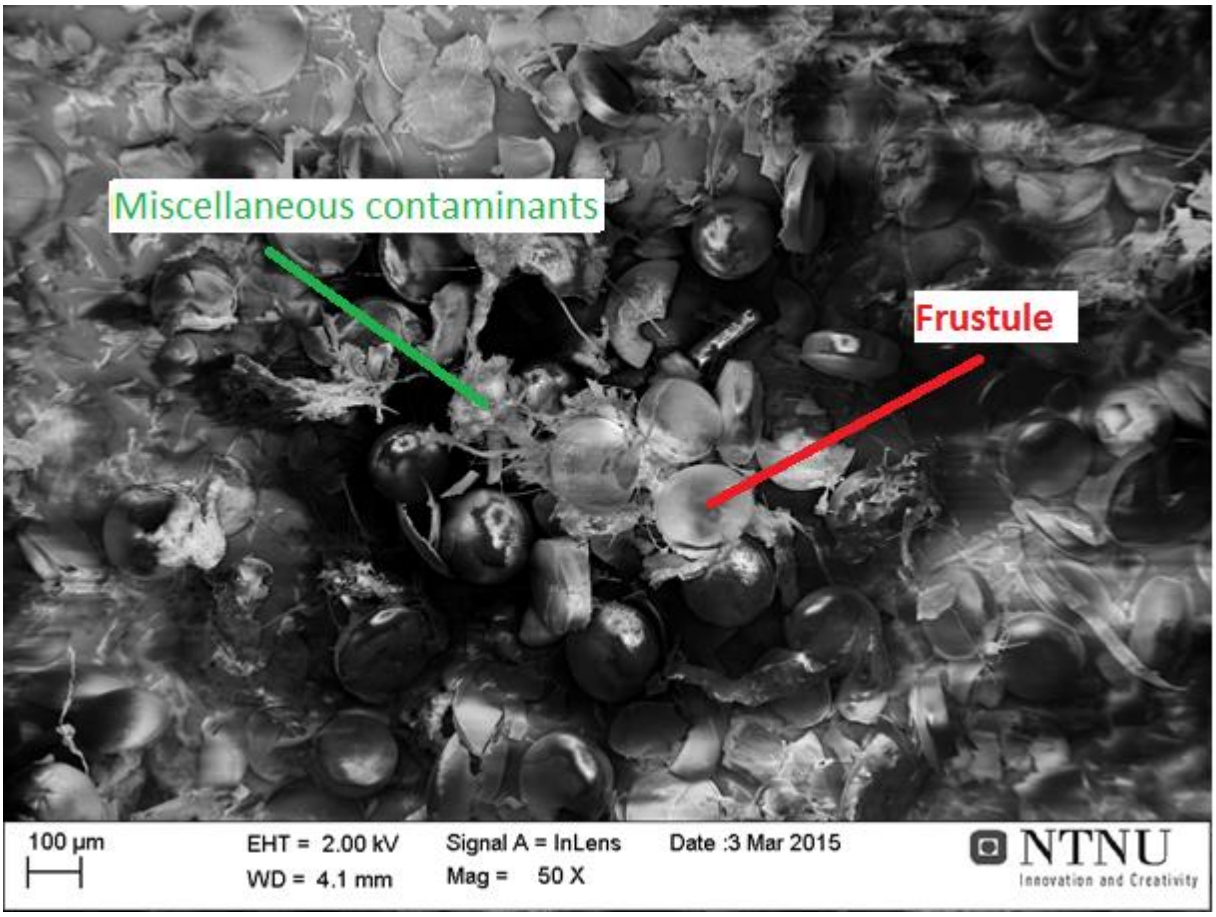

FIGURE 31 OVERVIEW-BEFORE

In the overview image we can see the general state of the frustules before the heat treatment. From this we can see that the frustules going into the reaction are in various degree of completeness, some intact, and others broken down to smaller flakes and pieces. We can also see collections of other artefact that are not frustules, but gatherings of miscellaneous contaminants.

Image quality is poor due to charging of the sample.

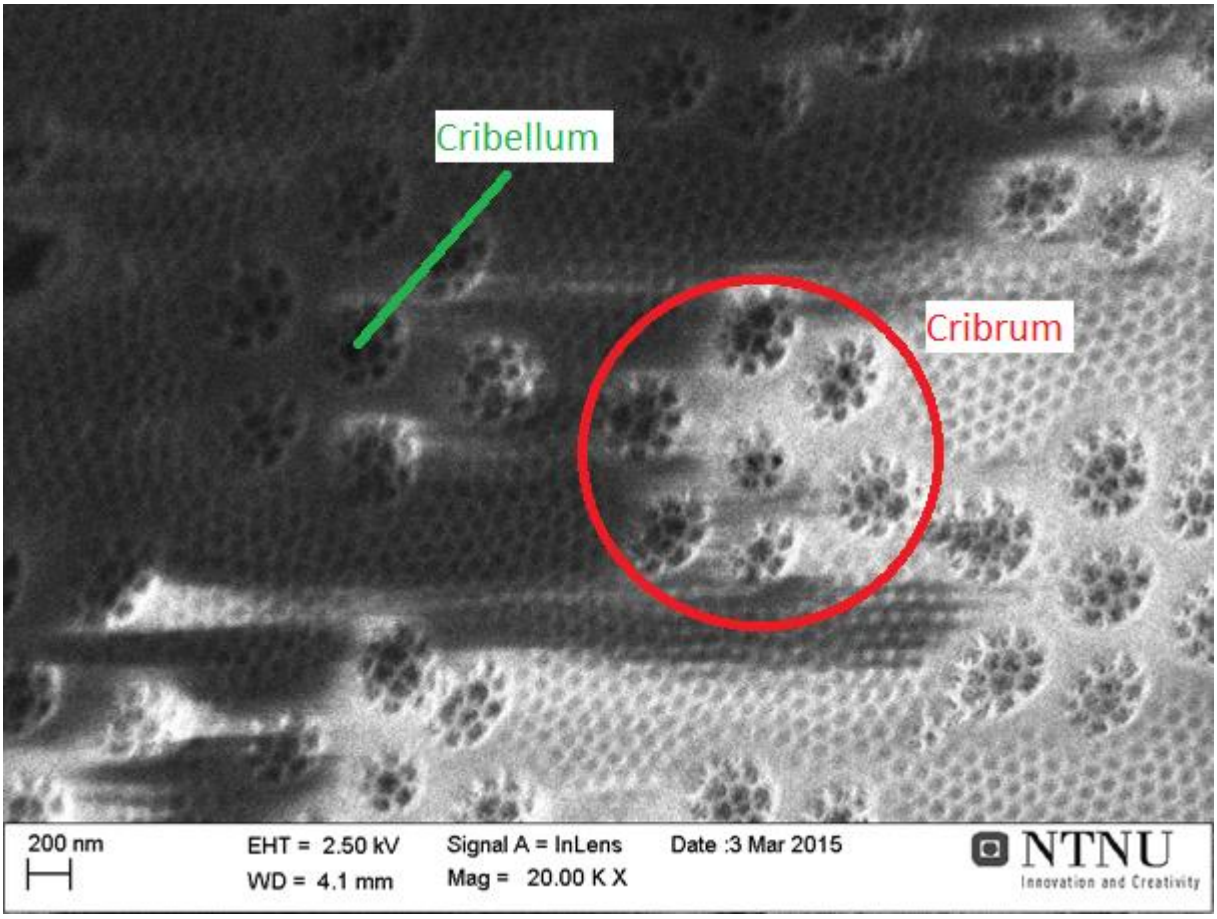

FIGURE 32 DETAILS-BEFORE CRIBRUM AND CRIBELLUM

Here we can see a close up image of the outside surface of a frustule. The holes in series of seven in a circle are the holes in the cribrum. The texture covering the holes are the cribellum. We can see that before going through the reaction, both are very well preserved.

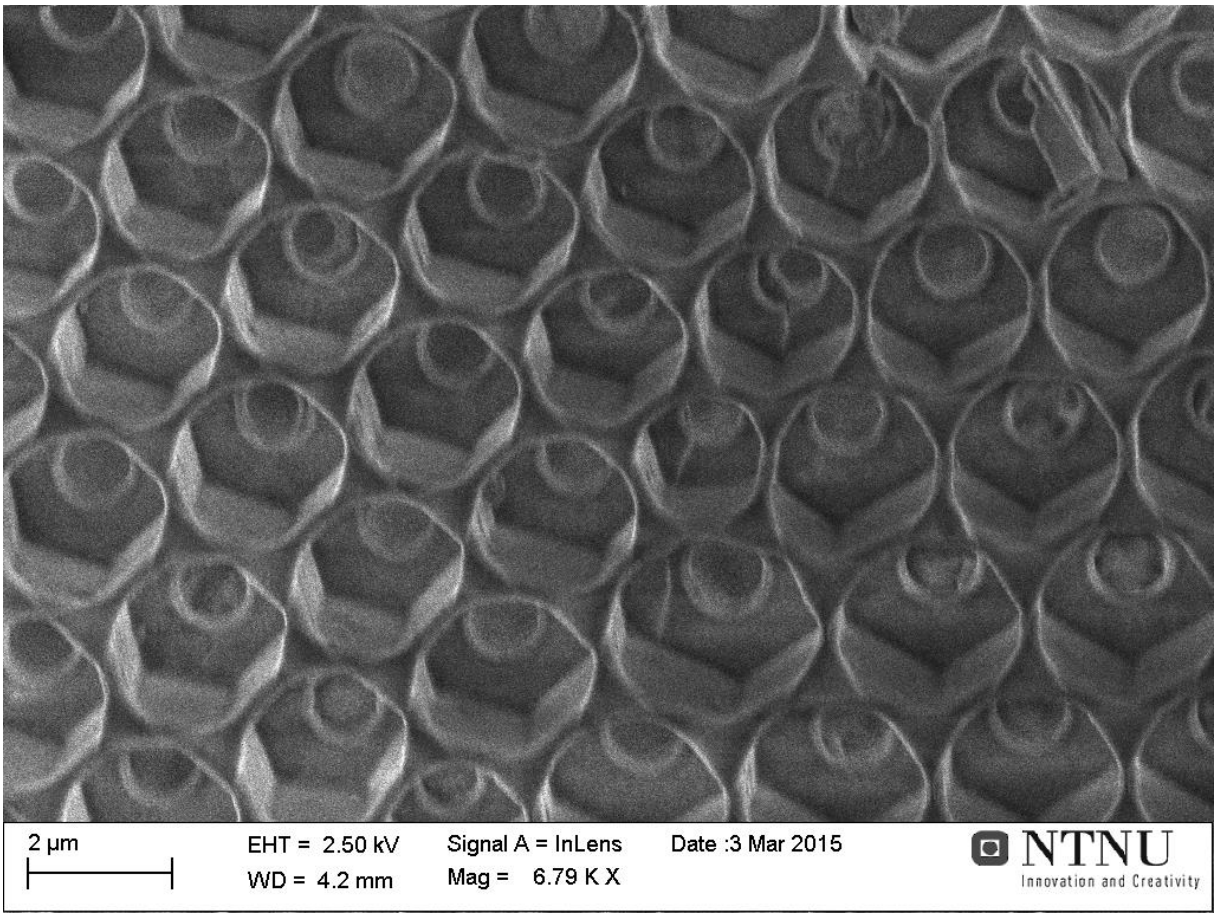

FIGURE 33 BEFORE-DETAILS AREOLA

In figure 33 we can see the areola before being treated by the reaction process. The areole lies directly beneath the cribrum, and each one of the holes seen here corresponds to a set of seven holes like the ones seen in the previous image.

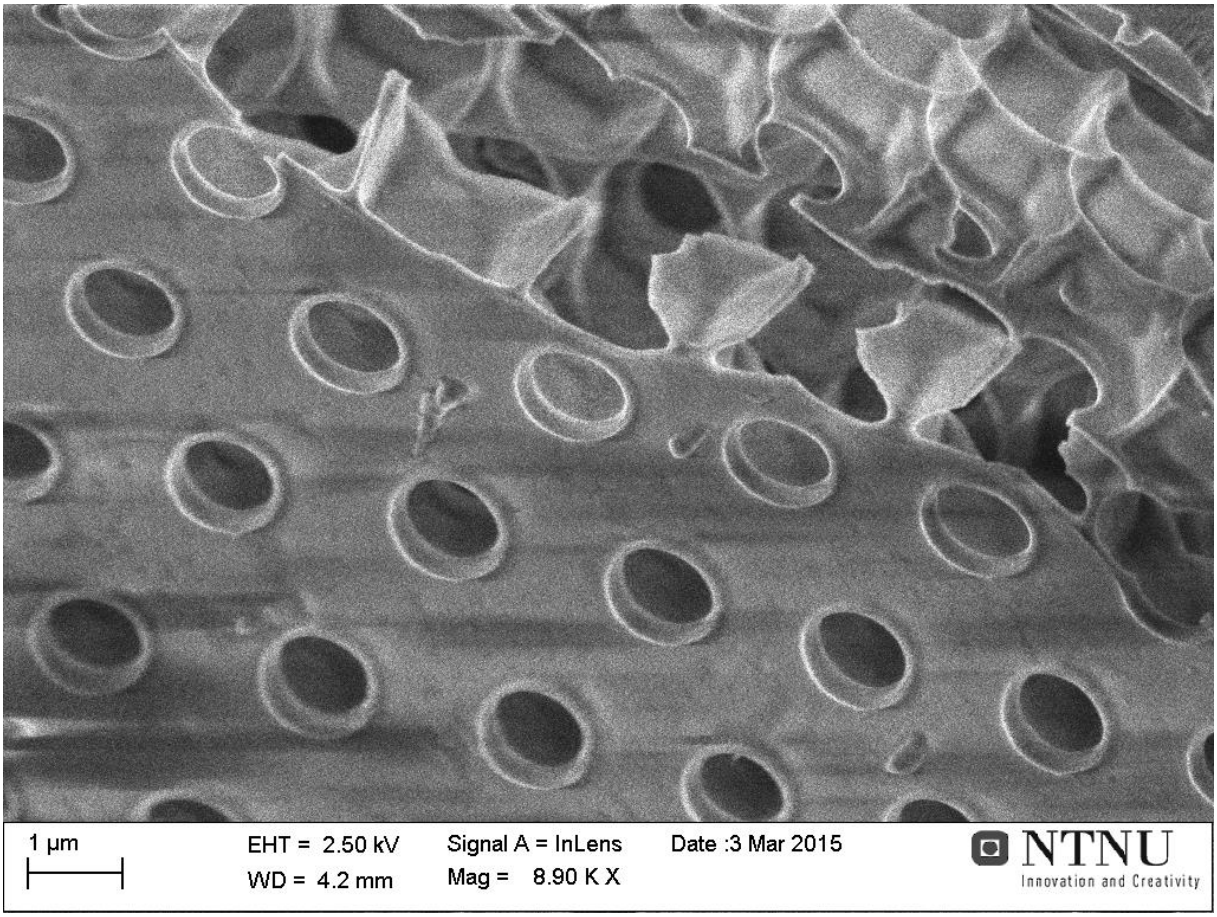

FIGURE 34 BEFORE-DETAIL AREOLA-FLIPPED

In figure 34 we see the same part of the frustule as we saw imaged in figure 33, but flipped around and seen from the other side. This is the foramen. Each one of the holes seen here are the ones seen at the bottom of the areola seen in figure 33.

4.2.2 Sample 1-Plain

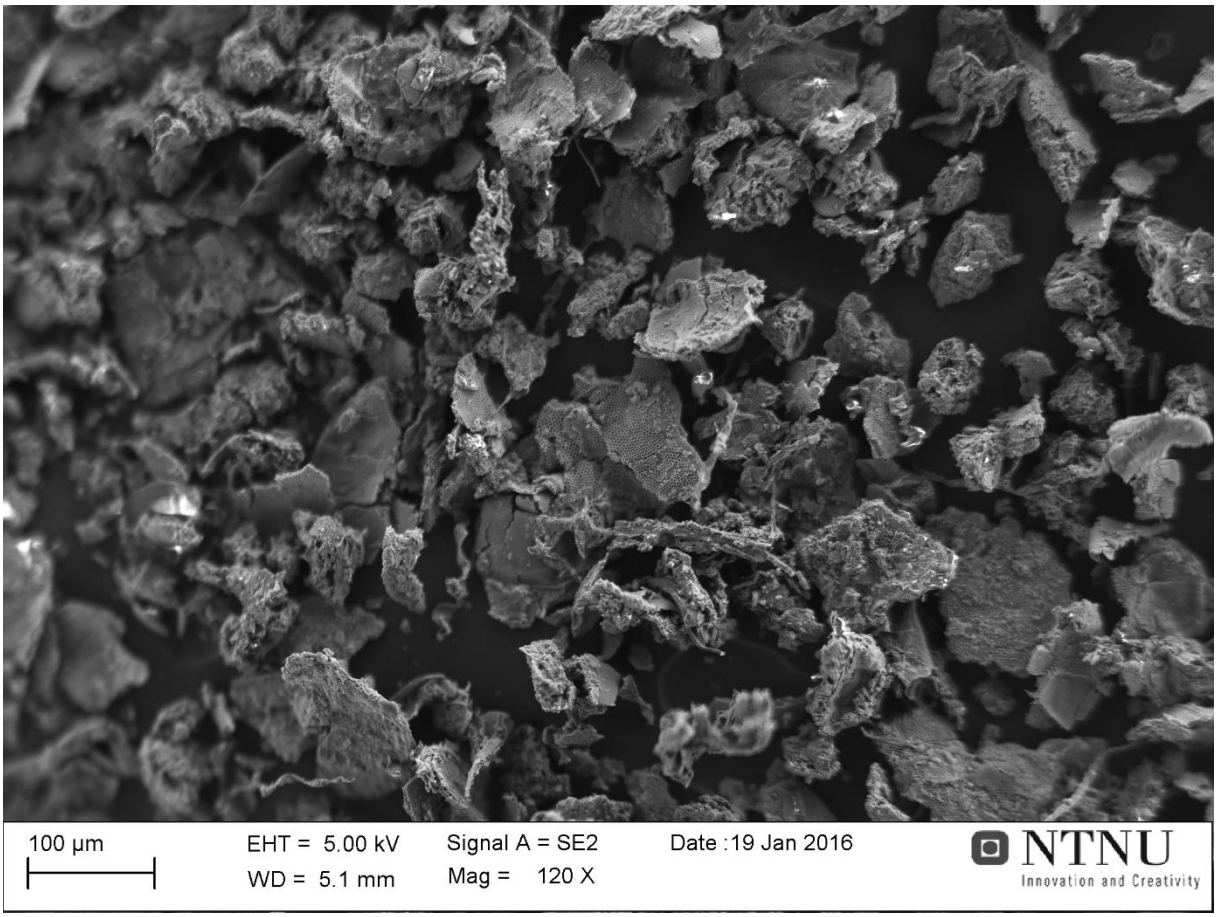

FIGURE 35 1-PLAIN-OVERVIEW

From the overview image of sample 1-Plain we see that the general state of the sample is rather poor, in that it looks like almost none of the frustules have survived process and storage whole. We see a smattering of frustules crushed into small pieces mixed with a lot of other contaminants.

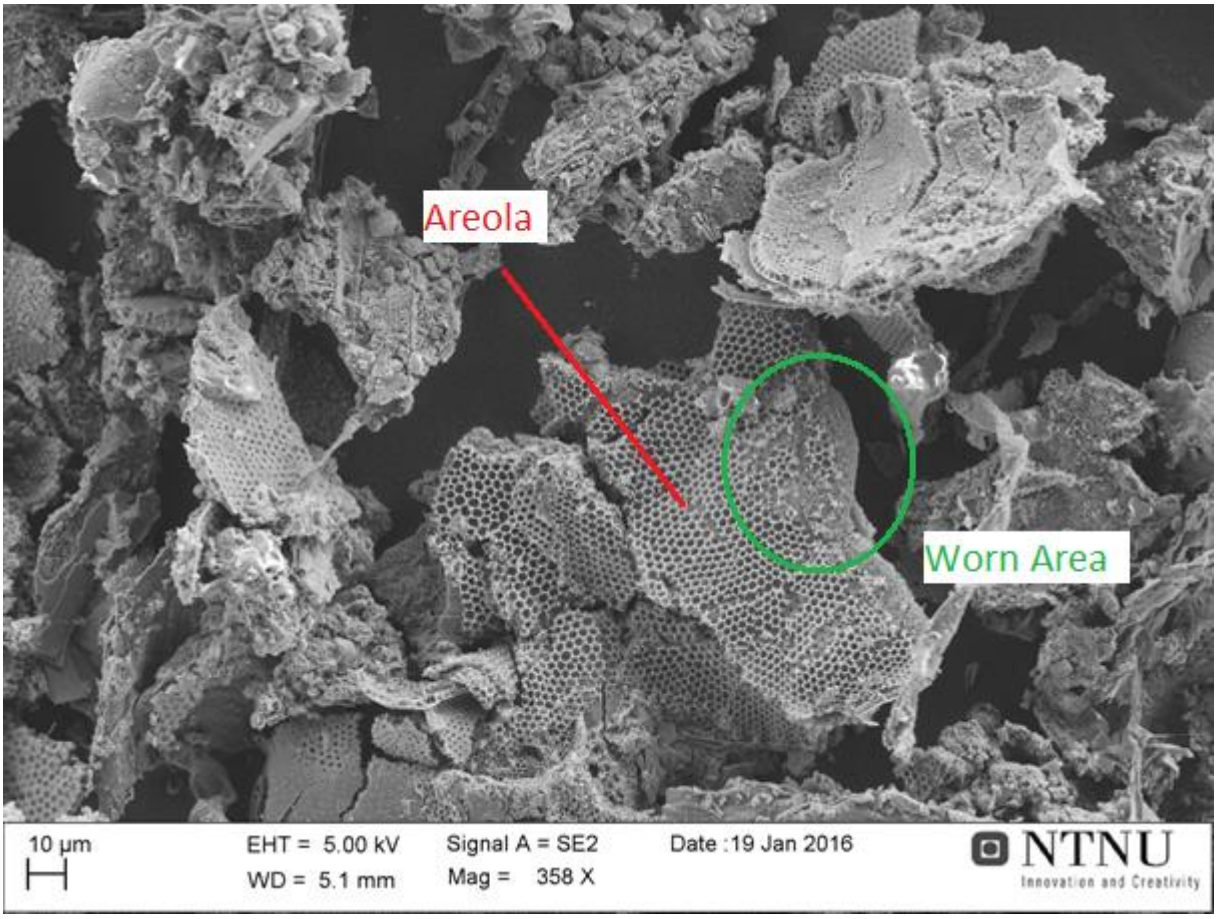

FIGURE 36 1-PLAIN-FRUSTULE

Given the high degree of destroyed frustules we see in on the overview image for the same sample it was very difficult to find an, even slightly, intact frustule. On the largest textured flake in the image we are able to see the areola. Some of the areola appears to have been worn away.

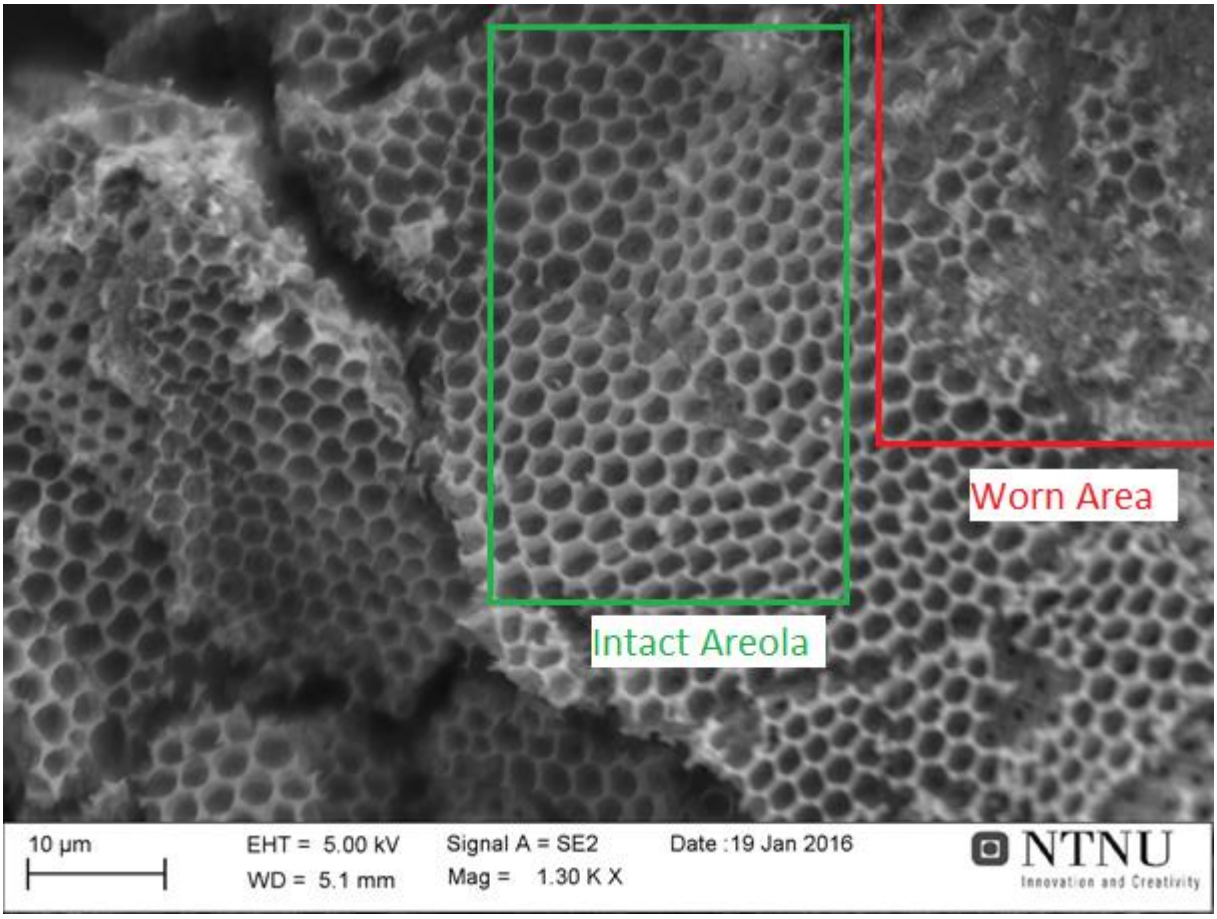

FIGURE 37 1-PLAIN-DETAIL1

We see, again, the areola of the frustule. In the upper, right corner of the image we can see that it looks to have been worn away from the cribrum. Elsewise, the areola appears intact.

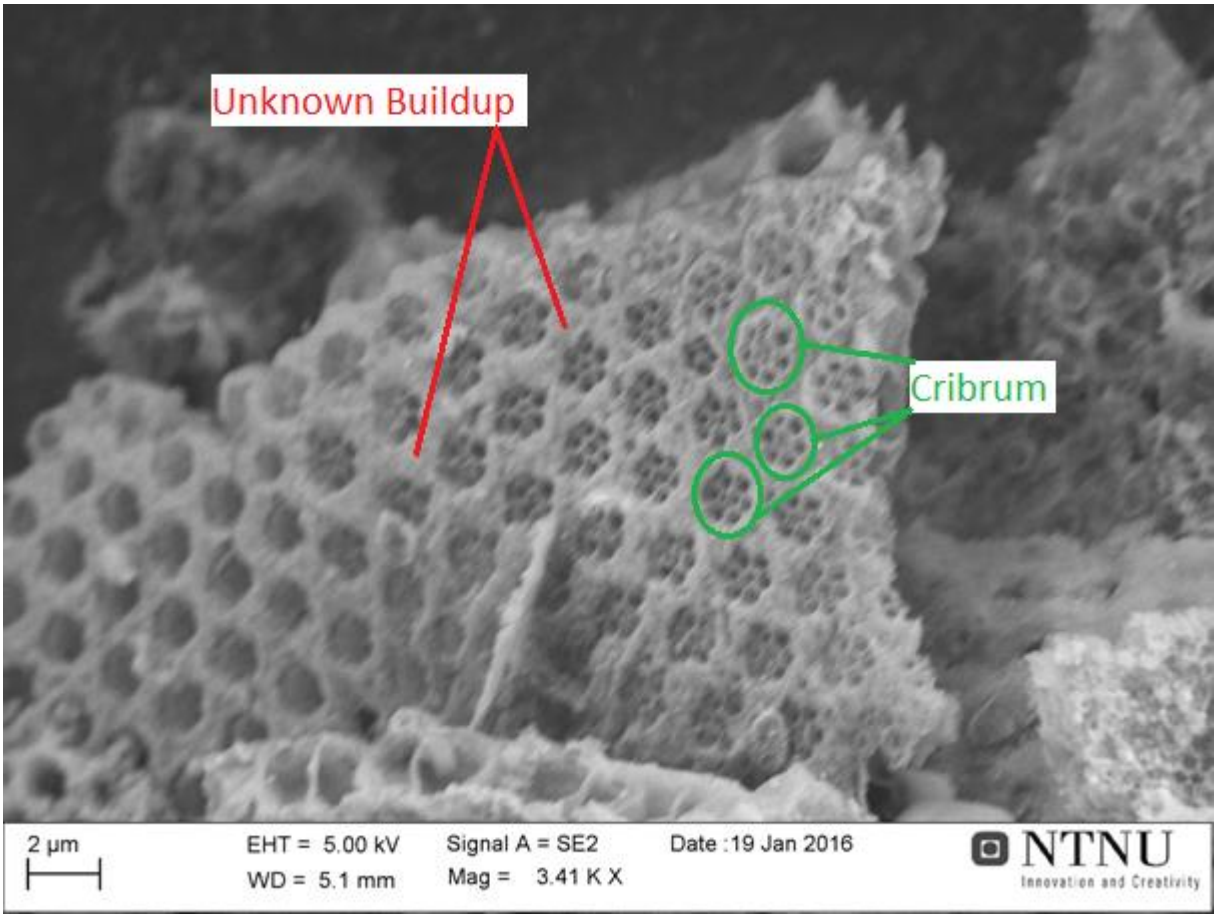

FIGURE 38 1-PLAIN-DETAIL2

We can clearly see the cribrum of the frustule. It looks undamaged by the process. There also appears to be a buildup of a layer of unknown composition on the surface between the holes in the cribrum.

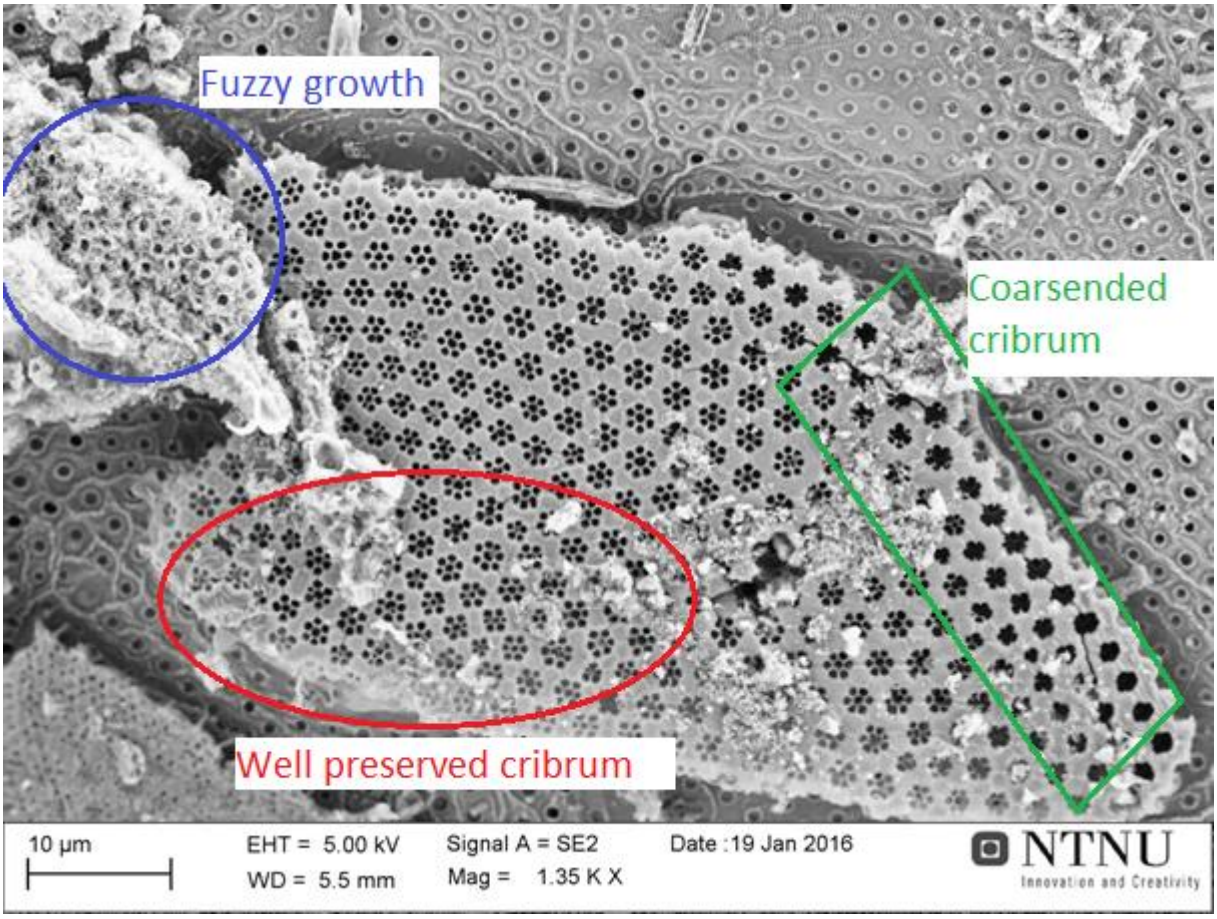

FIGURE 39 1-PLAIN-DETAIL3

In figure 39 we see a layer of cribrum on top of a layer of areola. The cribrum looks very well preserved at the center of the frustule (lower left of the image), but seem to loose detail and coarsen further out to the edge of the frustule. A layer of unknown, fuzzy growth can be detected on the surface of the flake in the upper left of the image.

4.2.3 Sample 2-Powder

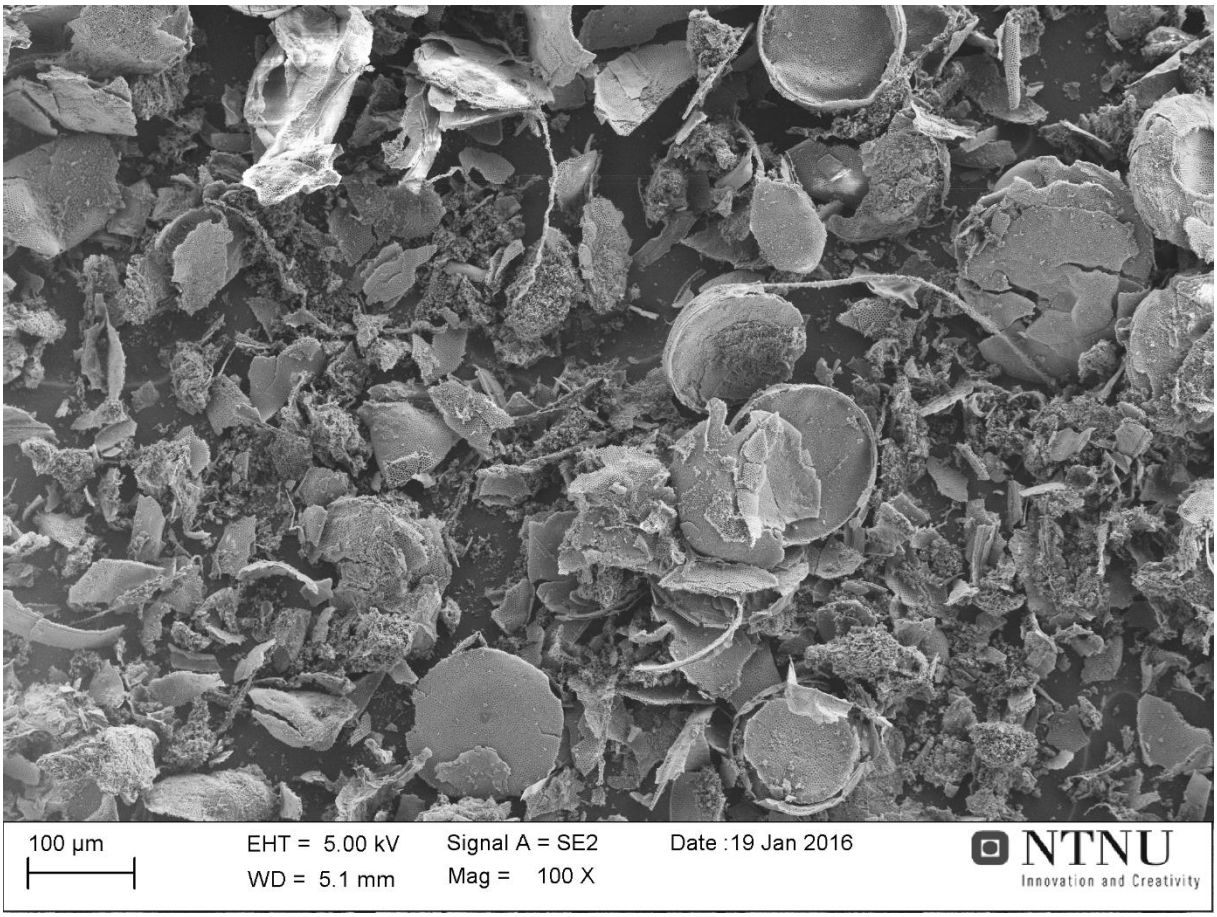

FIGURE 40 2-POWDER-OVERVIEW

The overview image of sample 2-Powder show that the frustules are broken down to small pieces. Several, mostly intact plates of epivalve and hypovalve can be seen. We also see a lot of other dust particles. Those are probably the carbon powder added to the reaction and agglomerated into bigger particles during the heat treatment.

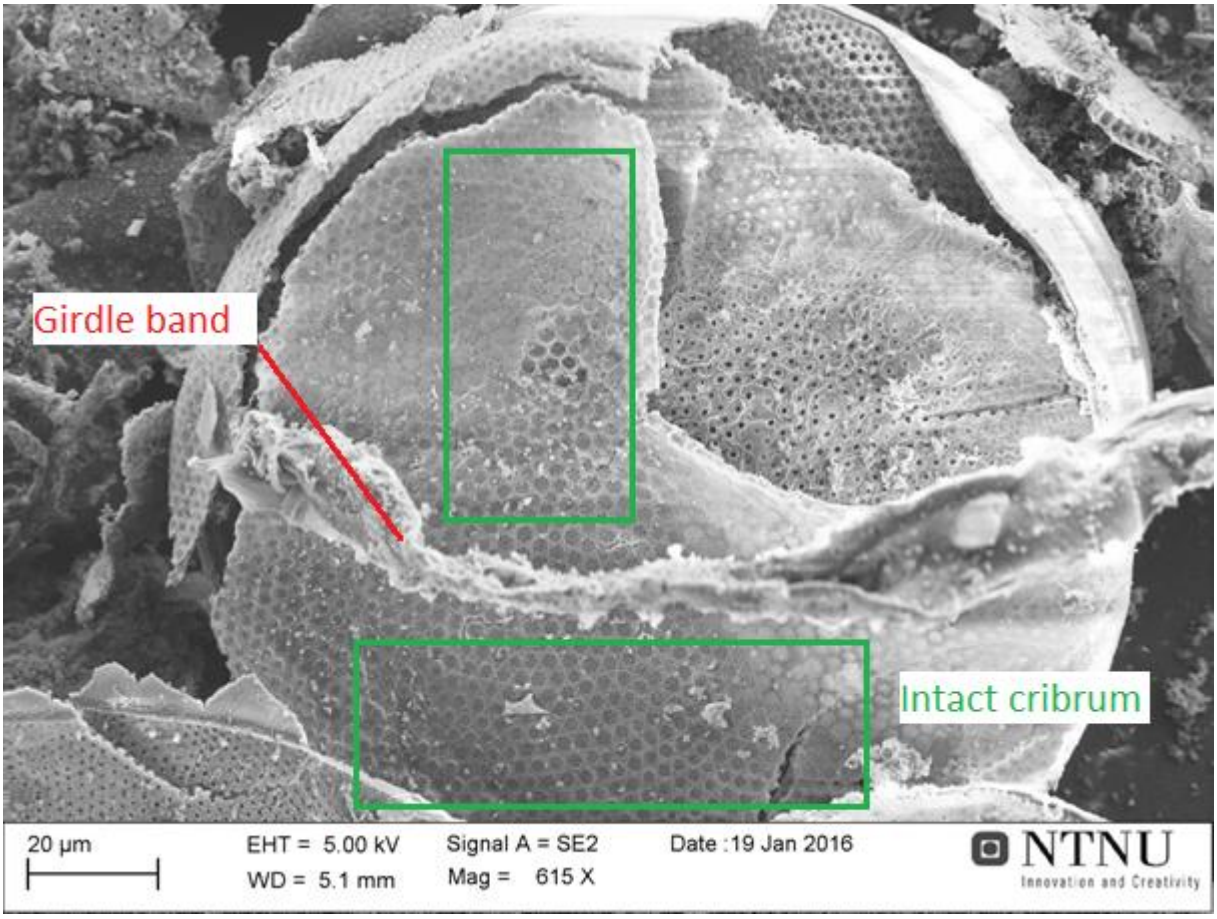

FIGURE 41 2-POWDER-FRUSTULE

In the frustule image we can see the whole of a cracked frustule. We see no large scale degradation of the nano-architecture, and it looks like the cribrum is, to a large degree, intact.

In the foreground we can see a long line extending across the image. It looks to be part of a girdle band that has deformed during the reaction process.

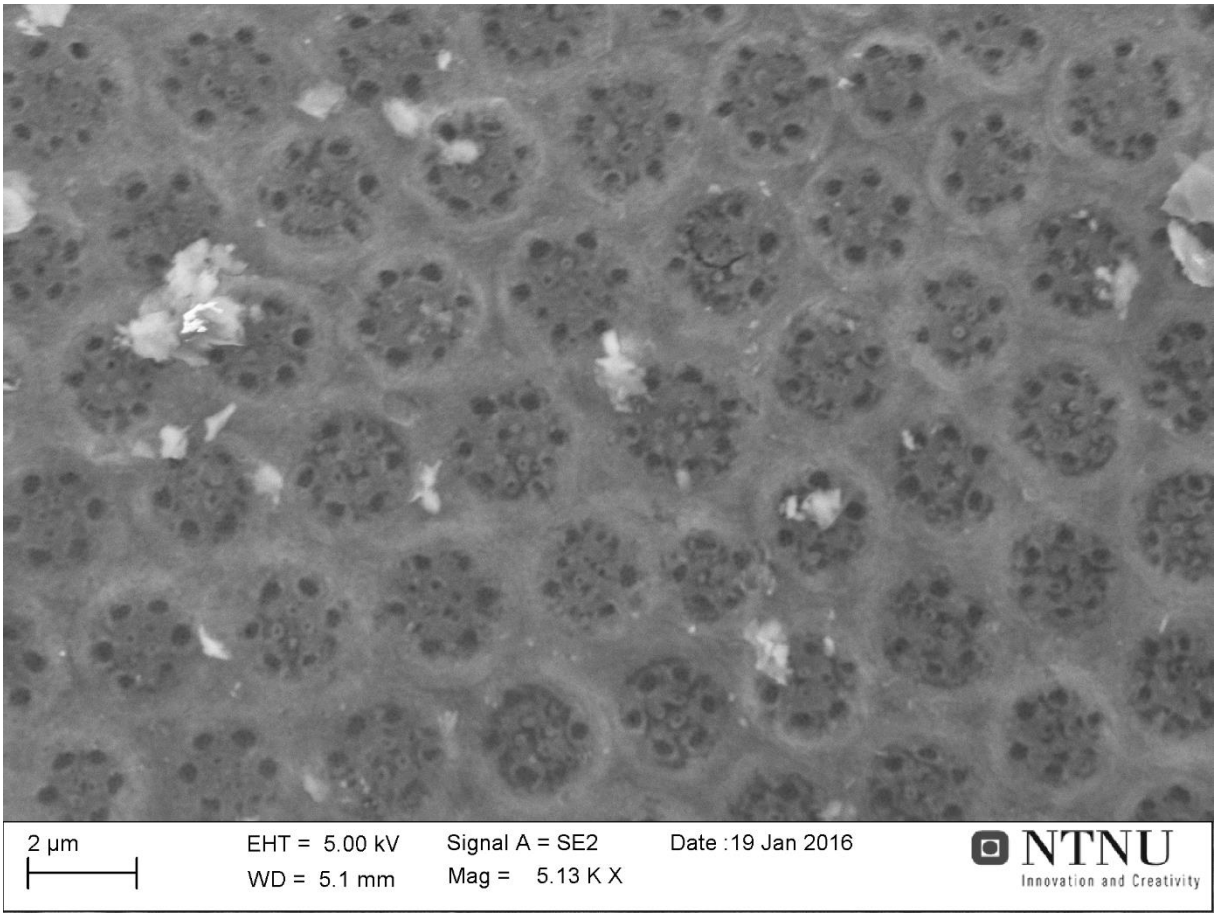

FIGURE 42 2-POWDER-DETAIL1

Taking a closer look at the cribrum we can see it is mostly intact, but looks to have undergone some amount of coarsening when compared to what we see in the images from sample 1-Plain.

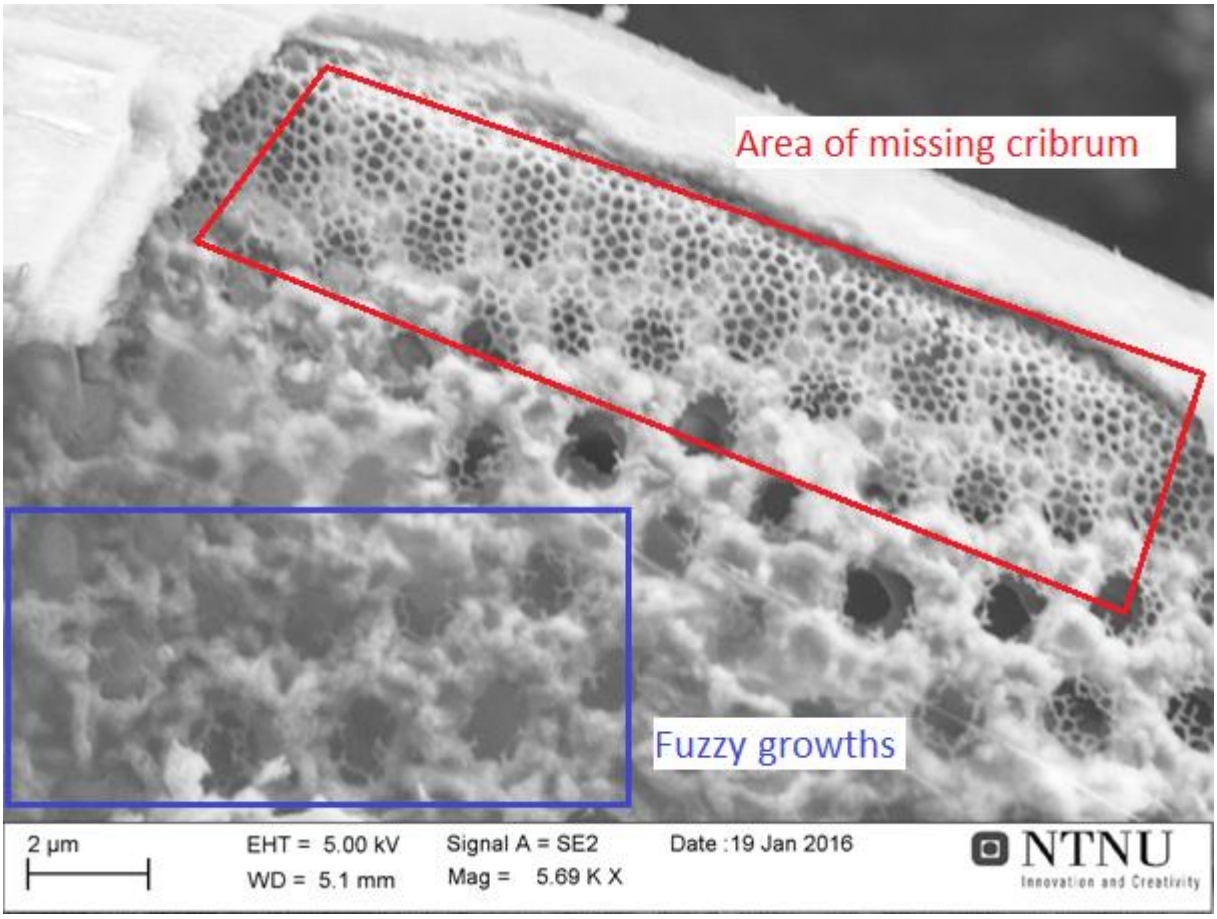

FIGURE 43 2-POWDER-DETAIL2

We see here the same fuzzy growths seen in sample 1-Plain. We can also see that some of the cribrum disappears as it gets close to the girdle band of the edge. We saw in sample 1-Plain that the fine details of the cibrum disappeared towards the edge, while here it is the flat parts between the holes that has disappeared and the fine mesh details have remained.

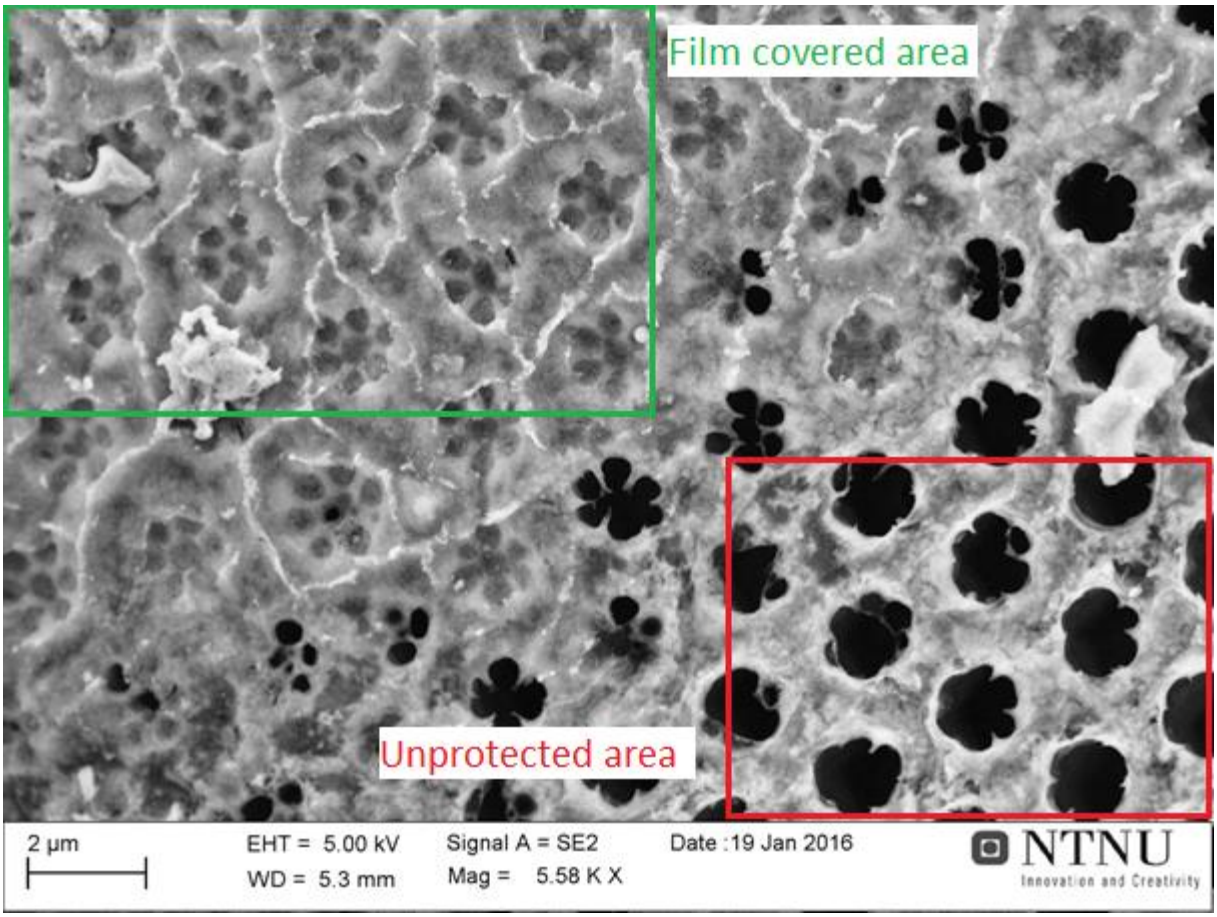

FIGURE 44 2-POWDER-DETAIL3

We can see in figure 44 that some kind of film is covering parts of the cribrum in the upper left part of the image while at the bottom right half of the image, the cribrum appears worn away. The cribrum looks to be less worn down at the parts covered by the film.

4.2.3 Sample 3-Oil1

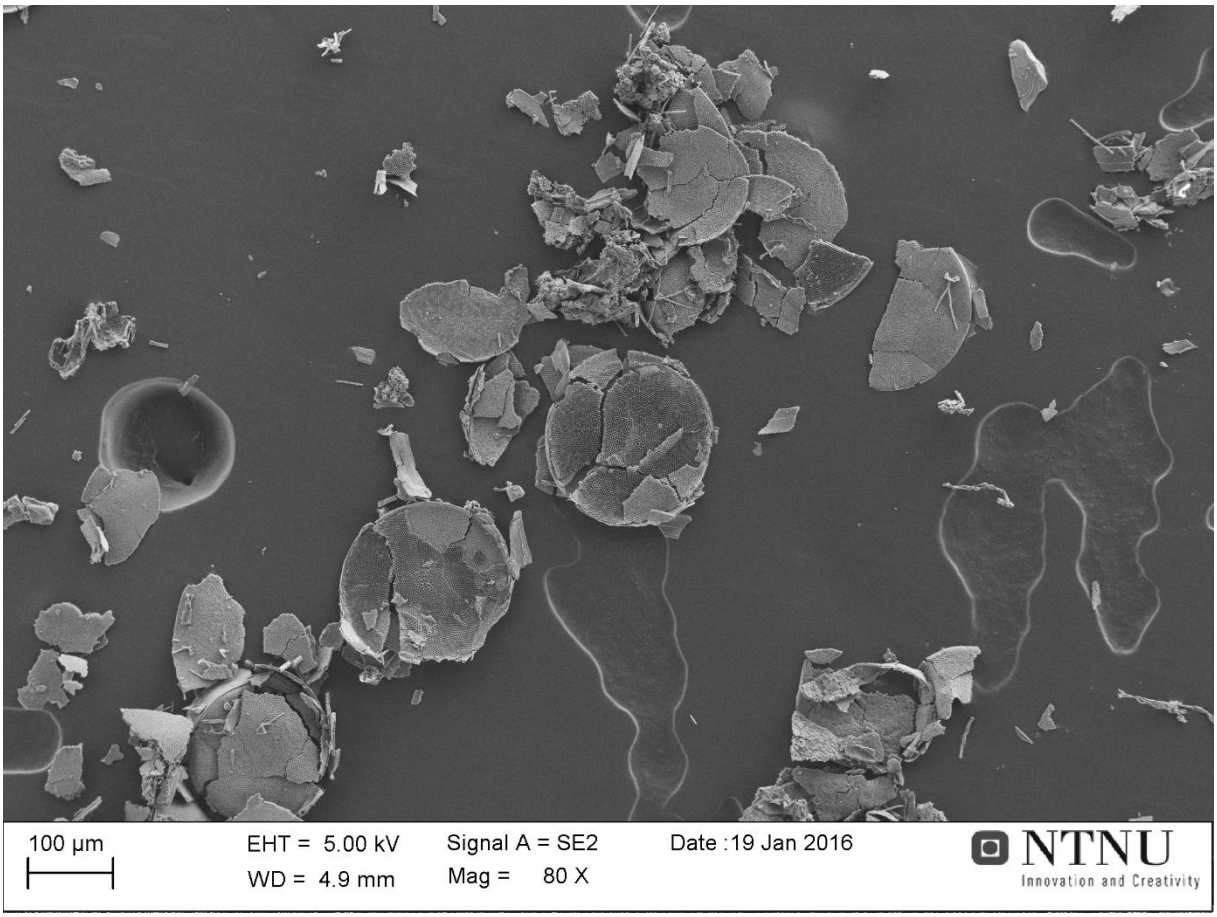

FIGURE 45 3-OIL1-OVERVIEW

The overview image of sample 3-Oil1 we see a lot less sample material than in the other overview images. This is because, as stated before, much of this sample was lost when the reaction caused the steel mesh holding the frustules in the reactor to break. Because of this we can see shapes and features of the carbon tape used to mount the frustules in the microscope in the background.

The state of the frustules that are present appear to be about the same as in both sample 1-Plain and 2-Powder; that being mostly cracked crushed into smaller pieces.

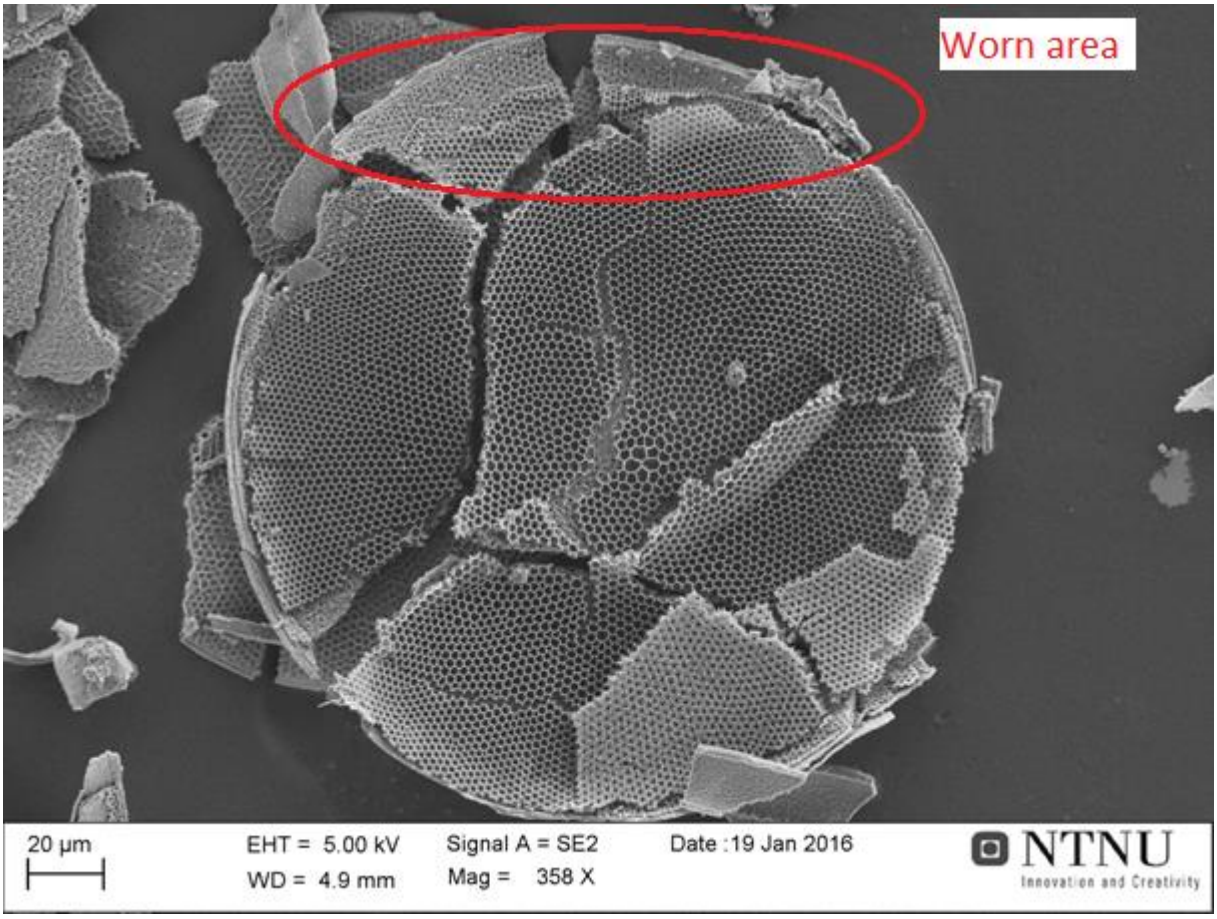

FIGURE 46 3-OIL1-FRUSTULE

We see from the frustule image of sample 3-Oil1 that the areola is intact but a little worn down along the edge at the top of the image. This is much the same as seen in the other samples.

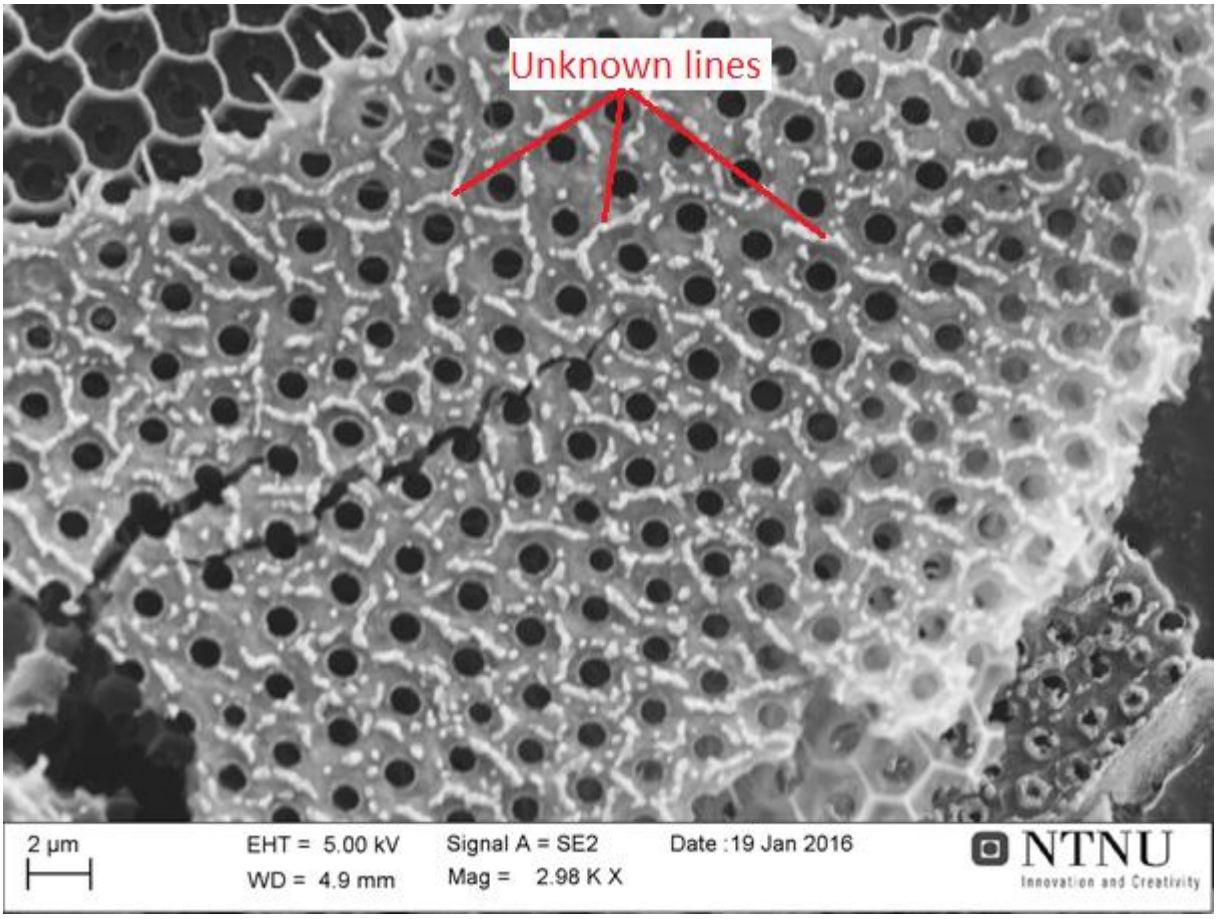

FIGURE 47 3-OIL1-DETAIL1

We see here the foramen. It looks like some white substance has gathered in lines between the holes.

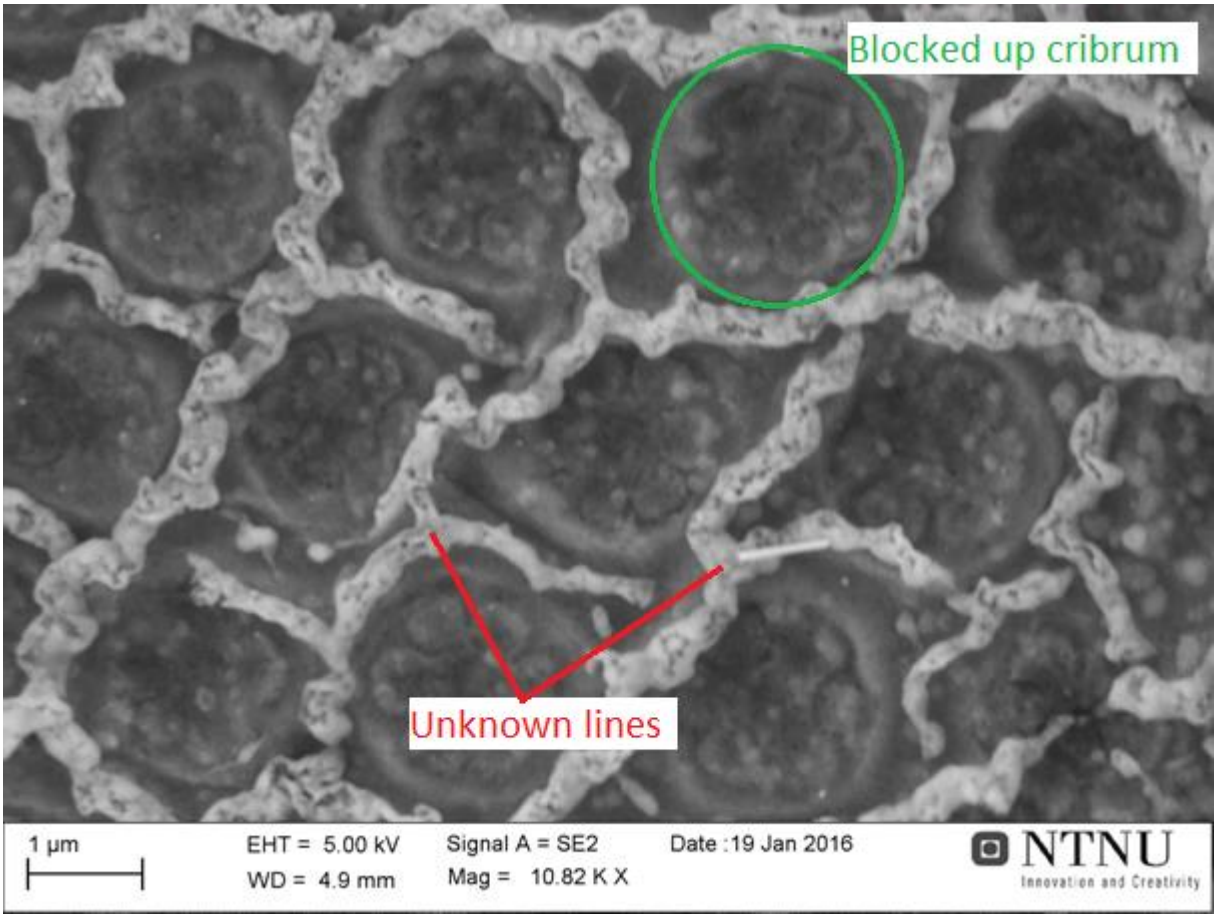

FIGURE 48 3-OIL1-DETAIL2

Looking closer at the cribrum of the first sample that was added oil we can see that the holes in the cribrum looks to be blocked up. This can possibly be the same film we saw in sample 2-Powder where it looked to protect the cribrum.

We also see the same lines we saw in the 3-Oil1-Detail1 image, though this time they are located at the surface of the cribrum rather than on the areola.

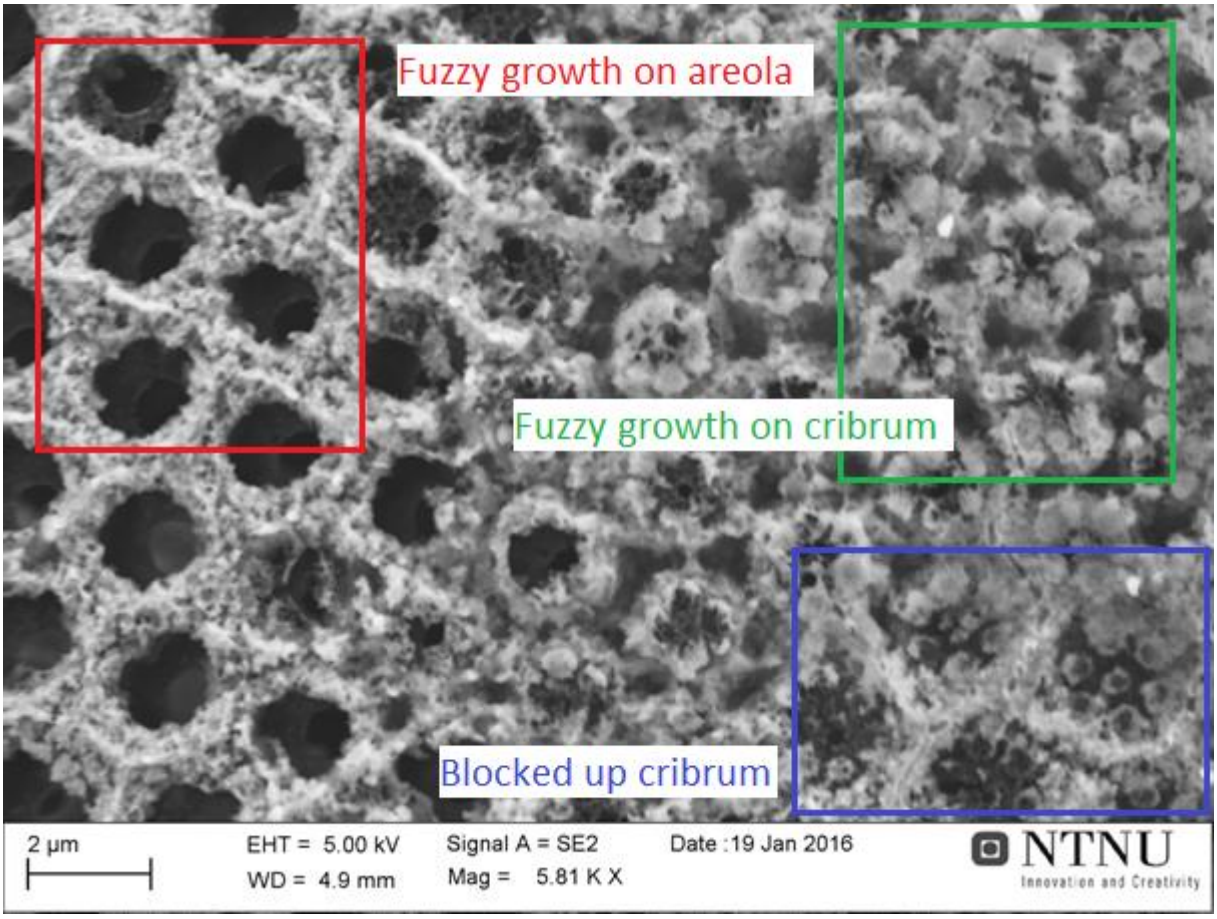

FIGURE 49 3-OIL1-DETAIL3

This image shows what looks like the same fuzzy growths as found in sample 2-Powder, though much more of it. It covers both the areola (left side of the image) and the cribrum (right side of the image). It looks like it covers the cribrum to the extent that it blocked up its holes like seen in the 3-Oil1-Detail2 image.

4.2.4 Sample 4-Oil2

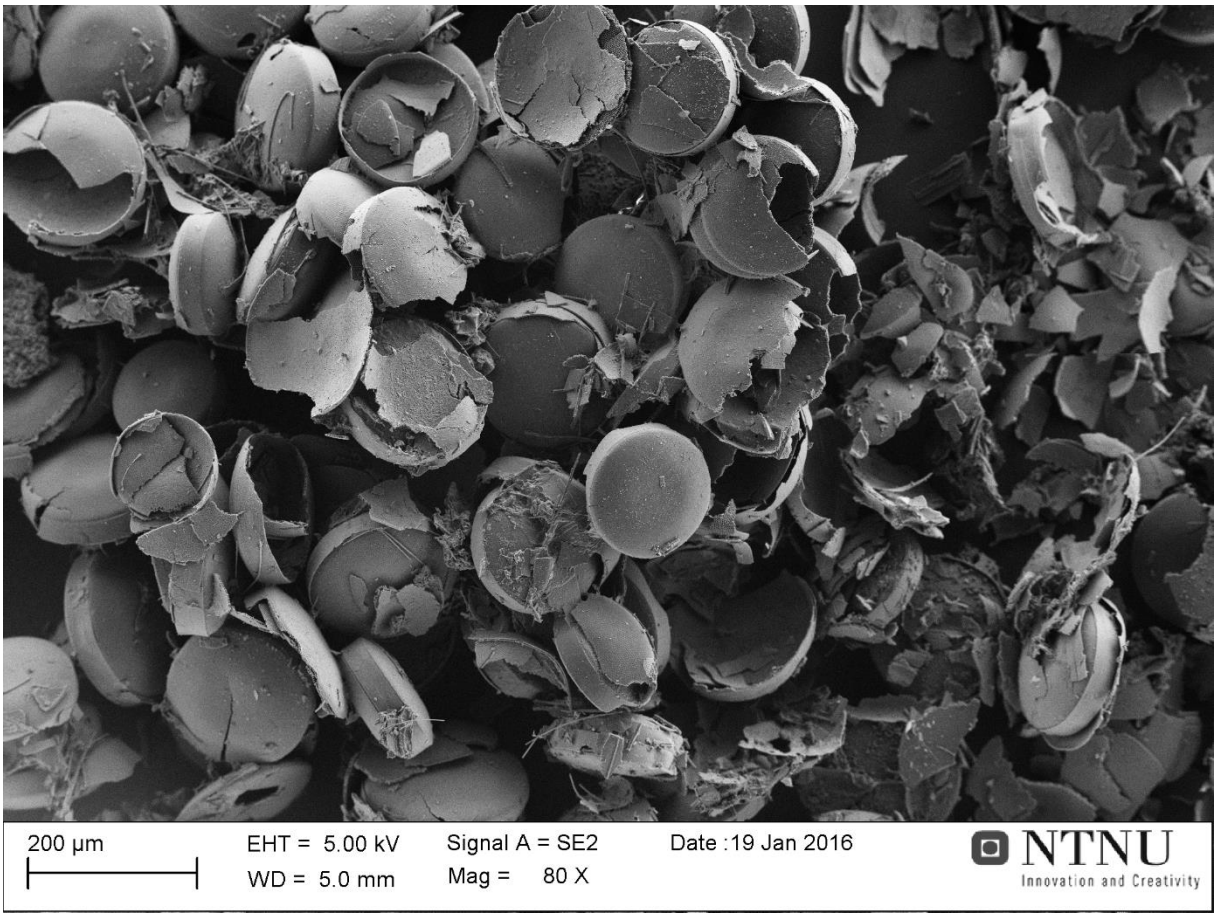

FIGURE 50 4-OIL2-OVERVIEW

In the overview of sample 4-Oil2 show frustules in a much better state than the previous samples. We can see several mostly intact frustules and large pieces.

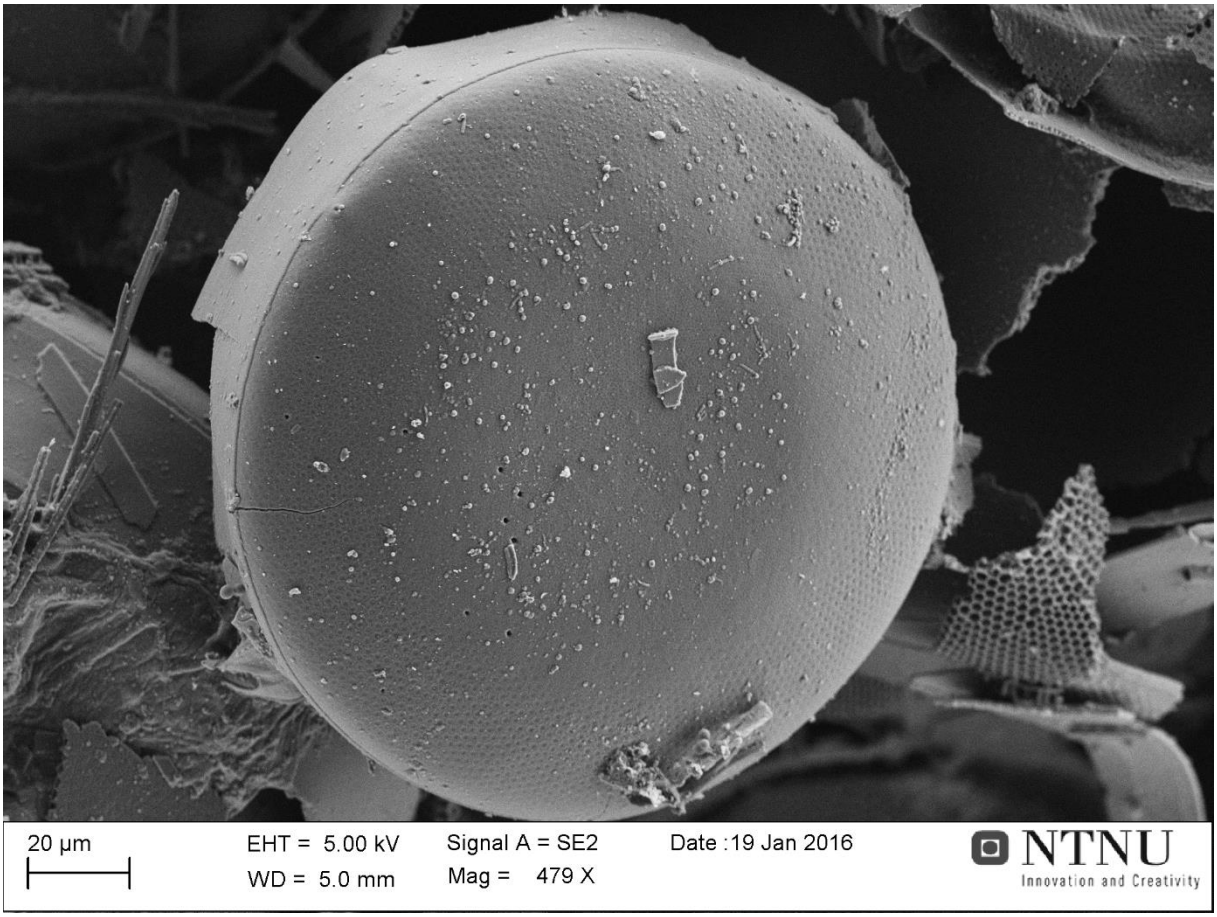

FIGURE 51 4-OIL2-FRUSTULE

Looking at a single frustule it looks completely covered by a film. This could be the same film seen covering parts of a frustule in sample 2-Powder, but here it looks to be covering the features of the frustule at a much larger degree. A different interpretation is that this is not a film at all, but rather just the result of the coarsening the cribrum that can happen during the heat treatment during the reaction process.

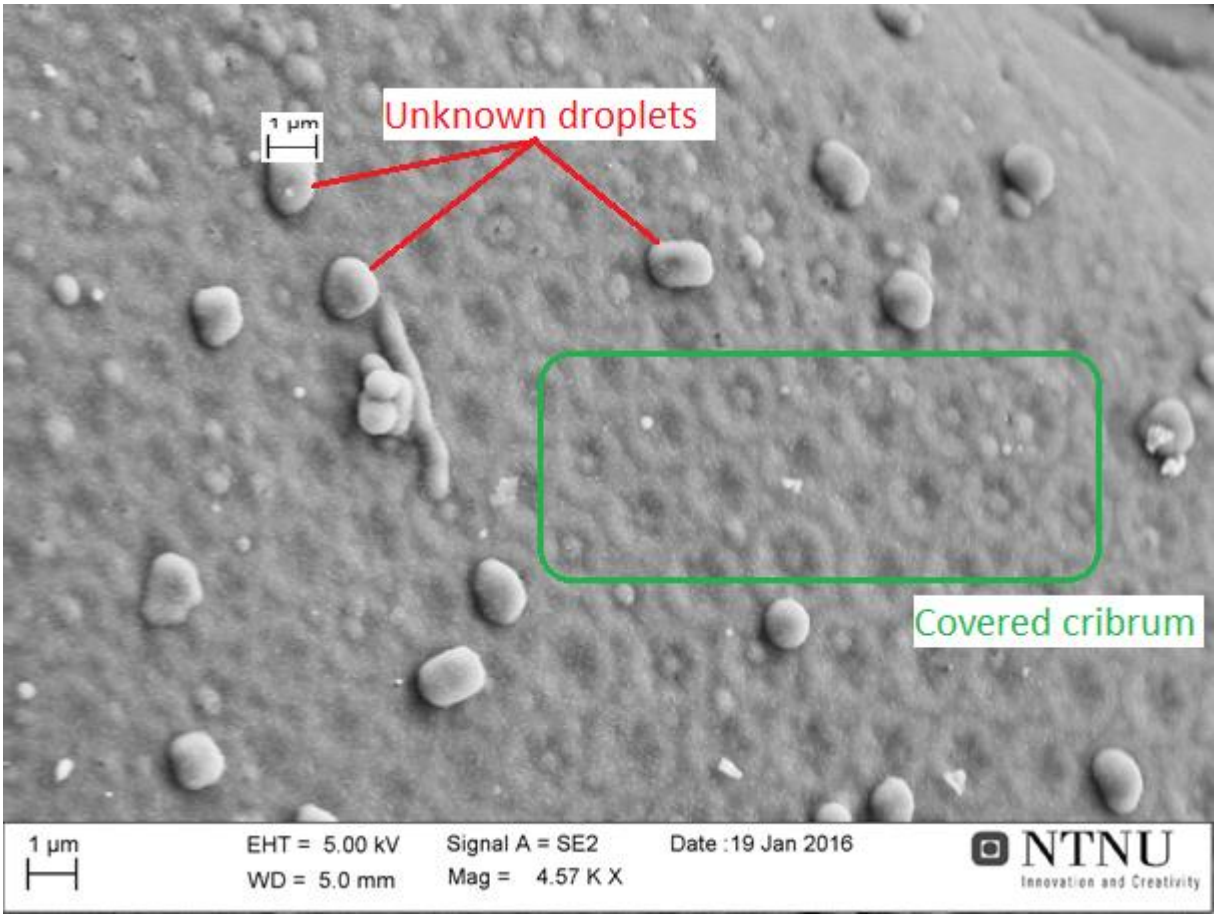

FIGURE 52 4-OIL2-DETAIL1

Looking closer at the same surface we see in 4-Oil2-Frustule we can see that the cribrum is completely covered by the hypothesized film or coarsening. We can also see what looks like small droplets with approximately 1 µm diameter.

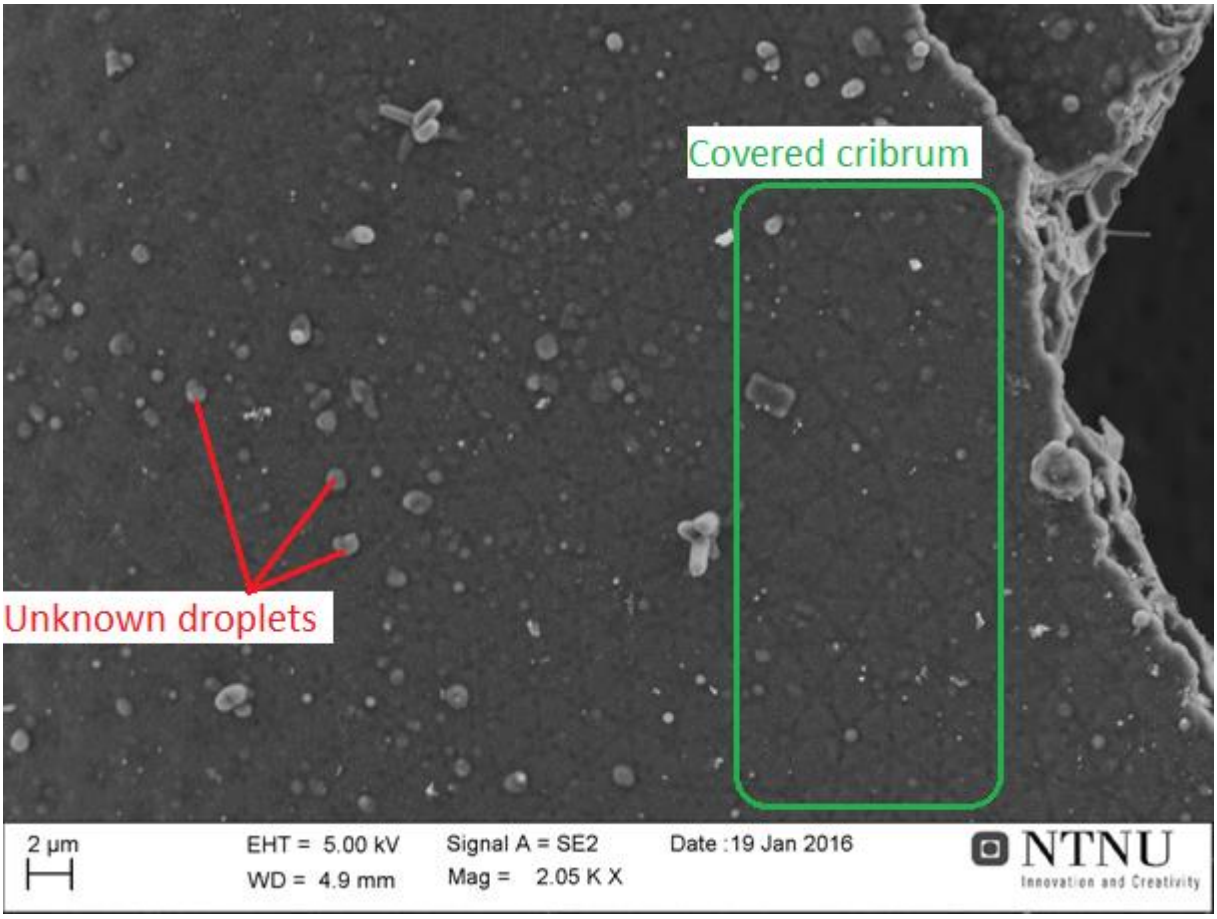

FIGURE 53 4-OIL2-DETAIL2

Looking at a different cribrum surface, we see the same film or coarsening covering its features as we saw in the 4-Oil2-Detail1 image. The same droplets can also be seen speckled across the surface.

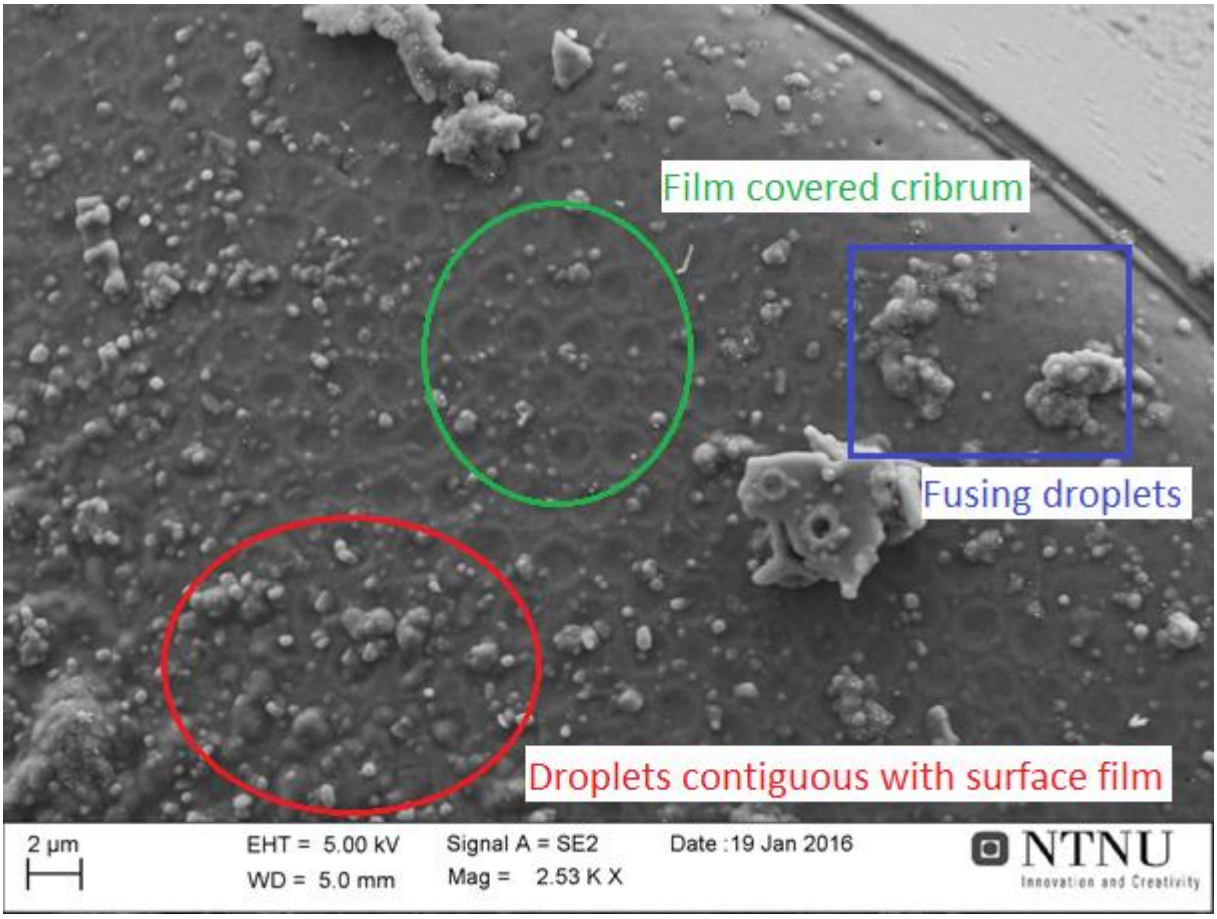

FIGURE 54 4-OIL2-DETAIL3

Looking at more detail images, we can see further examples of this hypothesized film covering the cribrum. Looking at the bottom left part of the image, it looks like more of the droplets have formed and agglomerated together into bigger droplets. It also looks like these bigger droplets are fusing with, or are contiguous with the surface. This would mean that the droplets and the film likely are of the same substance.

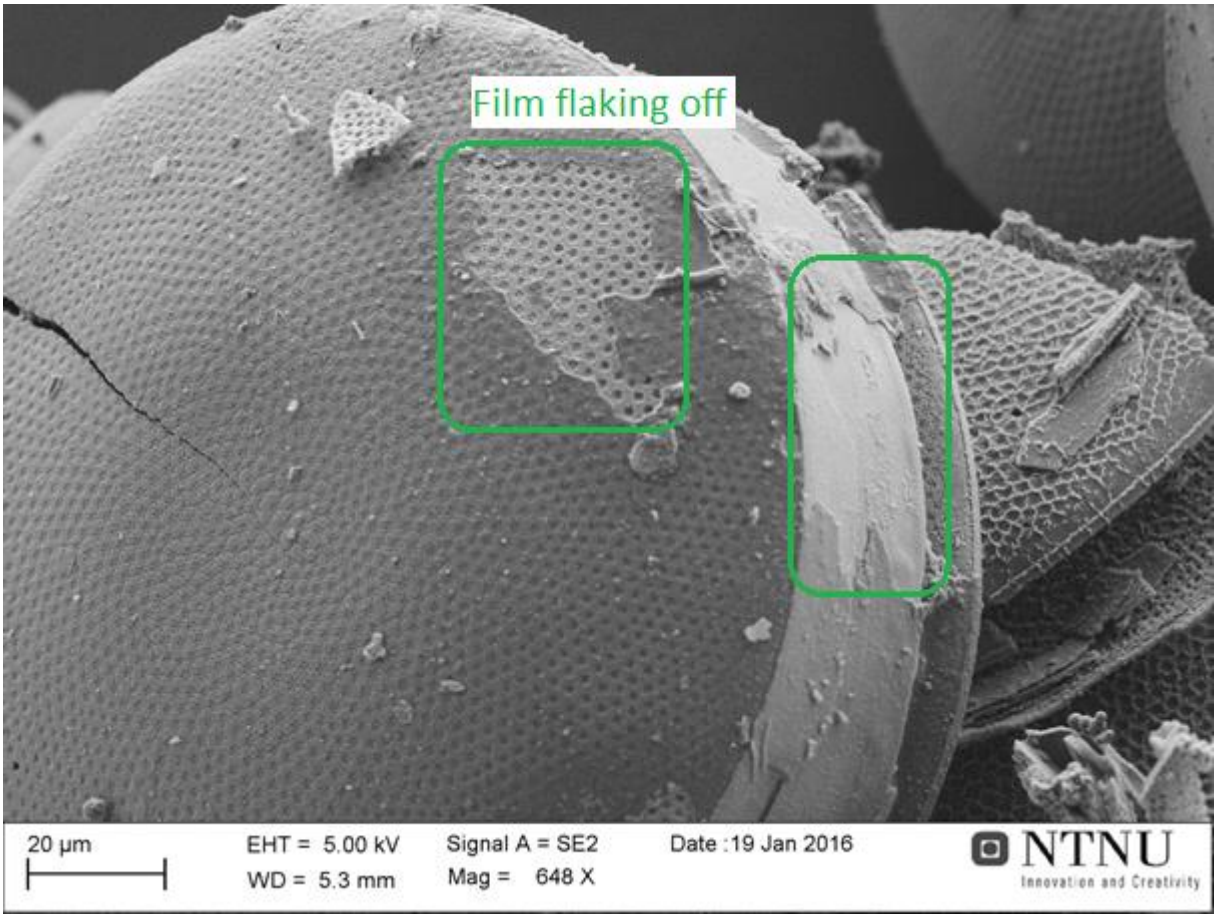

FIGURE 55 4-OIL2-DETAIL4

In this image we can clearly see that what we before hypothesized was either a film or coarsening of the cribrum, most certainly is a covering film. We can say this from the fact that we can see the film flaking off, revealing the underlying details. The same flaking off can be seen along the girdle band of the frustule.

4.2.5 Sample 5-Oil3

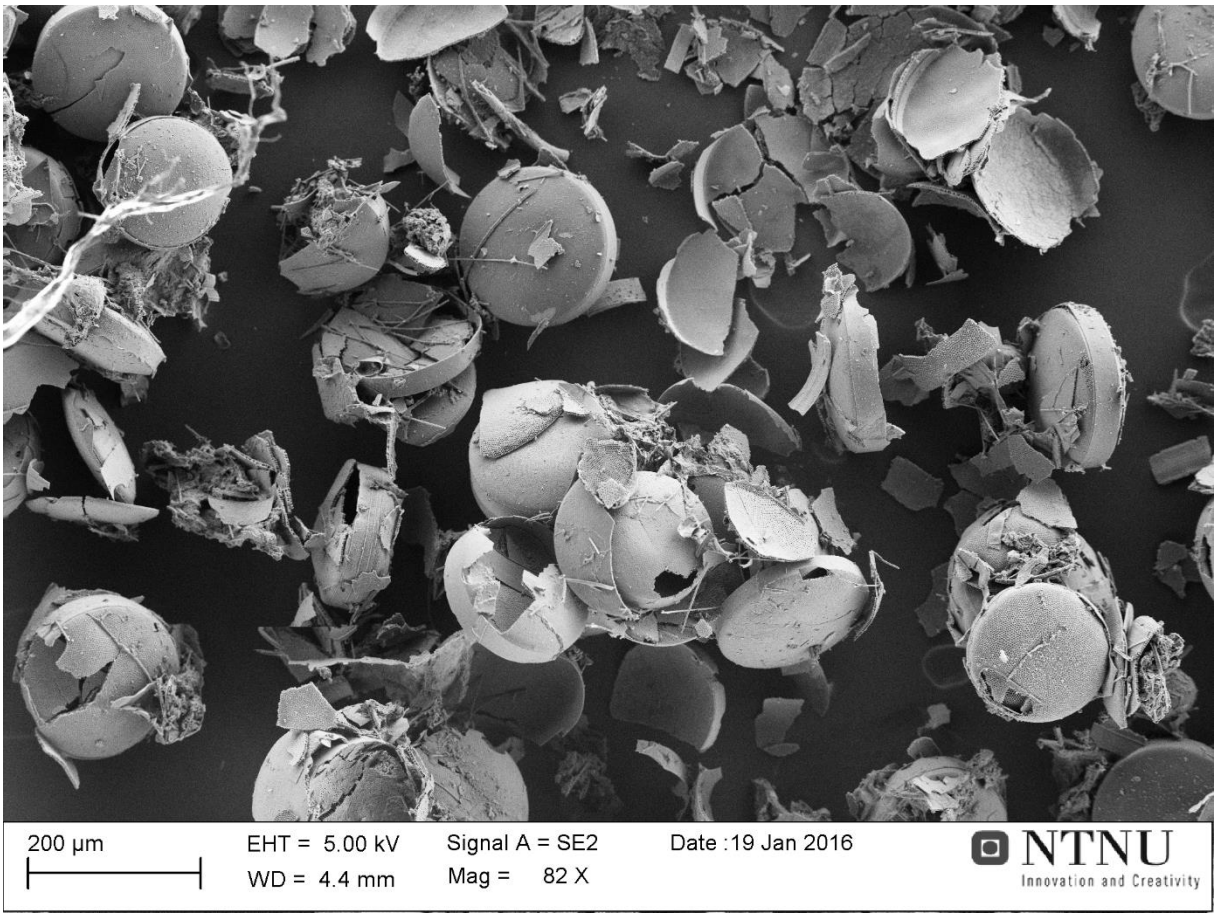

FIGURE 56 5-OIL3-OVERVIEW

The overview image of sample 5-Oil3 we see several frustules, some more or less intact, others, broken down to smaller flakes. This is similar to what we see in all the other samples.

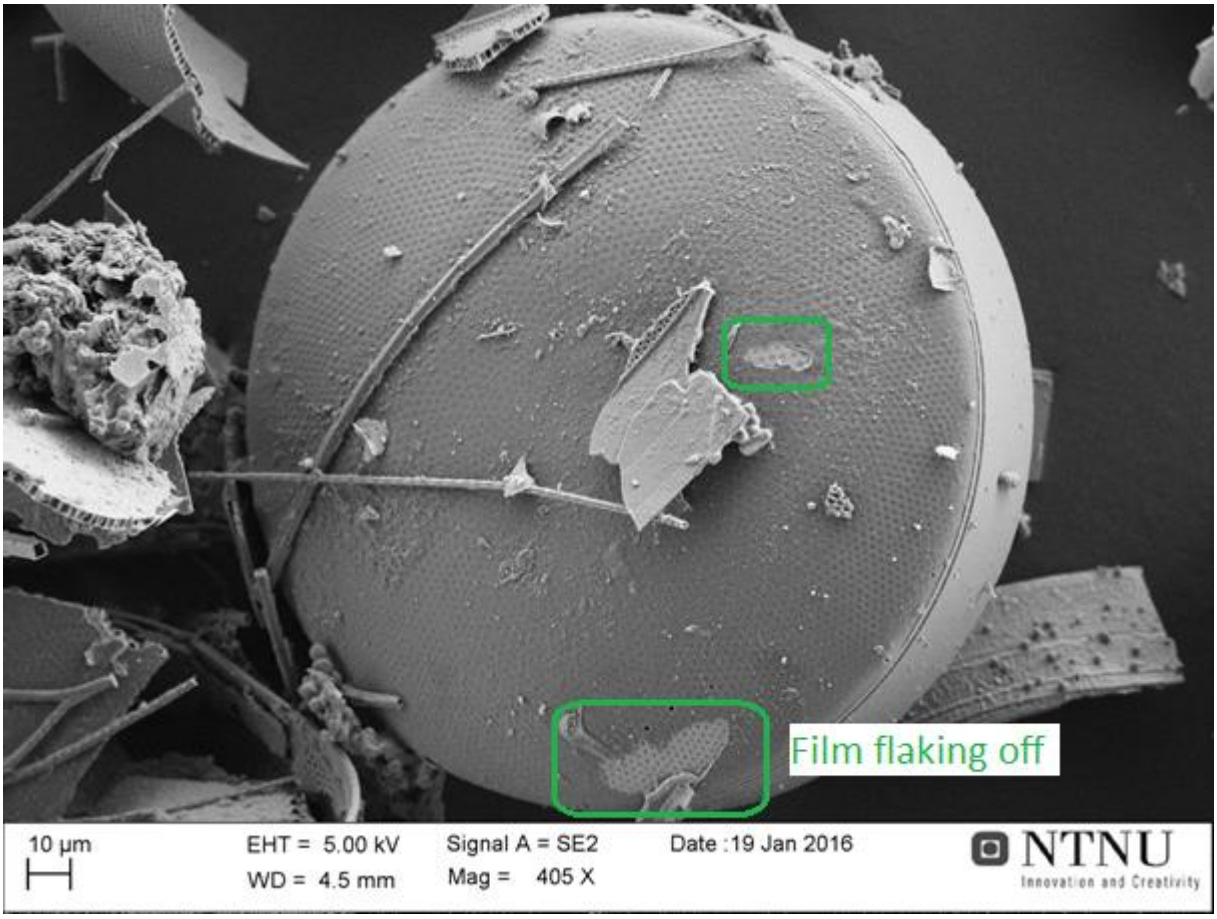

FIGURE 57 5-OIL3-FRUSTULE

Looking at a single frustule, it is clear that the same film observed in sample 4-Oil2 is covering the frustule. We can also see two places where the film is flaking off, revealing the underlying cribrum.

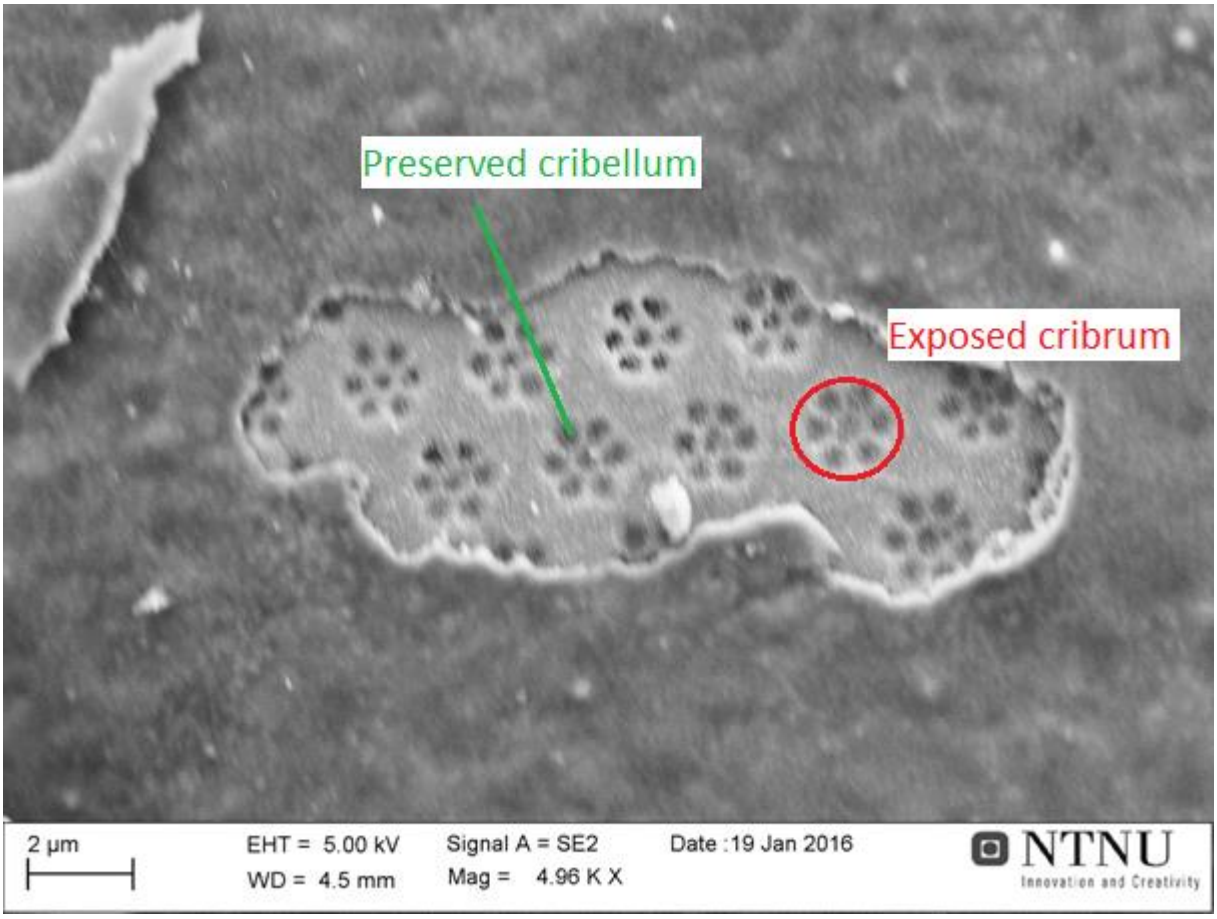

FIGURE 58 5-OIL3-DETAIL1

Zooming in on one of the places where the film has flaked off we can see that the cribrum hiding beneath is very well preserved. Looking at the texture covering the holes of the cribrum, it may even still have the cribellum, the smallest features of the frustule structure. This may again indicate that film protects the details in the frustule structure from chemical stresses and prevents it from being worn down or undergo coarsening.

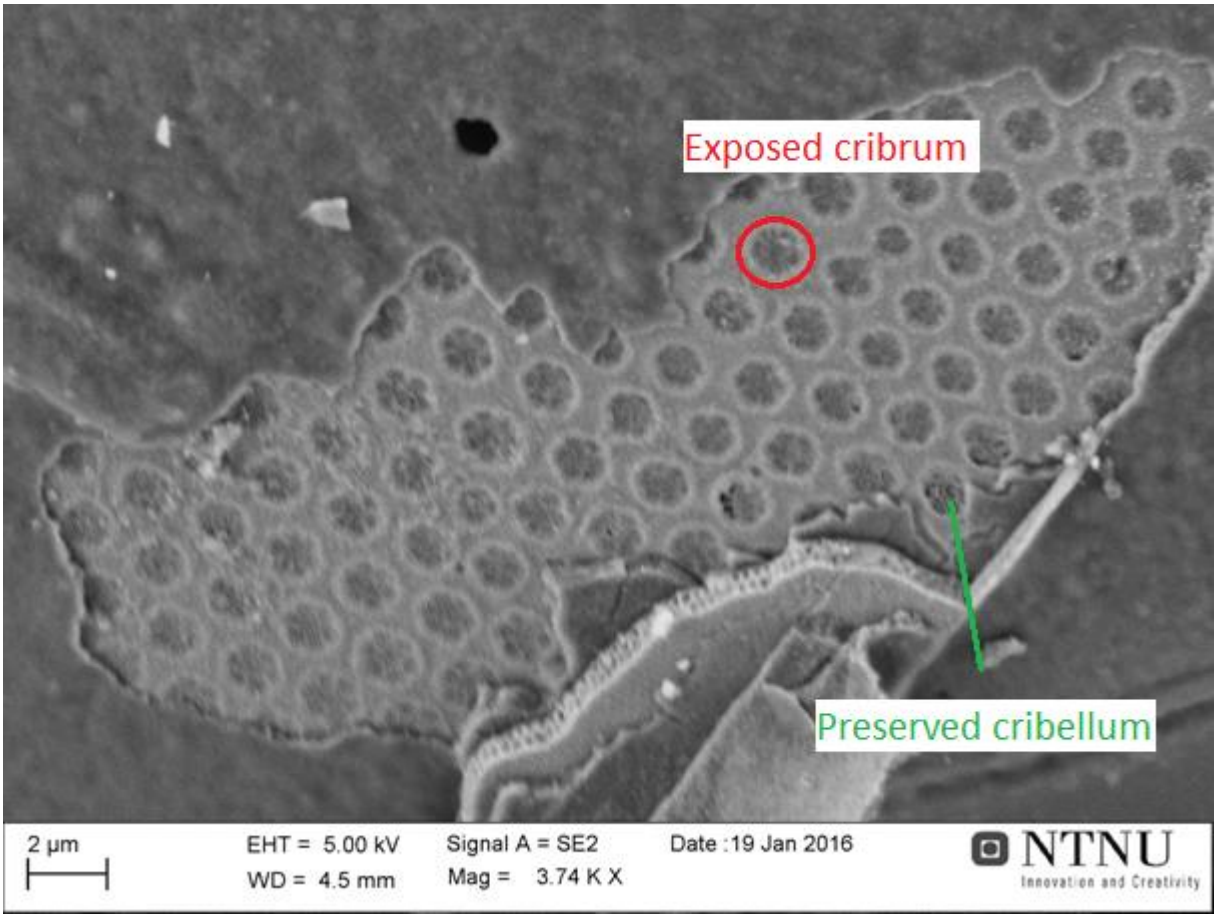

FIGURE 59 5-OIL3-DETAIL2

Looking at the other place we saw the film flaking off, we see the same we saw in image 5-Oil3-Detail1. Where the film has flaked off it reveals a very well preserved part of the frustule. By looking at the texture covering the holes in the cribrum, it looks like the cribellum is preserved.

4.3 TEM Results

To evaluate whether using TEM as a viable analysis tool in future works, a series of different operating modes was used. A short description of how those modes function is described in the theory part of this thesis.

4.3.1 STEM

The pictures gained by scanning tunnelling electron microscopy gives a clear view of the nano-structured architecture of the frustules. Since the image is made by electrons passing through the sample, rather than bouncing off the surface of the sample, we do not get as good of a view of the topography of the sample as you would in, for instance a scanning electron microscope. Particularly when looking edge-on the walls of the areola like in 2BF3k and 1BF10k the image is blurry and unfocused.

Though a much easier SEM might be just as well on the 1k-10k X Magnification ranges, the TEM allows for much higher magnifications. Figure 64, 67, 69 and 71 show magnification at 600k times, much higher than any SEM may view a sample. The lines we are able to see at this scale are actually row and rows of atoms. The microscope is able to detect atomic planes that are oriented edge on towards the electron beam.

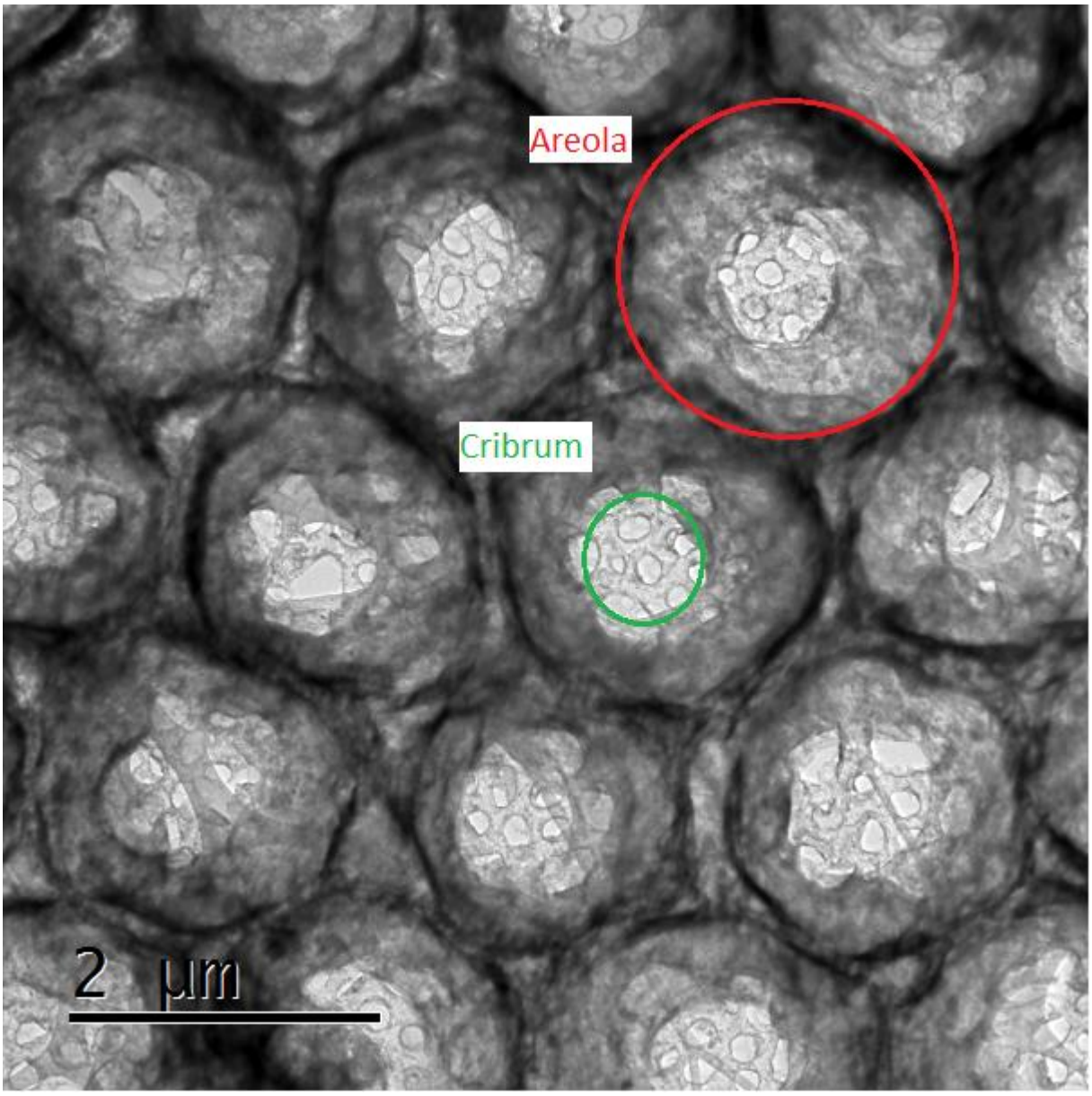

FIGURE 60 2BF3K

In the 2BF3k image, we see through the areola of the frustule and down on the underlying cribrum, meaning we see the frustule from the inside out.

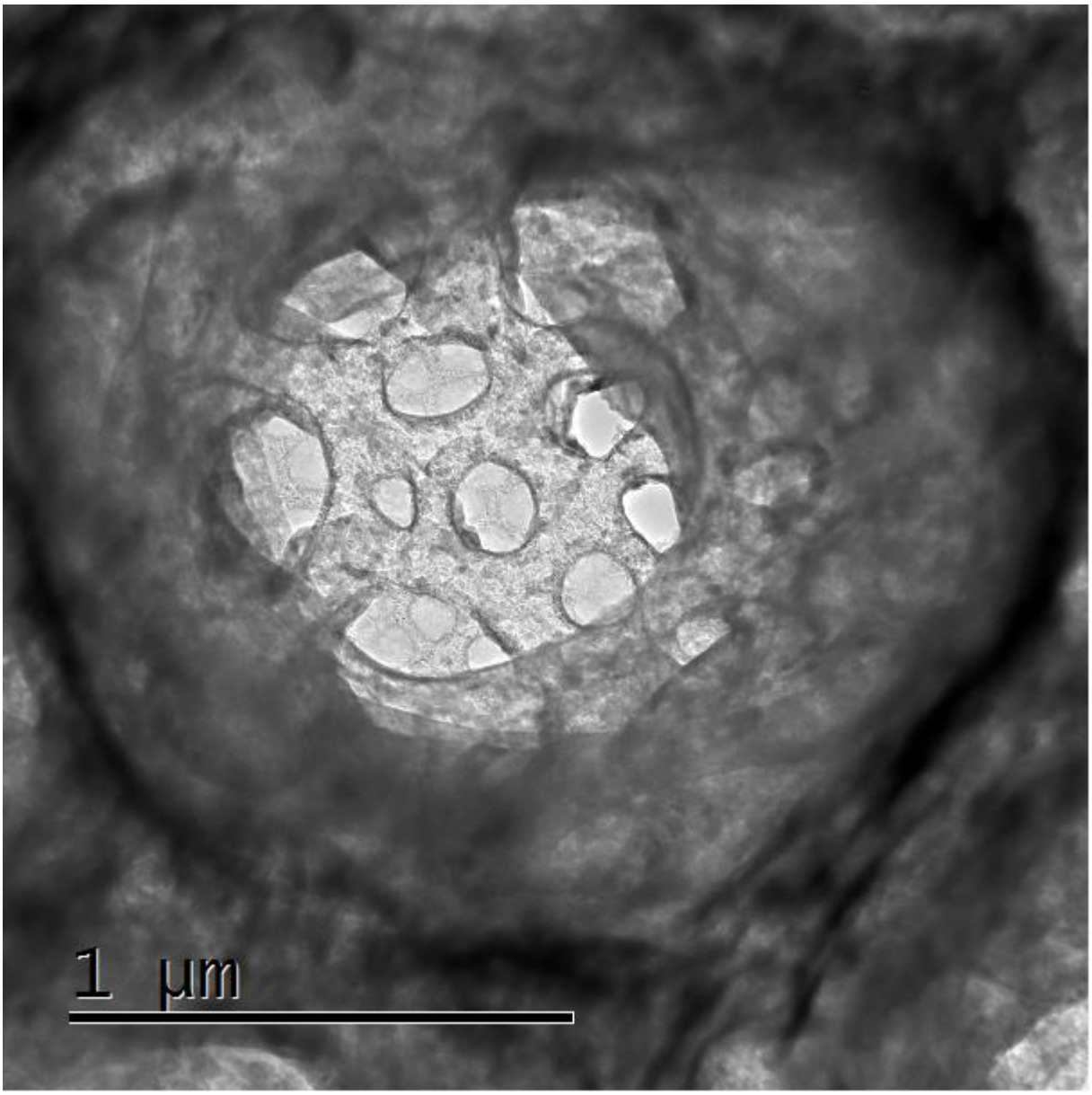

FIGURE 61 1 – BF 10K

Zooming in towards one of the areolas in the previous images, we are again able to see the cribrum much the same as we would be able in a SEM.

4.3.2 High Resolution Images

Figures 64, 67, 69, and 71 show high resolution images if parts of the frustule. These are images with magnification far exceeding what a scanning electron microscope is capable of. The magnification in these images are at 600,000 times.

Figures 62 and 63 shows the area of the sample used to collect the high resolution image. To be able to get a high resolution image we must use a part of the sample that is as thin as possible to not get too much obstruction of the electron beam. For this end, the following high resolution images are taken of the edge of a fragment of the sample, at the bottom of an areola.

The large area with lines stretching across the left part of Figure 62 is not a feature of the imaged sample, but rather the film on which the fragments of the sample is contained.

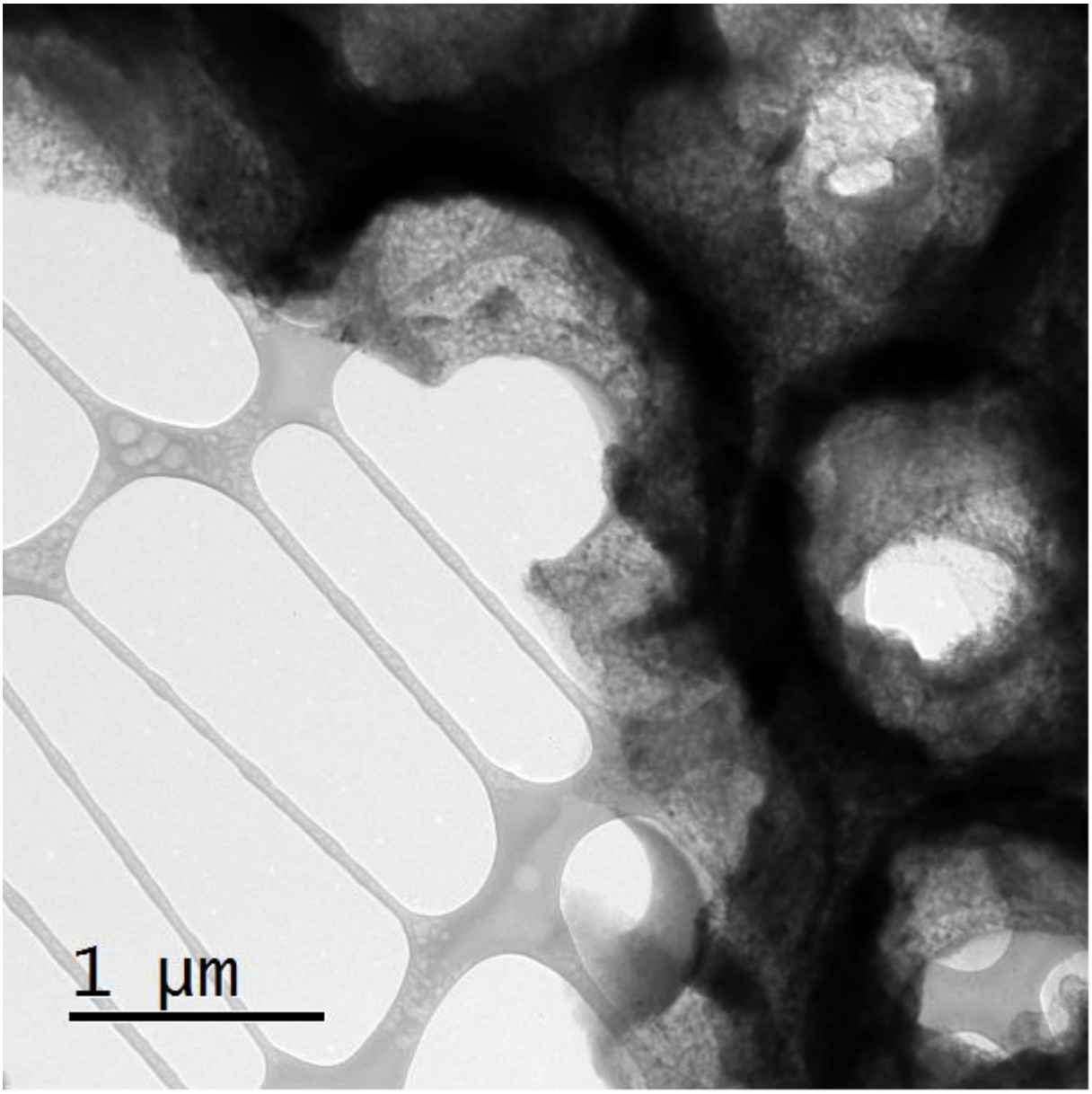

FIGURE 62 3BF5K OVERVIEW IMAGE SHOWING THE EDGE OF ONE OF THE FRUSTULE FRAGMENTS USED FOR TAKING THE HIGH RESOLUTION IMAGES.

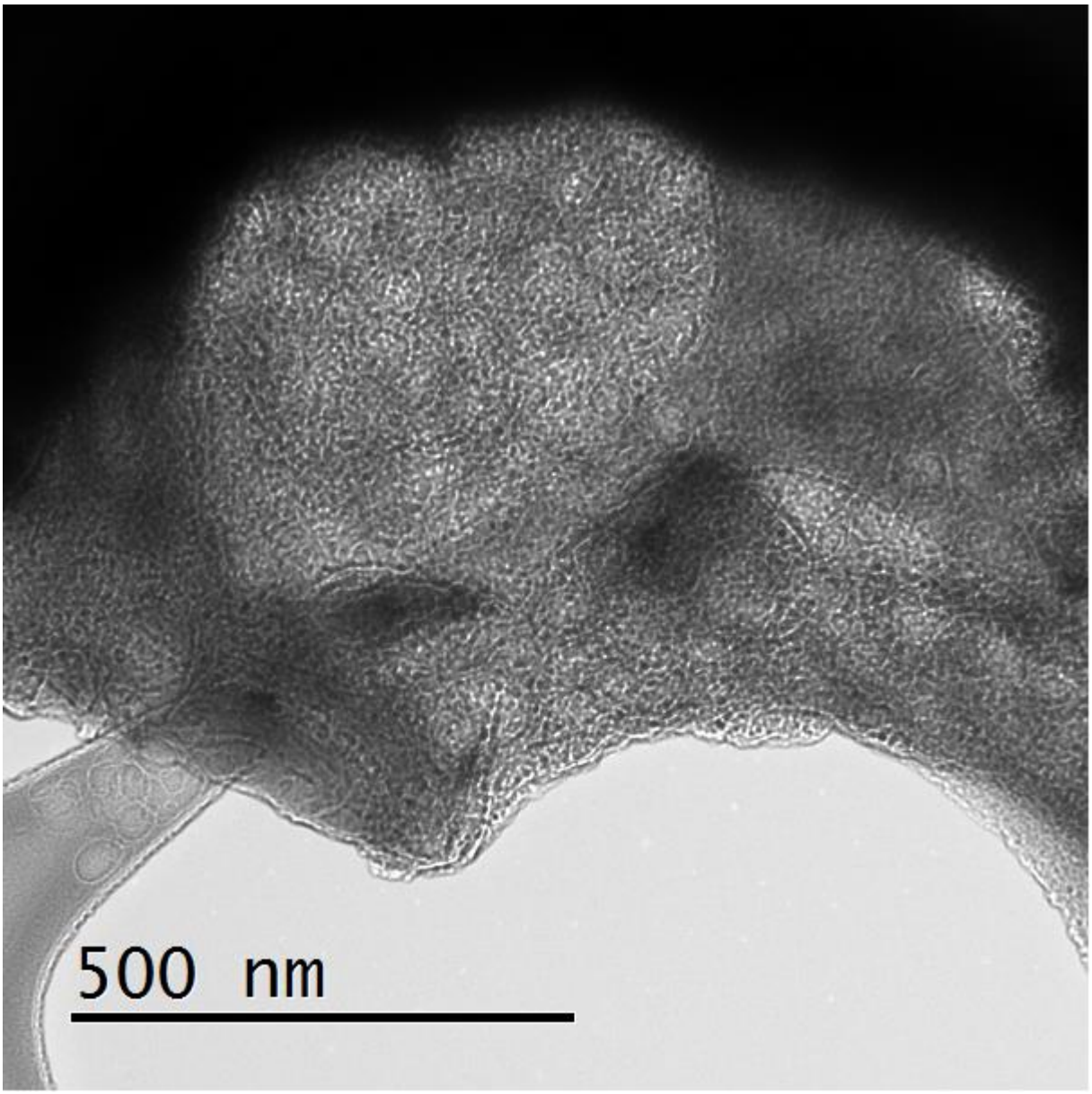

FIGURE 63 CLOSER IN OVERVIEW IMAGE FOR THE EDGE OF THE SAMPLE FRAGMENT USED TO COLLECT HRSTEM.

Looking closer at the area imaged, we start to see more details. It might look like we are able to see a lot of small texture details of the sample in figure 63, but that is in fact an effect of charging in the sample that effects the electron beam.

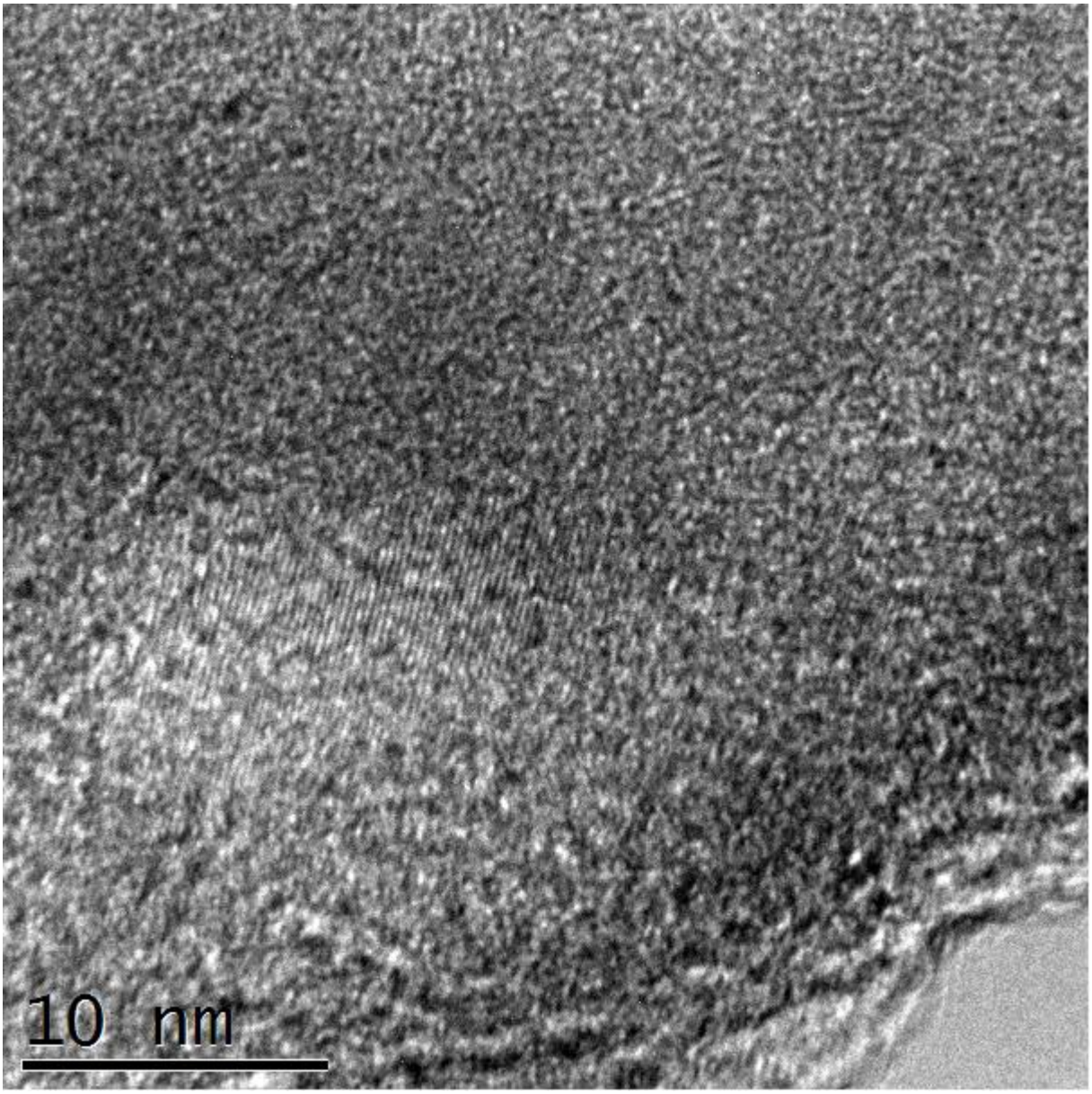

FIGURE 64 3HR600K

Looking closely at these images we can see a pattern of lines streaking across the sample. These lines are the atomic planes of the crystal structure of the sample seen edge on. They are only seen at the parts of the sample where the planes of the crystal lattice just happen to orient themselves towards the electron beam.

In figure 65 we have taken the image in figure 64 and converted it through a Fourier transformation which creates an image similar to the diffraction images (A). From that we are able to highlight the parts of the image that we find interesting (B), and then transform the image back again to get what we see in figure 66.

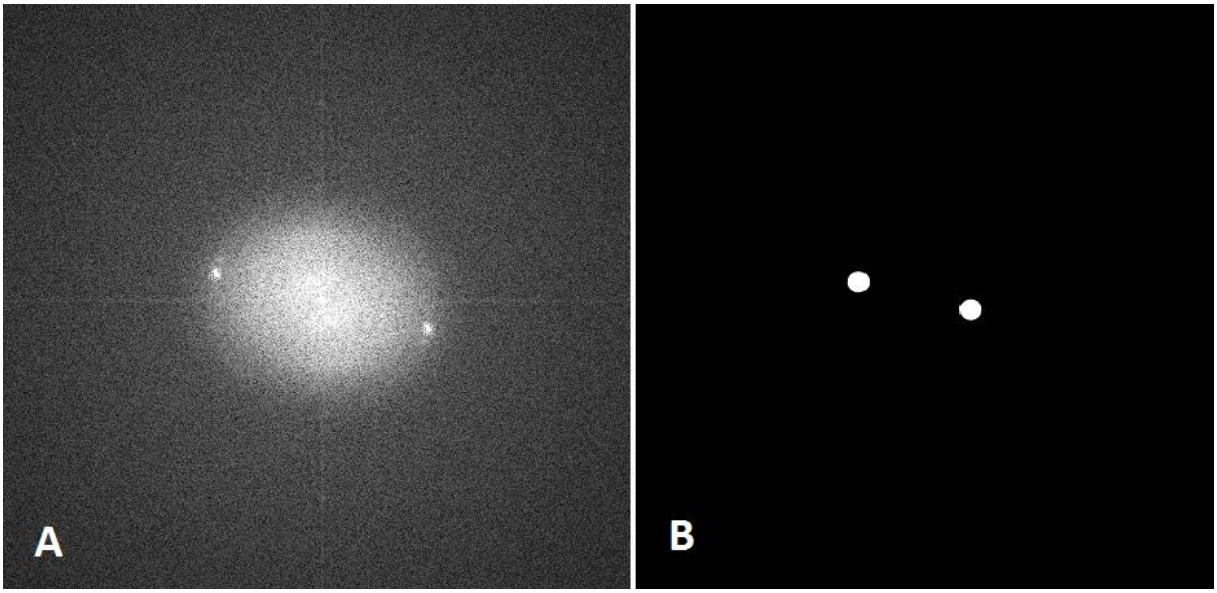

FIGURE 65 THESE IMAGES SHOW THE INTERMEDIATE STEPS FOR CREATING THE INVERSE FOURIER IMAGE OF FIGURE 66 FROM FIGURE 64. WE SEE THE FFT (FOURIER TRANSFORM) OF THE IMAGE SEEN IN FIGURE 64(A), CREATING AN IMAGE MUCH SIMILAR TO A DIFFRACTION IMAGE. TO THE RIGHT (B) WE SEE WHAT IS LEFT AFTER WE HIGHLIGHT THE BRIGHT DOTS THAT CORRESPONDS TO THE RELEVANT PARTS OF THE IMAGE, AND REMOVING ALL THE OTHER. THIS IS THE IMAGE THAT IS INVERSE-FOURIER TRANSFORMED INTO WHAT WE SEE IN FIGURE 66.

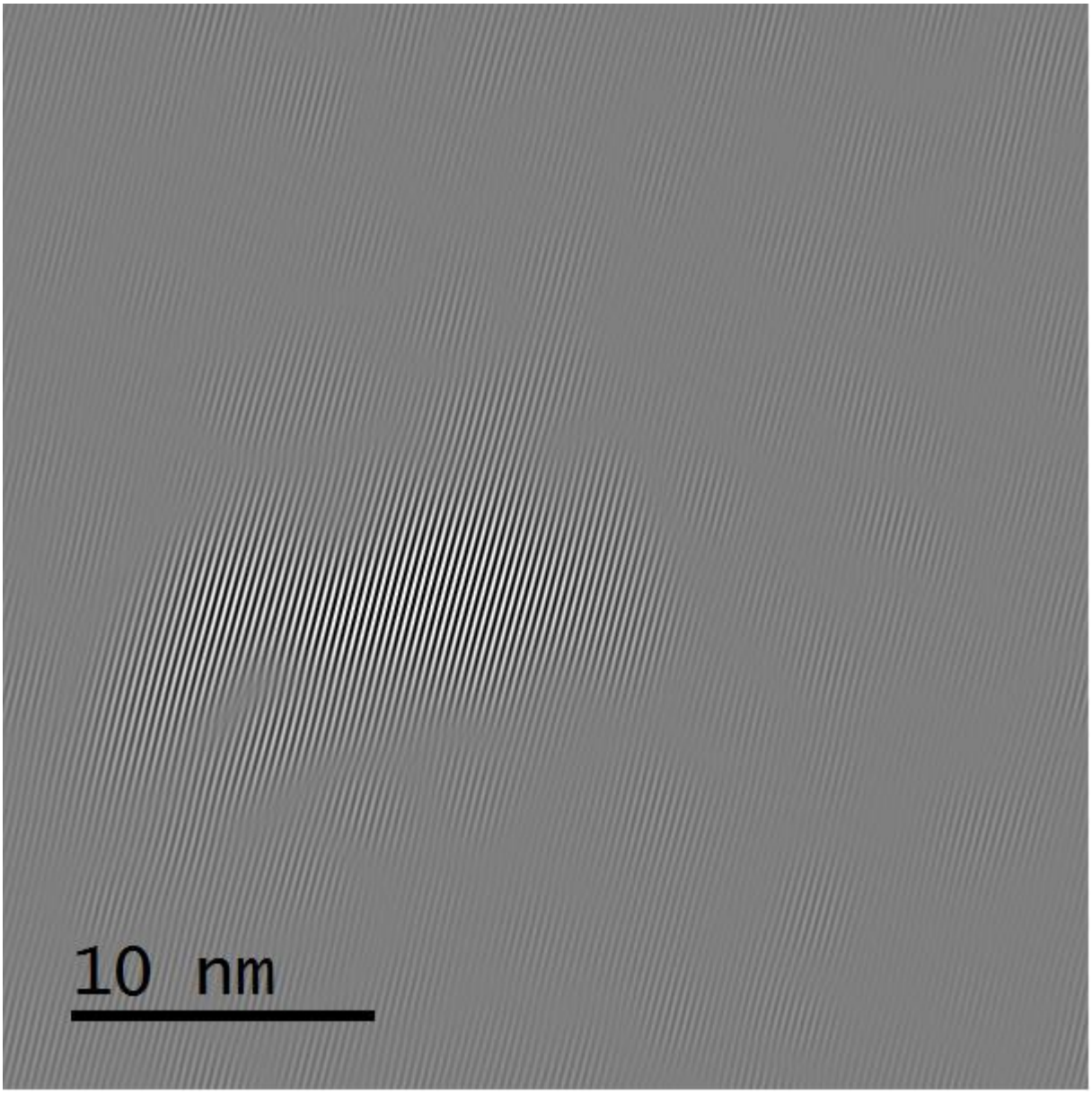

FIGURE 66 THE INVERSE FOURIER TRANSFORMED IMAGE FROM FIGURE 64. IN THE INVERSE TRANSFORMED IMAGE IT IS MUCH EASIER TO SEE AND MEASURE THE GRAIN.

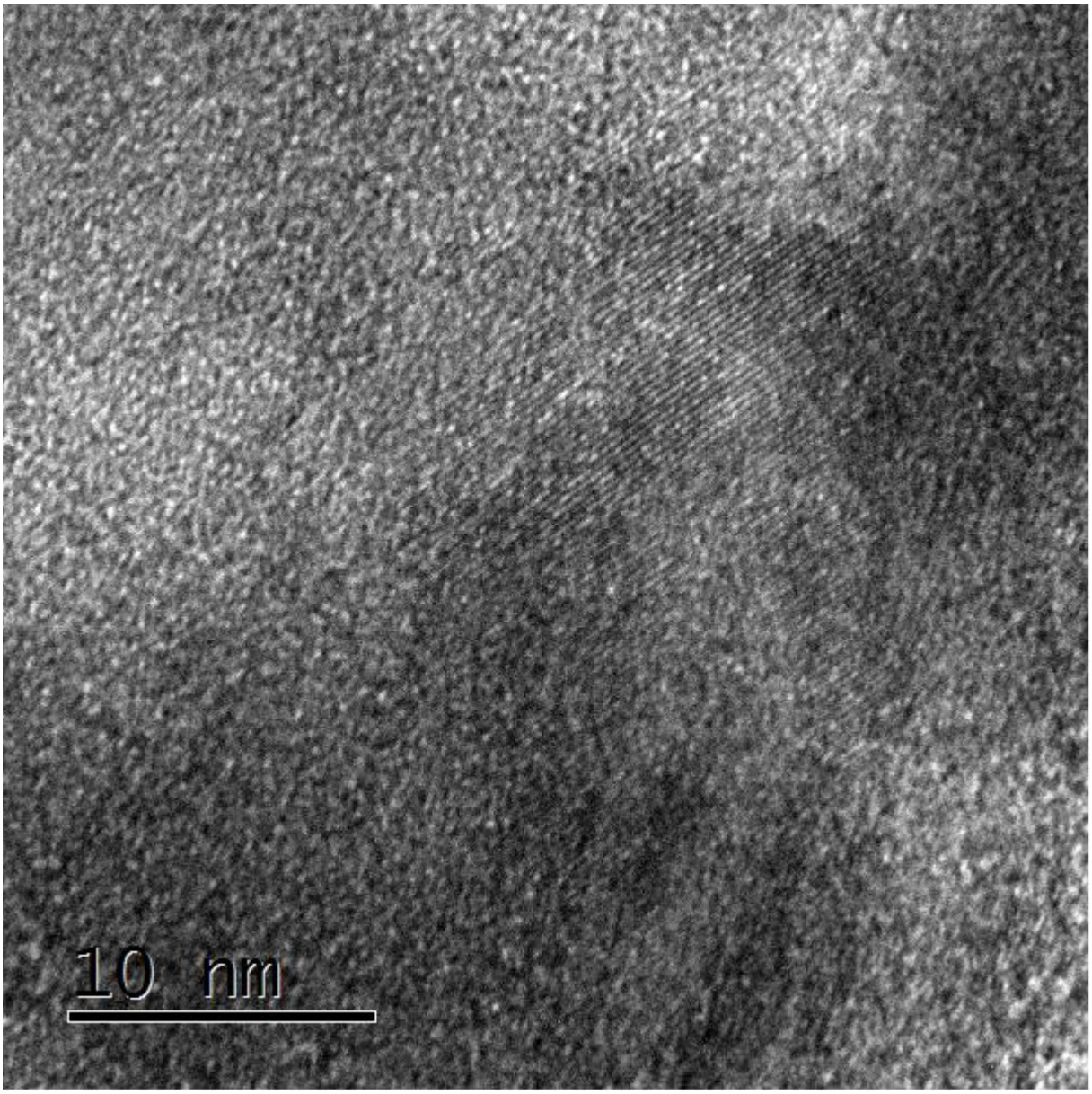

FIGURE 67 3-HR600K2

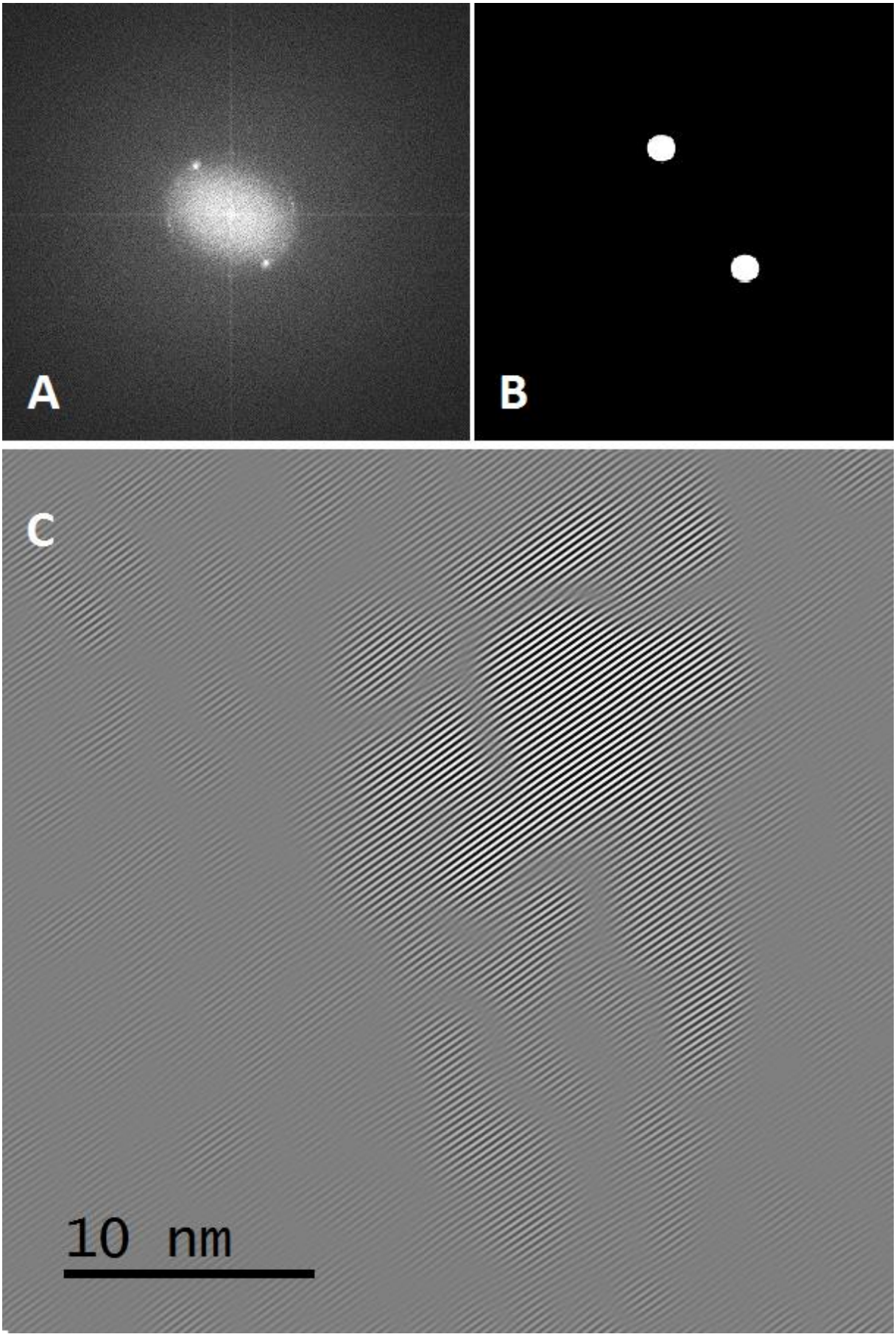

FIGURE 68 INTERMEDIATE (A, B) AND INVERSE-TRANSFORMED IMAGE (C) OF FIGURE 67.

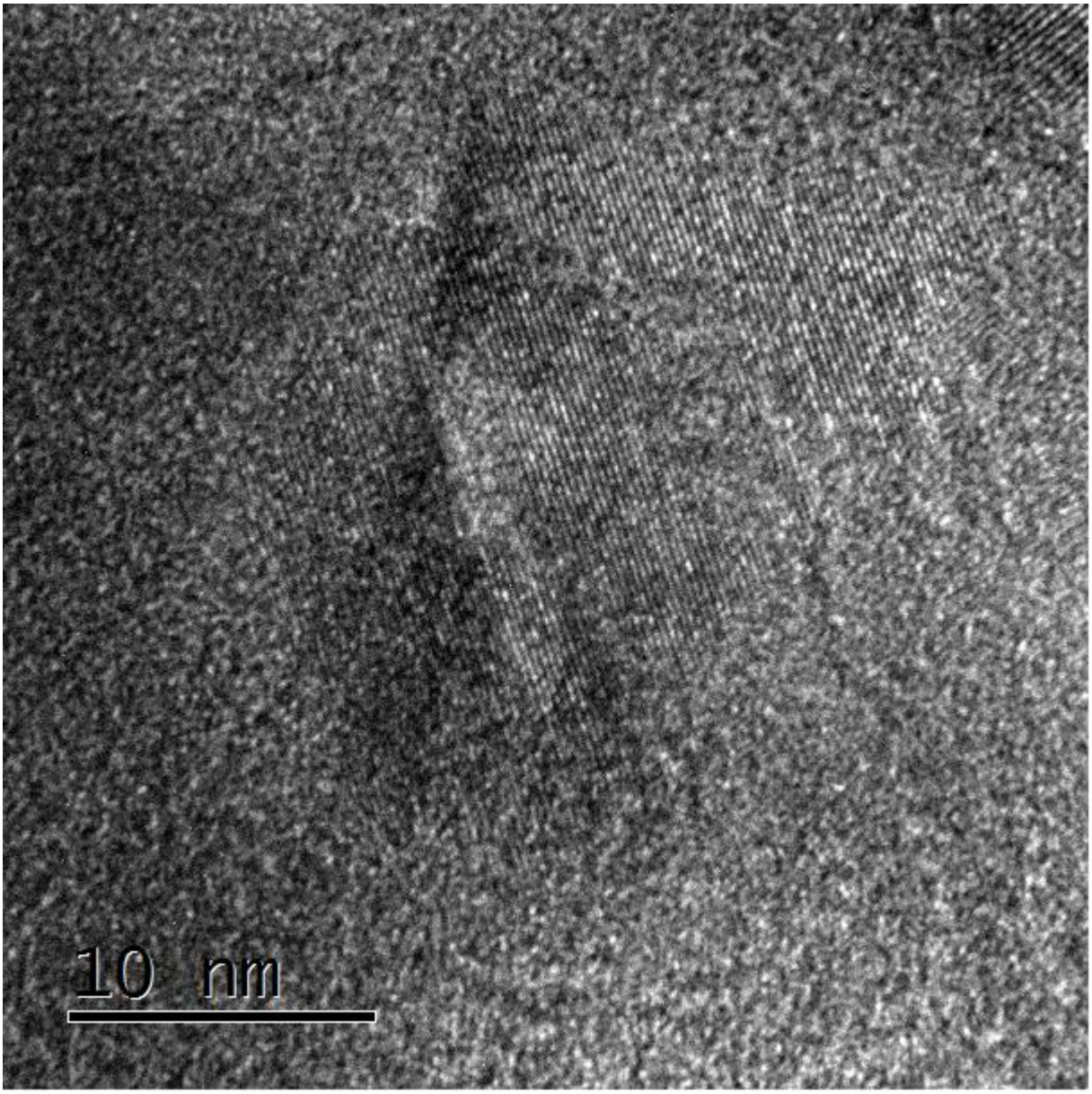

FIGURE 69 3-HR600K3

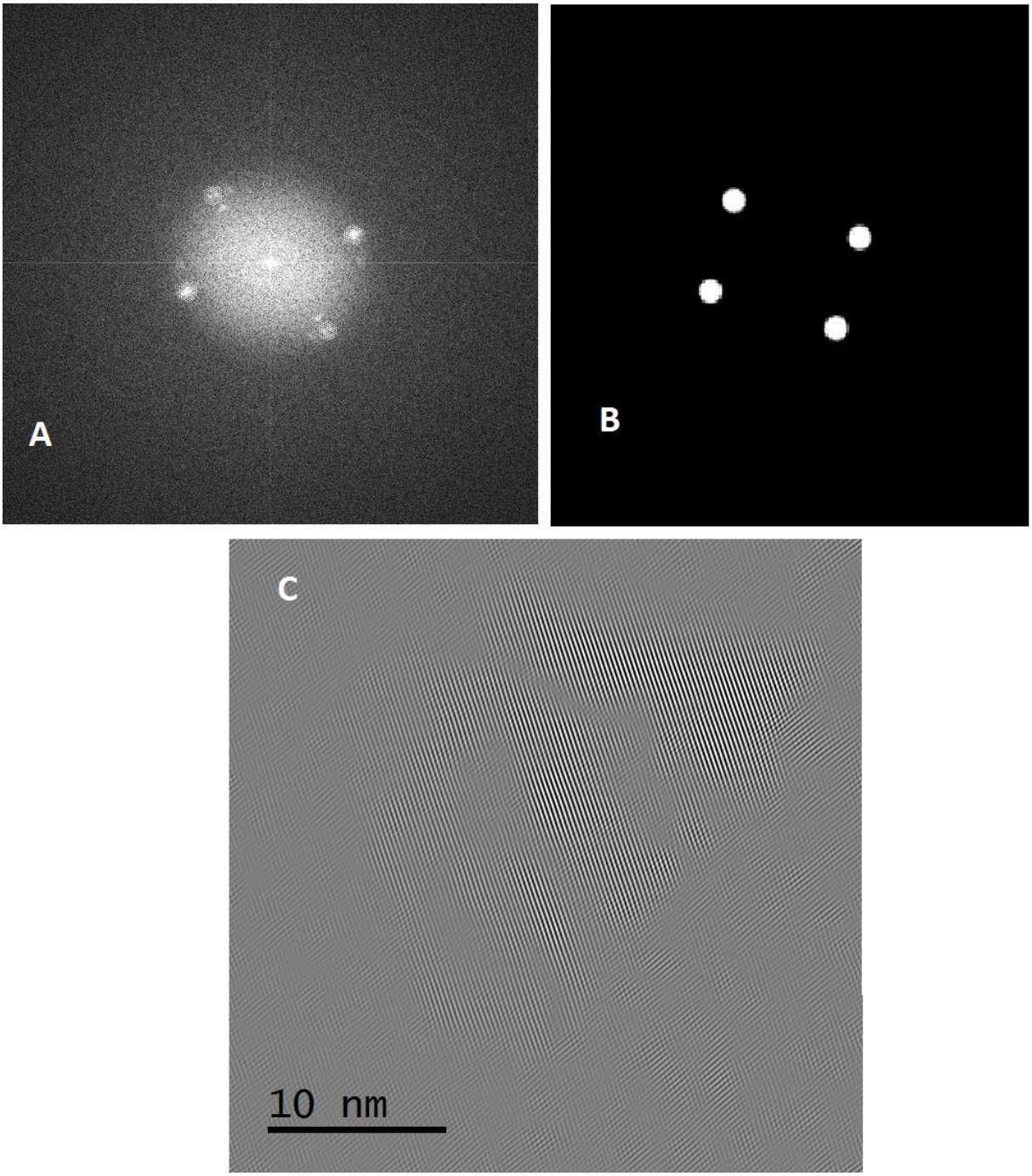

FIGURE 70 INTERMEDIATE (A, B) AND INVERSE-TRANSFORMED IMAGE (C) OF FIGURE 69.

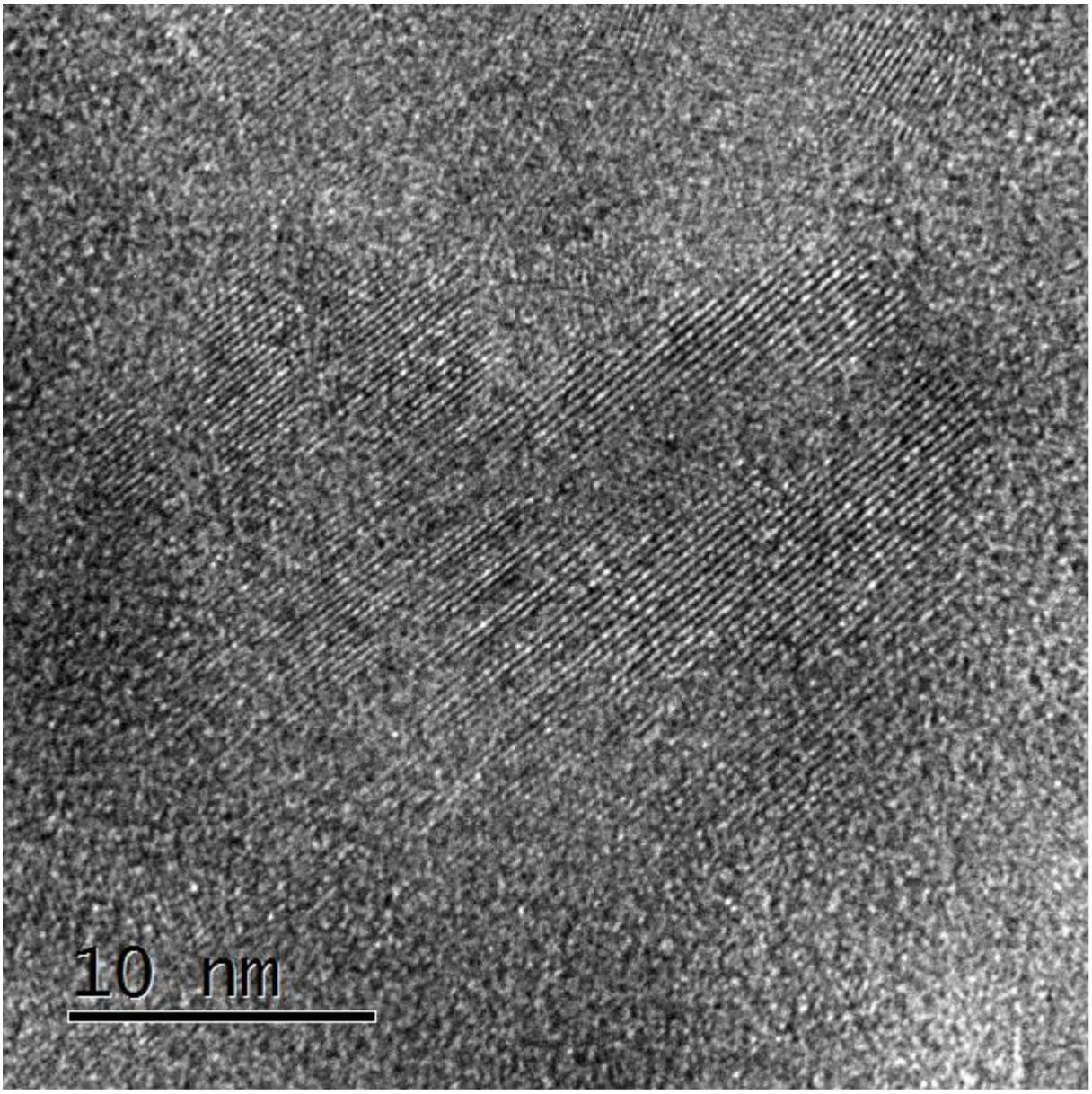

FIGURE 71 3HR600K6

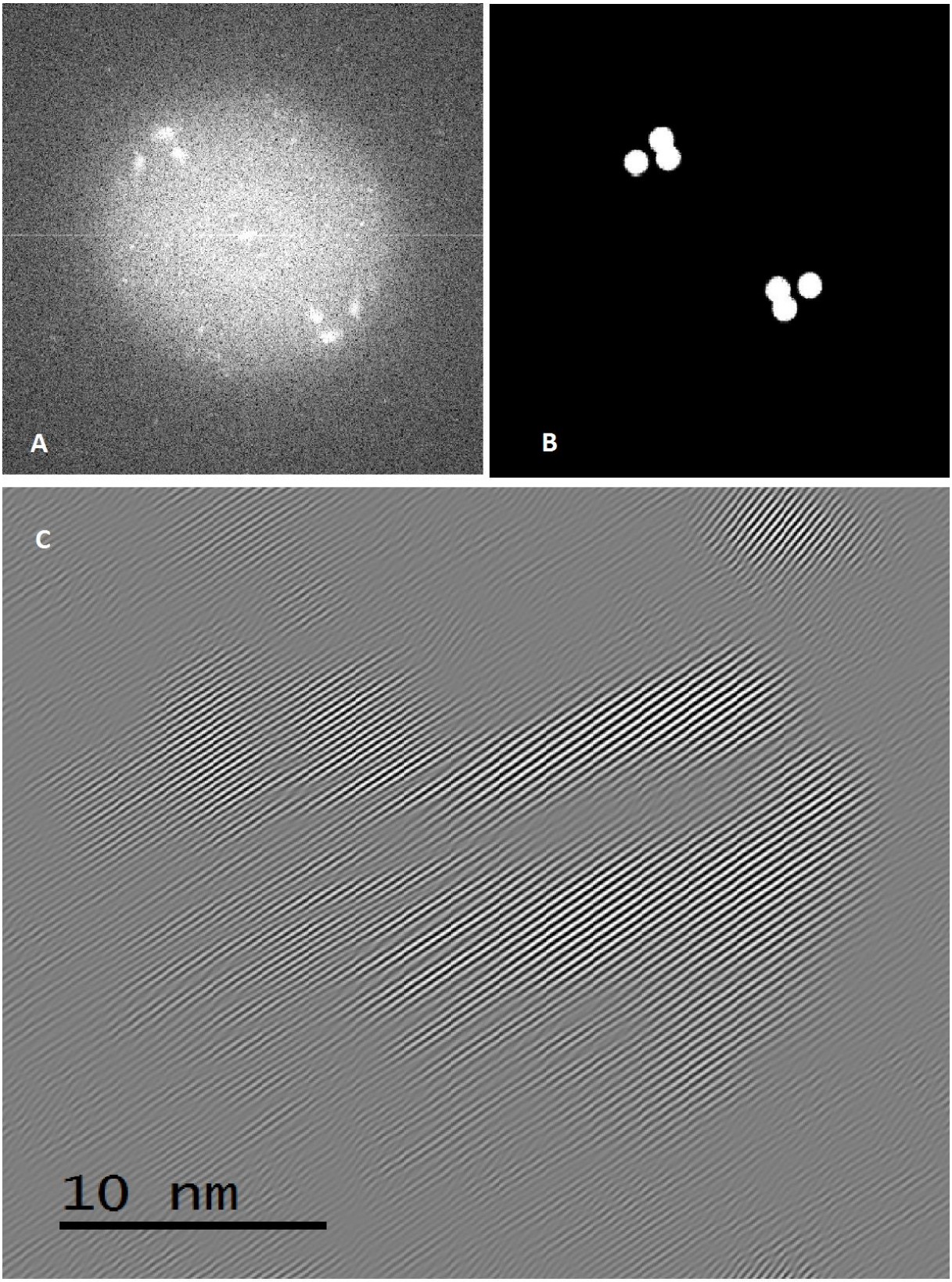

FIGURE 72 INTERMEDIATE (A, B) AND INVERSE-TRANSFORMED IMAGE (C) OF FIGURE 71.

If we assume that the grains are oriented randomly, we then get an accurate picture of the general grain size of the sample.

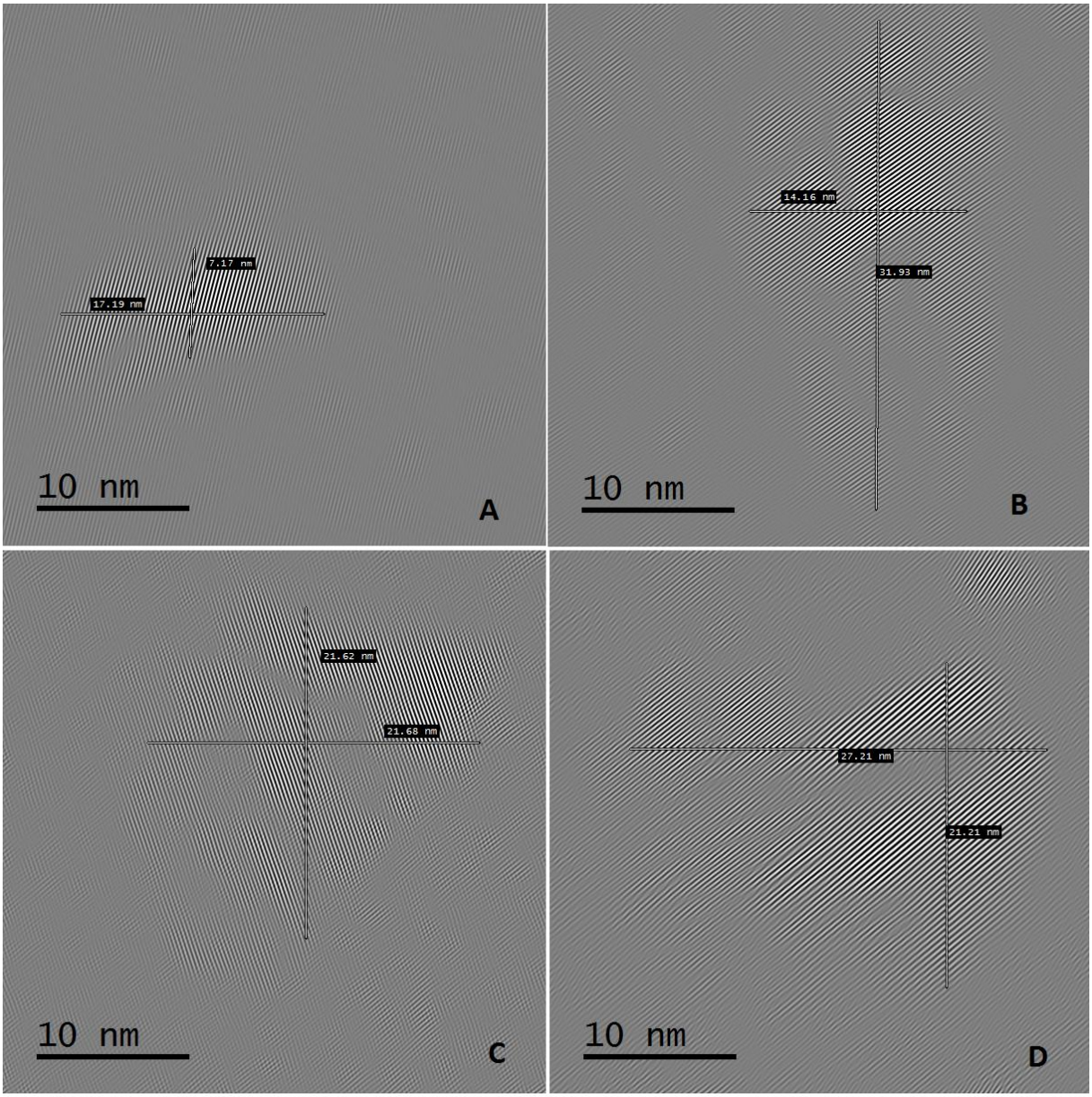

FIGURE 73 MEASURED SIZES OF THE GRAINS FOUND AFTER THE FOURIER TRANSFORMATION OF THE HIGH-RESOLUTION STEM IMAGES. 3-HR600K (A), 3-HR600K2 (B), 3-HR600K3 (C), AND 3-HR600K6 (D).

TABLE 6 GRAIN SIZE

	Crossection [nm]
A	17,19
A	7,17
B	14,16
B	31,93
C	21,68
C	21,62
D	27,21
D	21,21
Average	20,27

Using the distances measured in figure 73 we are able to determine an average grain diameter of 20,27 nm.

4.3.3 Diffraction

As explained in the theory, we are able to create diffraction images of the sample. The large, bright spot in the middle of the of the image, covered to not overpower the image and make us unable to see anything different, is the main beam of electrons passing straight through the sample. The diffracted parts of the beam are seen as secondary spots around the centre spot. As the beam passes through the material, a pattern will be formed corresponding to the material's crystal structure orientation. Using these patterns, we can identify which materials the beam is traveling through.

We can see a measuring rod in the diffraction images, but since we are really seeing reciprocal space where distances are inversed, and diffraction spots that appear close in reality has a larger distance between its diffracting planes and spots with a large distance from each other in the image actually has its planes closer to each other, this measuring rod cannot be used directly.

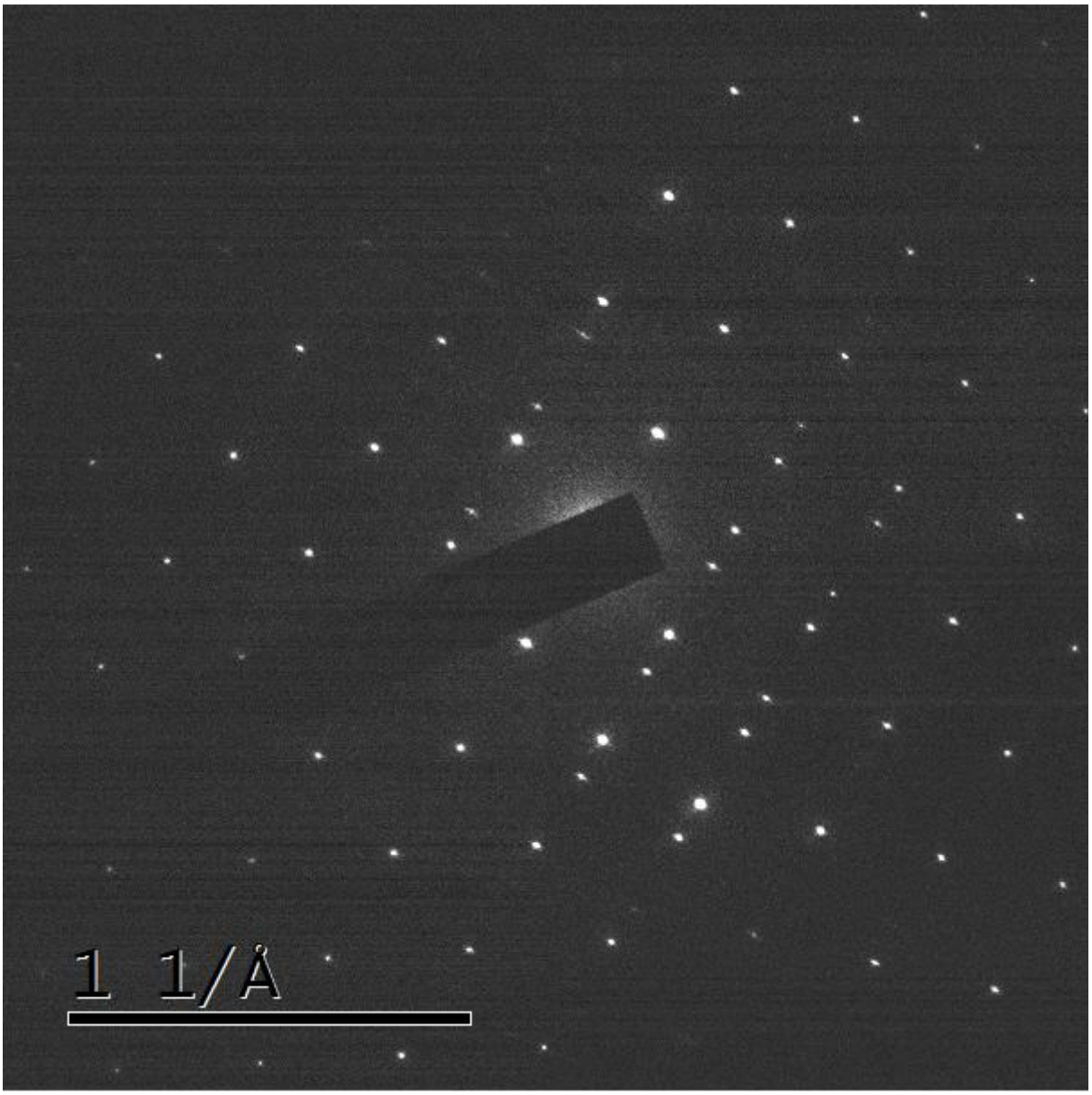

FIGURE 74 CALIBRATION IMAGE.

To correct this, we use figure 74 as a calibration image. The diffraction pattern in figure 74 is made using the same magnification as was used in the experiment. From this we are able to create a new scale bar that we can use to interpret the diffraction images.

By using the calibration image, we find that the scale bar of 1 1/Å is exactly 777 pixels. The “500” for the scale bar in the acquired images stands for 500 pixels, so that it its length. Then by dividing the measured number of pixels with 777 we will get a number in 1/Å

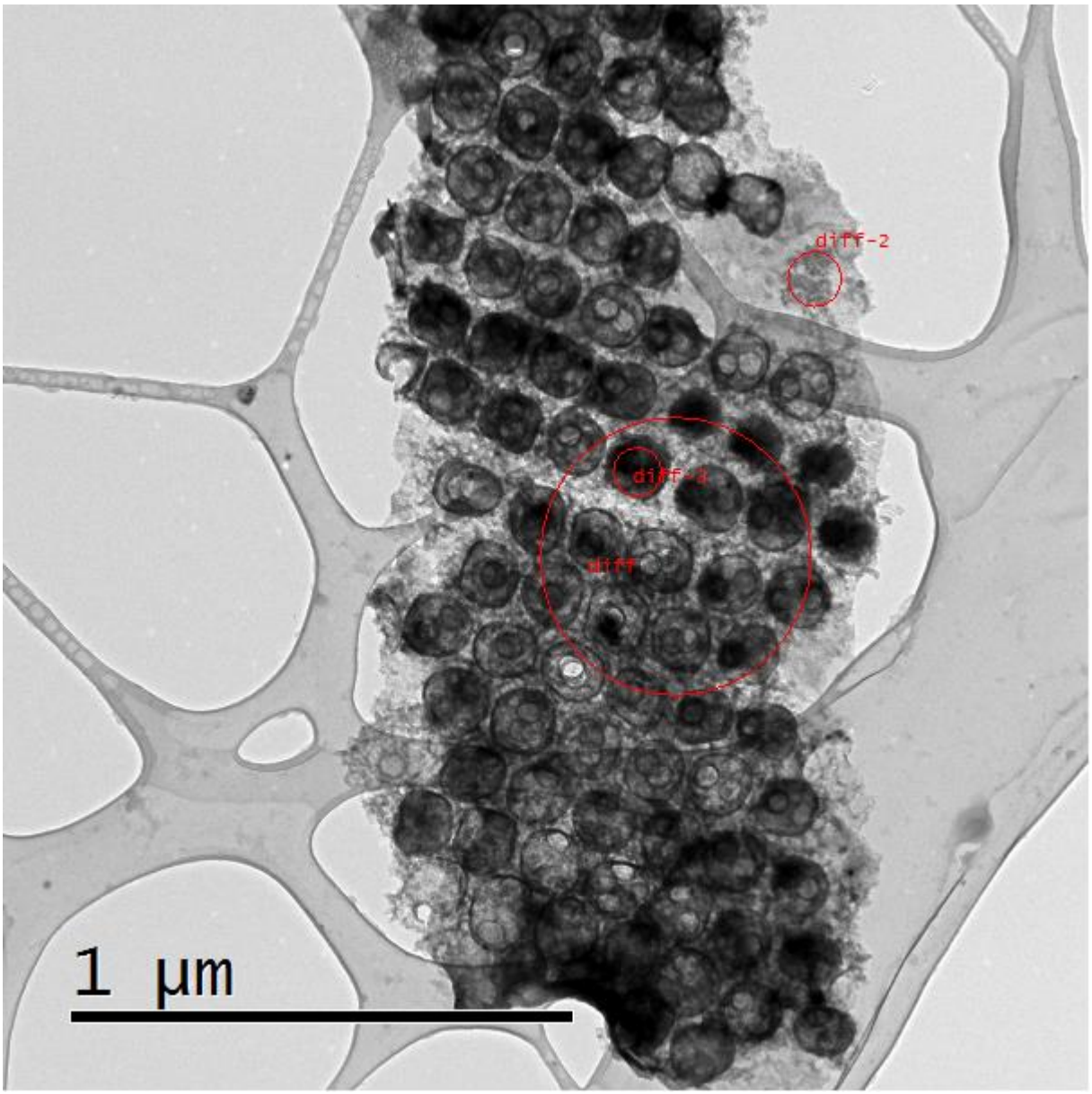

FIGURE 75 AREA USED FOR DIFFRACTION.

Figure 75 shows which areas was used for gathering diffraction images. The area marked “diff”, which contain several different features, was used to gather the diffraction image seen in figure 76. The smaller area marked “diff-2”, and contain only a thin edge area of the sample, was used to gather the diffraction image seen in figure 77. The area marked “diff-3”, which contains one of the darker areola features, was used to gather the diffraction image seen in figure 78.

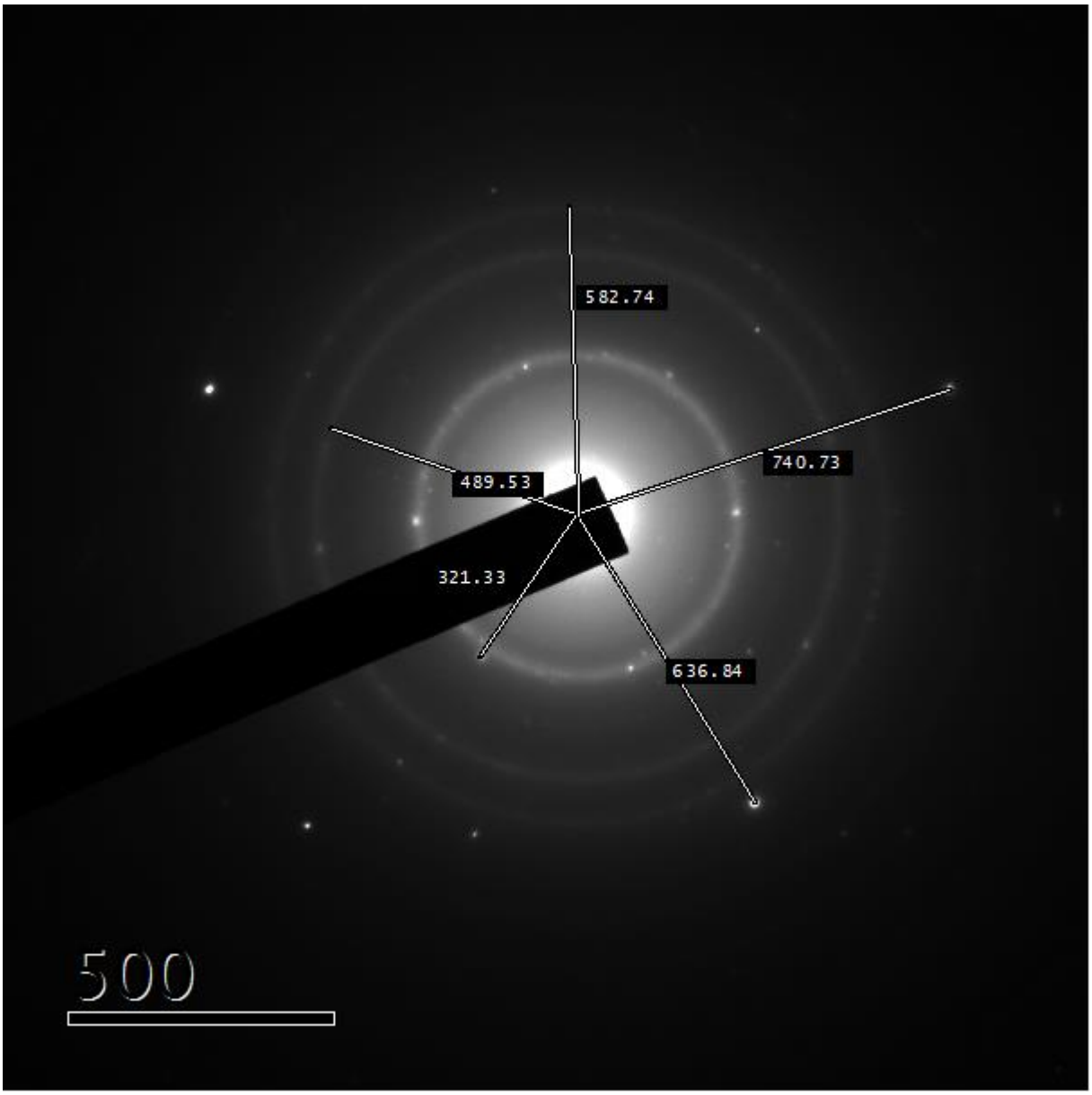

FIGURE 76 DIFF WITH SELECT DISTANCES MEASURED IN PIXELS.

TABLE 7 MEASURED DISTANCES IN DIFF

Measurment No.	Pixels	1/Å
1-1	321,33	0,413
1-2	489,53	0,630
1-3	582,74	0,749
1-4	636,84	0,819
1-5	740,73	0,953

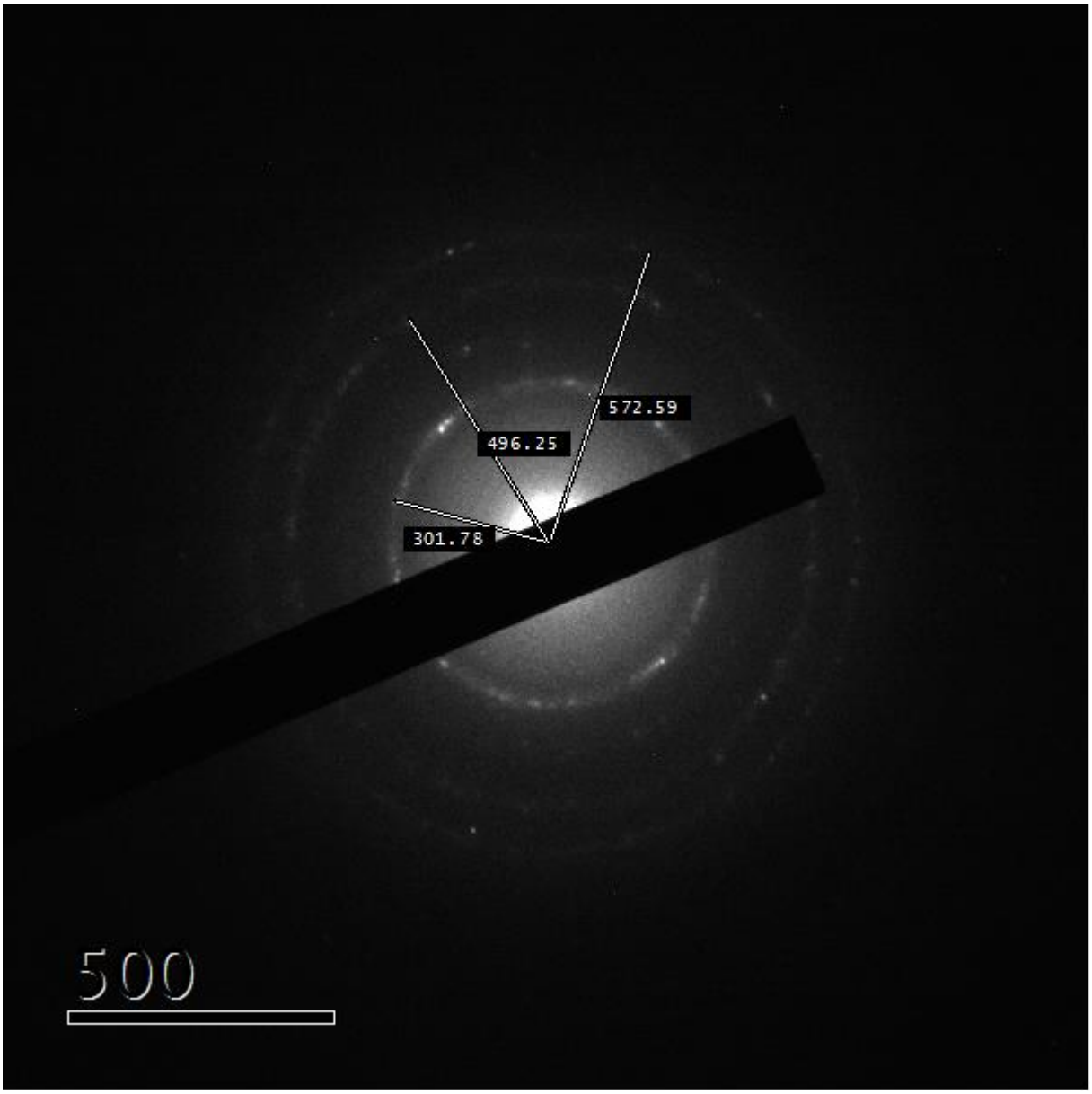

FIGURE 77 DIFF2

TABLE 8 MEASURED DISTANCES IN DIFF2

Measurment No.	Pixels	1/Å
2-1	301,78	0,388
2-2	496,25	0,638
2-3	572,59	0,736

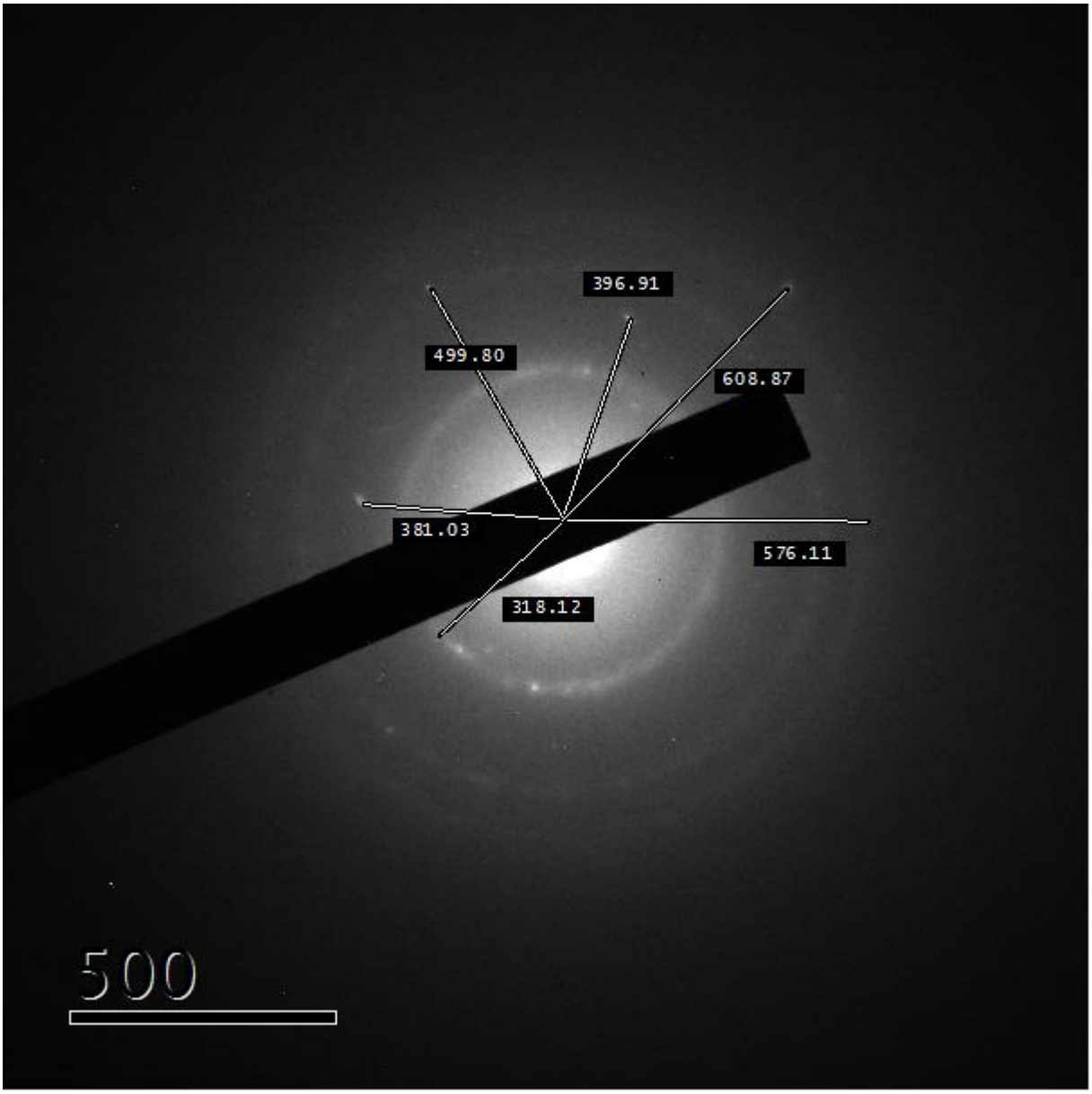

FIGURE 78 DIFF3

TABLE 9 MEASURED DISTANCES IN DIFF3

Measurment No.	Pixels	1/Å
3-1	318,12	0,40942085
3-2	381,03	0,4903861
3-3	396,91	0,51082368
3-4	499,80	0,64324324
3-5	576,11	0,74145431
3-6	608,87	0,78361647

Looking at the measurements from table 7, table 8, and table 9 we can find the measured plane distances [d_{hkl}]. All of these are displayed in table 10.

TABLE 10 DIFFRACTION MEASURMENTS

Measurement	D_{hkl} [Å]
1-1	2,418
1-2	1,587
1-3	1,333
1-4	1,220
1-5	1,048
2-1	2,574
2-2	1,565
2-3	1,356
3-1	2,442
3-2	2,039
3-3	1,957
3-4	1,554
3-5	1,348
3-6	1,276

There is an inaccuracy in these measurements stemming from the manual drawing of the measuring lines. By sorting them and looking at their relative differences, and because they are all gathered from the same sample containing the same crystals, we may assume that several of the measurements depict the same crystal.

If we sort our measurements after plane distances, measurements with similar plane distances can be grouped together. The error margin of each group is 0,16 Å.

TABLE 11 DIFFRACTION MEASUREMENTS GROUPED

Group	Measurements	D_{hkl} [Å] (Average)
1	1-5	1,048
2	1-4, 3-6, 1-3, 3-5, 2-3	1,3066
3	3-4, 2-2, 1-2	1,56866667
4	3-3, 3-2	1,998
5	1-1, 3-1, 2-1	2,478

To find out which compound each of these groups represents we must cross reference with a database of plane distances for relevant materials. Here we will use the compounds found during XRD analysis of the sample used for the TEM investigation.

Looking at the XRD results for the sample used in the TEM investigation, we have two tagged compounds. One is a silicon carbide compound with the database name “PDF 04-002-9070”. The other is a silica compound with the database name “PDF 04-014-2178”.

The *International Center for Diffraction Data* (ICDD), which maintains the database for powdered diffraction these patterns are taken from, has information in which crystallographic planes are causing the different tagged peaks in the XRD results. In table 12, this information is shown for the silicon carbide compound.

TABLE 12 PEAK POSITION, PLANE INDEXES, AND PLANE DISTANCES OF PDF 04-002-9070 (SIC) WITHIN THE RANGE OF THE OBSERVED TEM DIFFRACTIONS.

2Theta(°)	<hkl>	d(Å)
35,739	111	2,510
41,504	200	2,174
60,144	220	1,537
71,971	311	1,311
75,716	222	1,255
90,250	400	1,087
101,109	331	0,998

The data for the silica compound, PDF 04-014-2178, does not help much for our regard. The only peaks tagged in the XRD results of any size that we may use to pair with any of the diffraction groups we collected are around 2Theta=23°. According to the database, this corresponds to a planar distance of 3,86 Å. The furthest distance found in the TEM diffraction was 2,478 Å, so this does not help us much. Furthermore, if we were to try to find any matches in the database entry to the diffractions we found in the TEM, we would certainly be able to, but there are 40 possible planes with distances between 2,5Å and 2,0Å. Finding a match among them would mean nothing.

Because of this we appear to be restricted to looking at the carbide results and see what matches our TEM diffraction findings.

Comparing the groups in table 11 and the planes in table 12, we can detect a few possible matches.

The 111-plane with a plane distance of 2,510 Å is a possible match with group 5, being only 0,032 Å in difference.

The 220-plane with a distance of 1,537 Å is a possible match with group 3, being only 0,032 Å in difference.

The 311-plane with a distance of 1,311 Å is a possible match with group 2, being only 0,004 Å in difference.

The 400-plane with a distance of 1,087 Å is a possible match with group 1, being only 0,039 Å in difference.

4.3.4 Dark Field

Using the same fragment of frustule as was used for diffraction several dark field images was taken.

The diffraction image shown in figure 79 was captured and used to position the aperture.

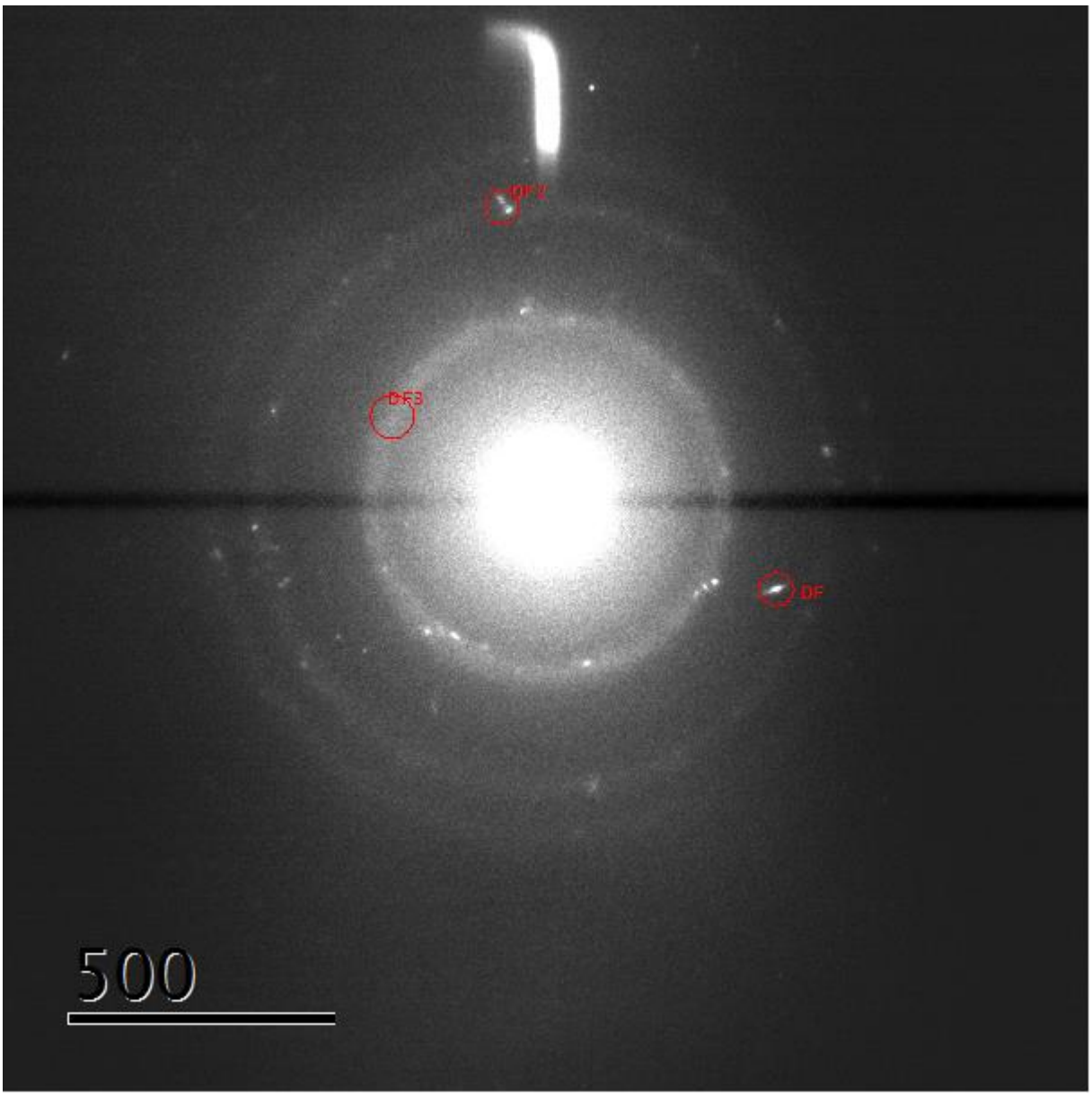

FIGURE 79 POSSESSIONS OF THE APERTURE USED FOR TAKING DARK FIELD IMAGES.

The aperture was placed at three different places in the diffraction image. One was placed on a bright node, not in a circle (DF). One was placed at a bright node within a circle (DF2). One was placed on a circle without a bright node.

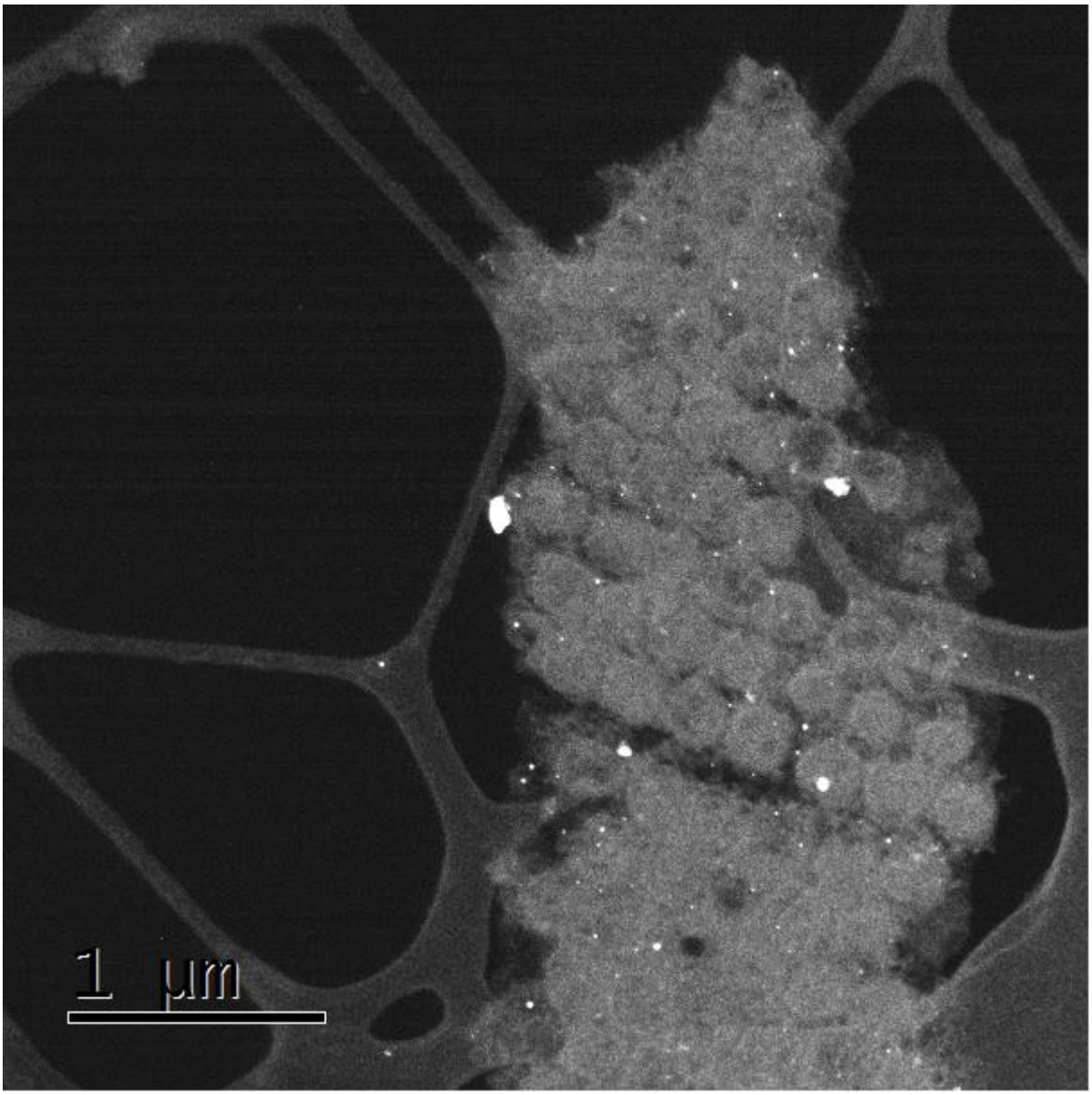

FIGURE 80 DARK FIELD IMAGE WITH APERTURE AT THE DF <FIGURE 91> POSITION

In figure 80 we see highlighted the parts of the sample with crystals creating the diffraction node marked in figure 79 as DF. We see this is mainly a few different spots on the sample fragment.

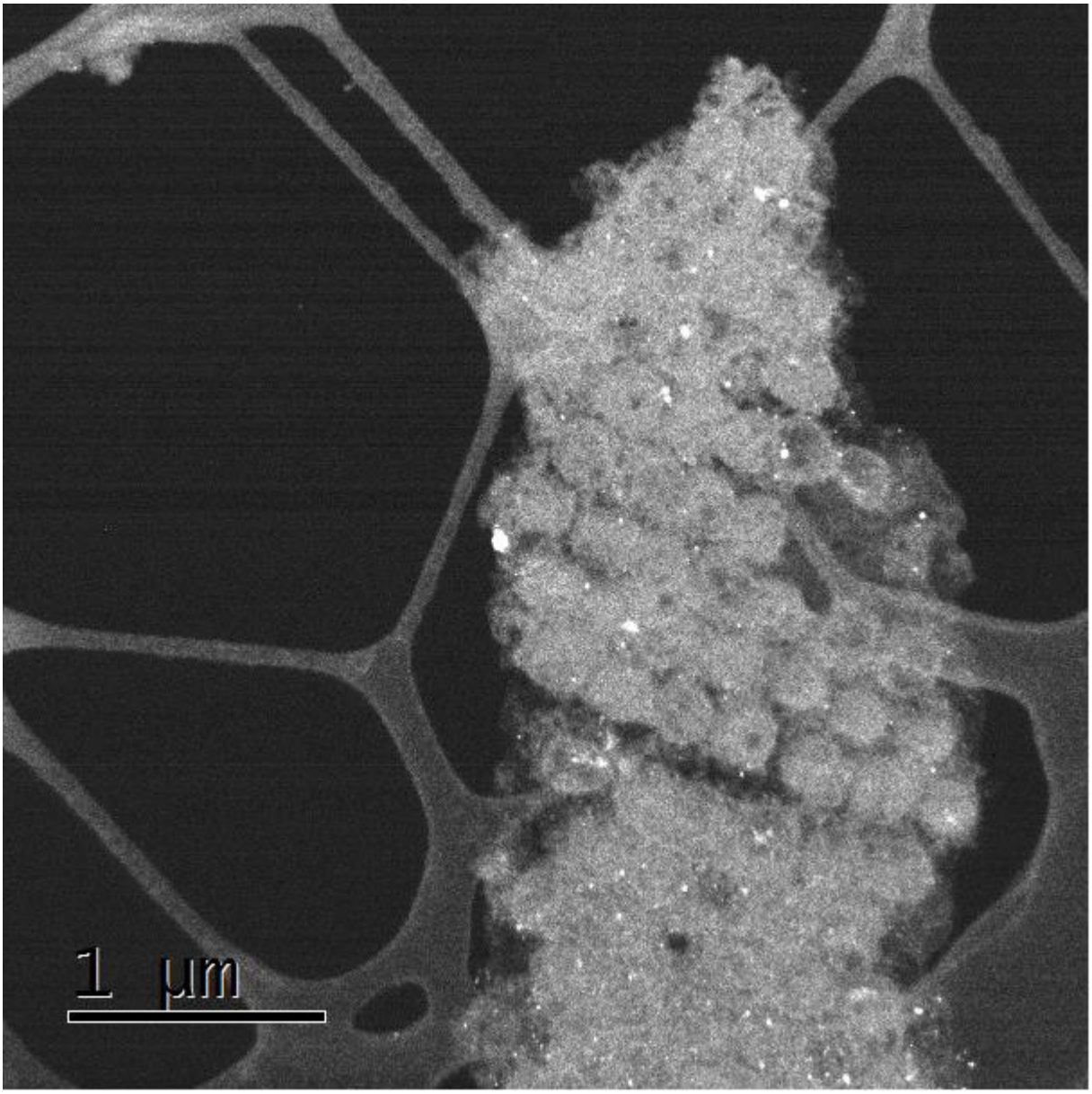

FIGURE 81 DARK FIELD IMAGE WITH APERTURE AT THE DF2 (FIGURE 80) POSITION

In figure 81 we see highlighted the parts of the sample with crystals creating the diffraction node marked in figure 79 as DF2. We see this is a much brighter image than figure 80, as more of the sample is highlighted.

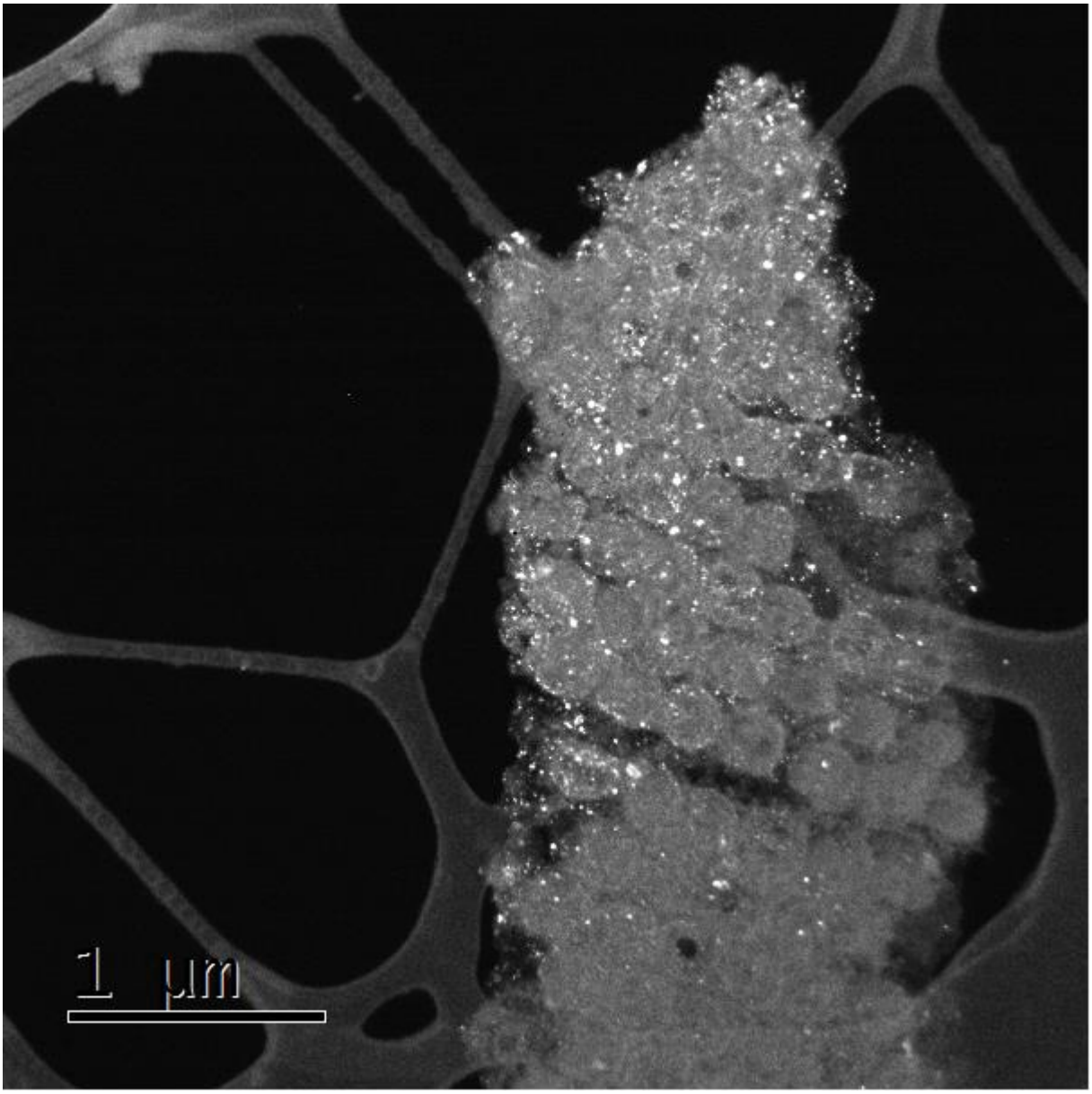

FIGURE 82 DARK FIELD IMAGE WITH APERTURE AT THE DF3 (FIGURE 80) POSITION

In figure 82 we see highlighted the parts of the sample with crystals creating the diffraction node marked in figure79 as DF3.

4.3.5 EDS

A penetrating EDS mapping was done on a small part of the sample. Figure 83 shows the area that was mapped. This area is a small part of the larger area seen in the dark field image study. The area was chosen as it contains several of the interesting features seen in the dark field study, including the "filled" areola, "empty" areola, thinner edge area, and an area outside sample for reference.

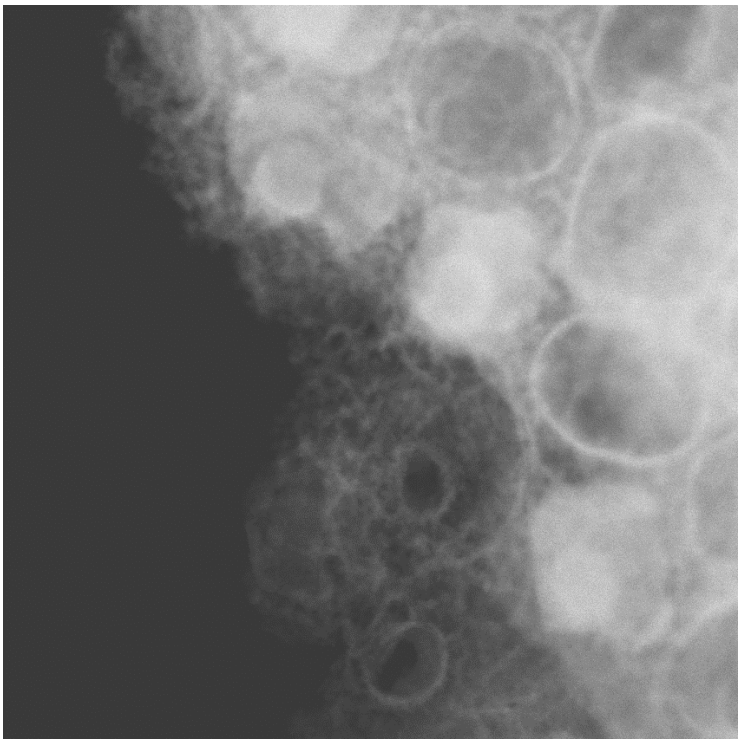

FIGURE 83 AREA USED FOR EDS MAPPING.

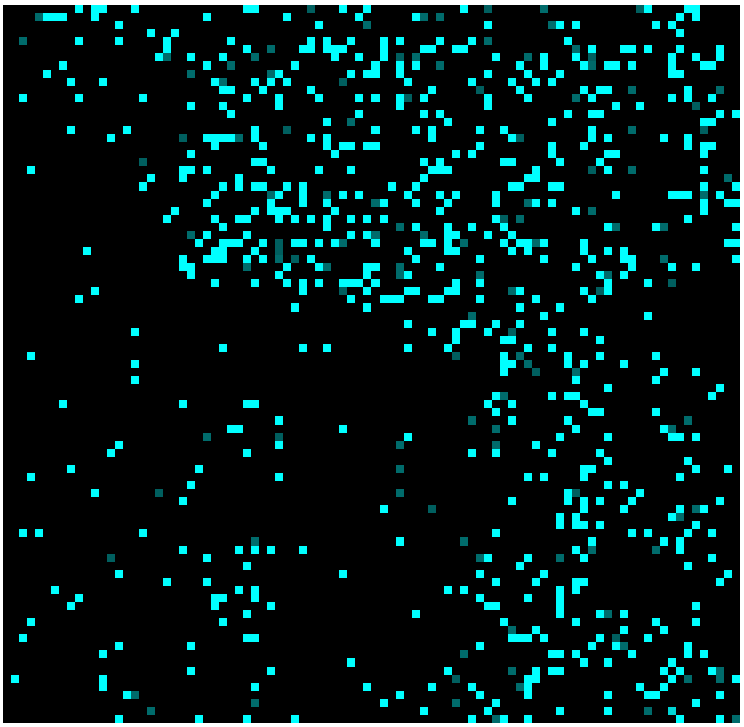

FIGURE 84 (C KA1) DETECTED CARBON IN THE AREA SHOWN IN FIGURE 83.

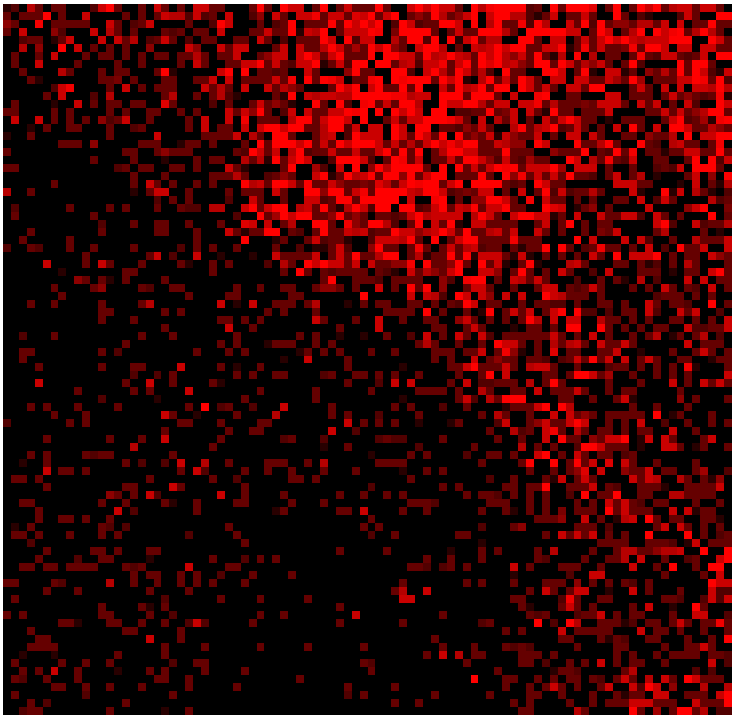

FIGURE 85 (O KA1) DETECTED OXYGEN IN THE AREA SHOWN IN FIGURE 83.

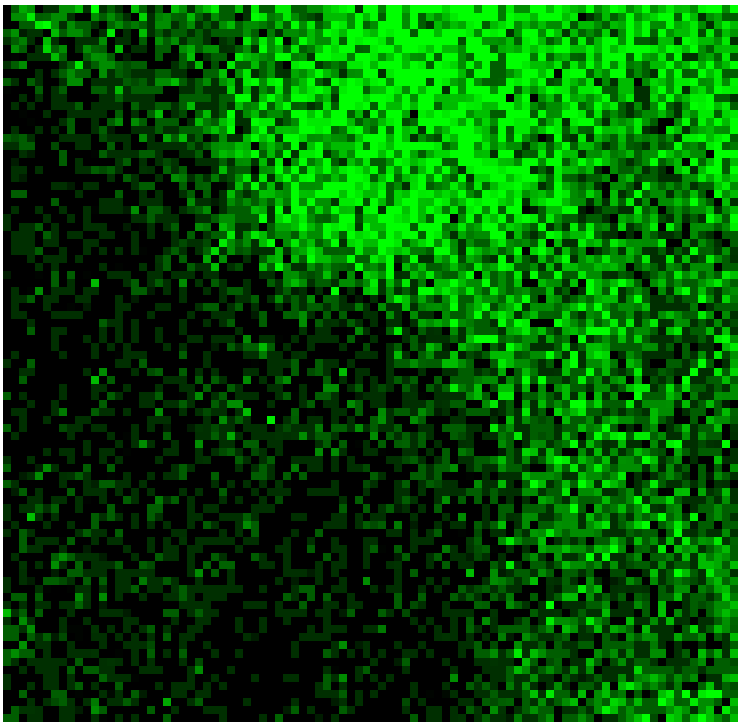

FIGURE 86 (SI KA1) DETECTED SILICON IN THE AREA SHOWN IN FIGURE 83.

5 Discussion

5.1 Reaction

5.1.1 Conversion

One of the main goals of this thesis is determining whether the frustules undergoing the described reaction do indeed convert from silica into silicon carbide. This question has been illuminated by several of the experiments we have conducted.

From the results of the XRD analysis of the frustules we can say that the reaction does create silicon carbide when added carbon in the form of oil. This is shown most clearly in the results from sample 4-Oil2, but is also supported by the results from sample 5-Oil3, as well as indicated by the results from sample 3-Oil1. In the diffraction results from sample 4-Oil2 we have an unambiguous silicon carbide signal. The peak 2Theta=36^{o} is a clear sign of the presence of silicon carbide in the sample.

We do not see the formation of silicon carbide in neither the sample added no carbon (1-Plain), nor the sample added carbon in the form of powder (2-Powder).

For the case of sample 1-Plain this can be explained by the lack of carbon. Though earlier results during internal research have showed the possibility of creating silicon carbide using only the organic carbon left over after the initial wash of the frustules, these results have not been consistently reproducible and are not published, though the sample used during the TEM investigation is one of them. From the results shown here we can say that without adding extra carbon, we get no formation of silicon carbide. For the case of sample 2-Powder, this likely comes from the fact that powder has a much smaller contact surface on which the reaction can take place. The carbon is present in the reactor, but it does not come in contact with the silica enough to create carbide. Another possible explanation could be that, as the reactor heats up, the oil boils and releases carbon compounds in the atmosphere while the powder does not do that to the same degree.

The formation of magnesium oxide is another indicator that conversion reactions are taking place. As the reactors are loaded in an argon atmosphere and sealed to prevent any gas exchange, there is no oxygen gas present to react with the magnesium. The only oxygen present in the reactors are bound in the silica. This means that, as we see the formation of magnesium oxide, it necessarily leaves silicon in other forms. As we only detect the presence of magnesium oxide in the samples that also contain silicon carbide, we can assume that the Si atoms which lost their oxygen went on to combine with the carbon that was present. The new proposed formula for the reaction taking place is then:

$$SiO_2 + 2Mg + C \rightarrow SiC + 2MgO \quad (9)$$

This is a simplified understanding of the reaction as it presumes that the carbon exists as free elemental carbon rather than as a mix of different organic compounds derived by pyrolysis from rapeseed oil.

Looking at results from XRD analysis of the glass replacements, we see no sign of and conversion into silicon carbide in any of the variations.

Following the same argument presented from the XRD analysis of the frustules, because silica is the only source of oxygen present in the reaction, the presence of magnesium oxide necessitates the formation of new silicon compounds. In the frustules we saw that when we found magnesium oxide, we also found silicon carbide. In the glass replacements a different reaction has happened. Instead of the silicon bonding with carbon it appears to either bond with magnesium (Glass1, Glass2, and Glass3) or stayed as elemental silicon (Glass3).

The TEM investigation is not able to tell us much about whether the conversion is happening or not. Firstly, the sample used in the TEM investigation was not part of the original experimental matrix used for the samples used in the XRD investigation. It was a sample from earlier experiments, and might have undergone a slightly different process. The sample used for TEM investigation was also a sample that had not been added any carbon when it underwent the conversion process, yet it still showed clear signs of having underwent conversion. That is a result that has not been reproduced by the XRD investigation done in this thesis. From this we can say that the sample used during the TEM investigation was not representative of the other samples used to investigate whether conversion occurs.

5.1.2 On the usefulness of the glass replacement, and what they can tell us about the reaction taking place.

Our experiments with the glass replacements shows what happens to a simpler form of silica when exposed to the same reaction we expose the frustules to. The silica on the replacements reacts with the magnesium gas and creates both magnesium-oxide-compounds and Silicon-magnesium-compounds, but no Silicon-carbide compounds. This appears to be true for both the case when carbon was added as a powder and when added as an oil. This is different from the results gained from our frustule samples. This would indicate that using glass replacements for investigating the reaction process is not a good substitute. This would also mean that the reaction that happens to convert silica into silicon carbide is very dependent, either on the microstructure of the material, as glass is amorphous while frustules are nano-crystaline, or porosity and surface area, as the glass is dense while the frustules are porous. Of these two, it is probably because of surface area, as this would fit with why we get conversion in the frustules when they were added oil and not powder.

Looking closer on each of the XRD results from the glass samples, we note a few interesting things.

As expected, the control sample (Sample 0) does not get any clear peaks in the XRD. This is because XRD detects crystalline structures, while the unprocessed control is amorphous glass. The wide peak-like formation we see between 2Theta=5-30^{o} comes from that corresponds to the average distance between the atoms in the glass of the sample. We can see the same “hill” in the results for sample 1, though flattened out because of the much longer y-axis. For Sample Glass0, y-axis goes to 8000 counts. For Sample Glass1, y-axis goes to 110000 counts, more than ten times as much, indicating a that much stronger signal.

Looking at the results from the sample; Glass1, where no carbon was added to the process, we see that the magnesium gas has reacted with the SiO_2 in the glass sample to create MgO and Mg_2Si. We also see that the new compounds do not have the amorphous glass structure and makes clear peaks in the diffractogram. We see no formation of any carbon compounds, which is expected since no carbon was added. The results from Glass1 show that in the absence of any additional carbon, the magnesium gas will react on its own, and extract oxygen from the silica that is present to some degree.

In the results from sample Glass2, which was added carbon in the form of nano-sized graphite powder, we see much the same result as from sample Glass1, but with the addition of a large peak at 2Theta=40^{o}. This peak is from the presence of the carbon in the sample, but as pure carbon, not attached to any of the other elements present. This means that even though the carbon was present during the reaction process, it did not take part in the reaction, and did not form compounds with either the silicon, nor the magnesium. For the case of reacting with silicon, this could be because there was limited contact between the reactants. There may be only a few points of contact between a powder and a glass surface. This explanation may not be used for the case of the magnesium. During the reaction, the reaction chamber is saturated with magnesium gas. From this we can confidently say that the magnesium gas will not react with carbon powder in the environment inside the reactor during the reaction.

Looking at the XRD results from the sample Glass3, which was added carbon as an oil, it may seem at first look as if though it shows no indication of the presence of carbon at all. This is probably not the case, though, as the peak tagged as Mg_2Si, positioned at 2Theta=40^{o}, is in the same place as the carbon peak for the sample Glass2. This means that the peaks overlaps and the peak we see in Glass3 contains both the carbon peak and the tagged Mg_2Si peak. Comparing again with the results from Glass2, we can see much the same peaks present. The large MgO peaks at 2Theta=43^{o} and

2Theta=62^{o} are the same for the two samples, as is 2Theta=73^{o} and 2Theta=58^{o} peaks for Mg_2Si. It does show the new addition of a pure Si compound having been created. This resembles the result of Z. Bao et.al. from 2007, where they managed to use magnesium gas to create nano-crystalline silicon from silica frustules at a temperature of only 650^{o}C. [45] We see no signs of the presence of silicon carbide. Combining this with what we have found out about surface area dependence, we can conclude that with low surface area for the silica, they will react to form elemental silicon and Mg_2Si, instead of the desired silicon carbide.

Also of note is the weaker signal compared to the Glass2 results. For Glass3, the highest result we get is at approximately 24000 counts, only 1/5 of the signal from Glass2. The reason for this is unknown, but it could be from something trivial like the position of the sample in the sample holder or the texture of the surface of the sample where the x-ray hit. Either way, it is not believed that it has had any effect on the result gained.

In none of the glass replacement samples do we see any peaks for silica, even though that is what the glass is made out of. This means that the temperature of 800^{o}C was not high enough, or one hour not long enough, to cause crystallization from the amorphous glass. Whether this means that it is also not high enough to cause changes in the grain size of frustules, we cannot say for certain, as the temperature required to change the size of a grain is different from what is required to form crystals, but we can interpret it as a weak indication that the crystal structure of the frustules is not largely effected by the temperature of the reaction.

5.2 On preservation of structure

As our ultimate goal is not only to achieve a conversion of the frustules from silica into silicon carbide, but doing it while preserving the nano-architecture that makes them behave as photonic crystals, a SEM investigation was done to look at how well the structure survived the process.

Looking at all the overview images taken of the different samples, it is clear that the overall survivability of whole diatom is poor. We can see that the frustules are flaked up and broken into smaller pieces. Few or none of the frustules were found to be completely intact, though intact hypo- or epivalves showing both areola and cribrum was found in all sample except 1-Plain, which had the highest amount of destruction.

This is probably caused by mechanical stresses during handling and storage. The frustules used during the experiment was also rather old, having undergone initial washing a whole year before undergoing the remaining steps of the described process. This will have given the frustules ample time to break down. The long storage cannot be the only cause, though. All the samples were stored an equal length of time, yet we still see clear differences in the degree to which the frustules are broken down. A particularly large difference is seen between the samples 1-Plain and 4-Oil2. For sample 4-Oil2 we are able to find a lot of frustules that are largely intact. This difference is seen in the comparison below.

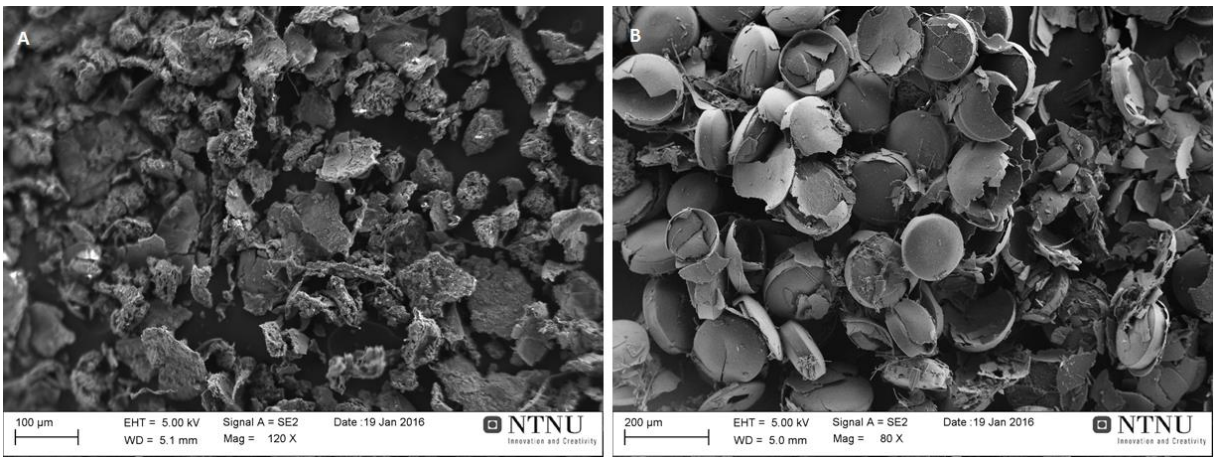

FIGURE 87 COMPARING THE OVERVIEW IMAGES OF SAMPLES 1-PLAIN (LEFT) AND 4-OIL2 (RIGHT) WE CAN SEE A STARK DIFFERENCE BETWEEN THE HOW INTACT THE FRUSTULES ARE.

There are at least two possible explanations for this difference. One is that the frustules underwent more stress during the process with no added carbon than the process with added oil. The only stated difference between the two samples are the addition of carbon in the latter. When the carbon was added, the oil was mixed in by filtering accompanied by some stirring by hand. One would expect this to incur additional breakdown of the frustules so that we had the inverse results; the carbon-added frustules being less intact than the ones without any added carbon. As we do not have that, this is likely not the cause of the difference.

The second possible explanation for this difference is that it is caused by a selection phenomenon when the frustules were loaded into the reactor. It is possible that, as the samples were made chronologically, beginning with 1-Plain and ending with 5-Oil3, the sample material had a bias for emptying its smallest parts out of the sample container first, leaving the larger parts to appear in the later samples. If this is the case, we would expect to see a gradual increase in the amount large and intact frustules going from the first to the last sample. We do see this to some degree, but a study using more reliable randomization of the sample materials would be required to say for certain.

Looking at the preservation of the structure on a smaller scale, it seems to vary greatly between the different samples. From the SEM images made of sample 1-Plain, we can see signs of chemical stress on the some of the cribrum where the smaller parts of it appears to have disappeared. The loss of only the smallest arts of the cribrum and that it looks to be a gradual degradation from the center indicates that this is probably a chemical degradation, and not caused by the same mechanical stresses that has worn down other parts of the frustules. It is possible that the finer details of the cribrum become thinner along the edges of the frustule, and that is why those parts have disappeared while the cribrum at the center has survived.

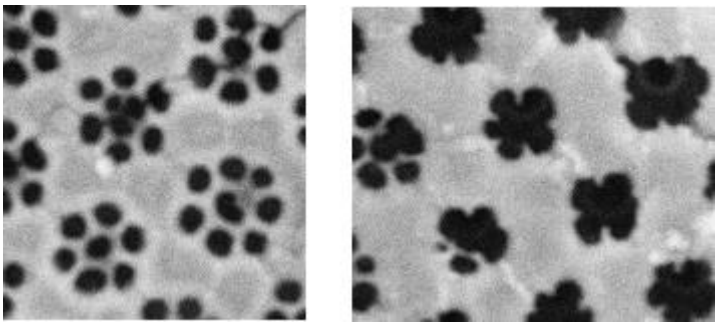

FIGURE 88 COMPARISON OF CRIBRUM FOUND IN SAMPLE 1-PLAIN. THE CRIBRUM CLOSER TO THE CENTER (LEFT) OF THE FRUSTULE IS BETTER PRESERVED THAN THE CRIBRUM AT THE EDGE (RIGHT).

The sample 1-Plain also showed areas where the areola is worn away. This is seen in figure 36 and 37. We also see the same wear in sample 3-Oil1. This is either caused by the same stresses that seem to have broken down the macrostructure of the frustules, or by the same phenomenon that causes the degradation seen in figure 88. Without further study we are unable to determine which.

In the sample 3-Oil1 we found areas where the cribrum appears to be blocked up. When we look at figure 49, this appears to be the fuzzy growths that are the cause of this blockage. The blockages seen in figure 48 is then the same phenomena seen from the other side of the cribrum.

In all the samples growths in various forms were found. In sample 2-Powder and 3-Oil1 we found fuzzy growths on both the cribrum and the areola. In sample 1-Plain, 2-Powder, 4-Oil2, 5-Oil3, and possibly also in 3-Oil1 we find a film covering the surface of the cribrum. In sample 4-Oil2 we find droplets formed on top of the film, and some places being contiguous with it. Considering the compounds available, all these features are likely deposition of carbon in different form deposited on the frustules during the reaction. This is supported by the fact that the samples which have been added the carbon as an oil appear to have a thicker film than sample 1-Plain, which had no added carbon, and sample 2-Powder, which was added carbon that was in less contact with the frustules. This matter should be studied further at a later point.

This film appears to protect the underlying structure of the frustule from degradation and coarsening. This can be seen by how, in sample 2-Powder, we have an image of an area only partially covered by a thin film where the uncovered parts are much more degraded than the parts that are covered.

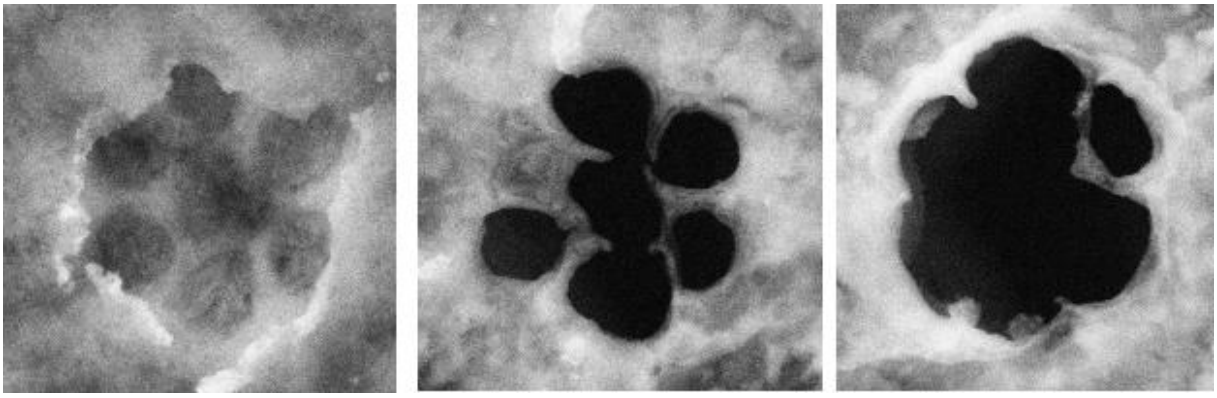

FIGURE 89 THE EFFECT OF THE FILM SEEN IN SAMPLE 2-POWDER ON PRESERVATION OF CRIBRUM. WE SEE CRIBRUM COVERED (LEFT), PARTIALLY COVERED (MIDDLE), AND UNCOVERED (RIGHT).

This can also be seen in samples 4-Oil2 and 5-Oil3 where the places where the film has flaked off appears very well preserved, even preserving the cribellum. If we try to compare these areas with how the cribrum looks before the process, it is not easy to do a direct comparison due to the quality of the images, but we are able to see that the smallest features of the frustule, the cribellum covering the cribrum has survived the process.

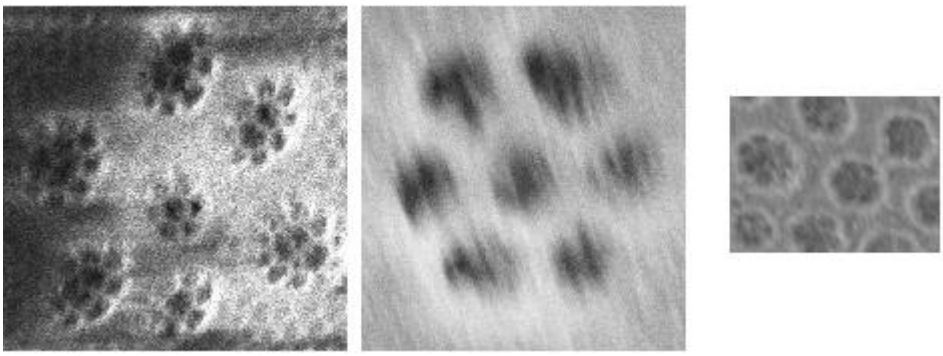

FIGURE 90 CRIBRUM BEFORE (LEFT) AND AFTER (MIDDLE AND RIGHT, FROM 5-OIL3). POOR IMAGE QUALITY ON THE AFTER IMAGE MAKES COMPARISON DIFFICULT, BUT IT LOOKS LIKE THE CRIBELLUM, THE FINE MESH COVERING THE SEVEN HOLES OF THE CRIBRUM, SURVIVED THE PROCESS.

From this it appears that during the reaction process, the carbon added to the reaction form a protective film on the surface of the frustules. This film appears to preserve the structure of the frustules to a remarkable degree, particularly in the samples that were added oil.

5.3 On the utility of TEM

5.3.1 On the utility of STEM and HRSTEM

One of the most impressive feats of a TEM machine is its ability to image a sample at incredible high resolutions. Whether this is of any use to us, though, is not certain. To decide whether this tool can be useful for our purposes, we need to ask and answer two questions.

Firstly, can the use of STEM tell us anything new that an easier SEM can not?

Secondly, is there any information relevant for our purposes to be gained at the scale where the use of HRSTEM is warranted?

To answer the first of these questions we may compare an image captured by STEM and one captured by SEM.

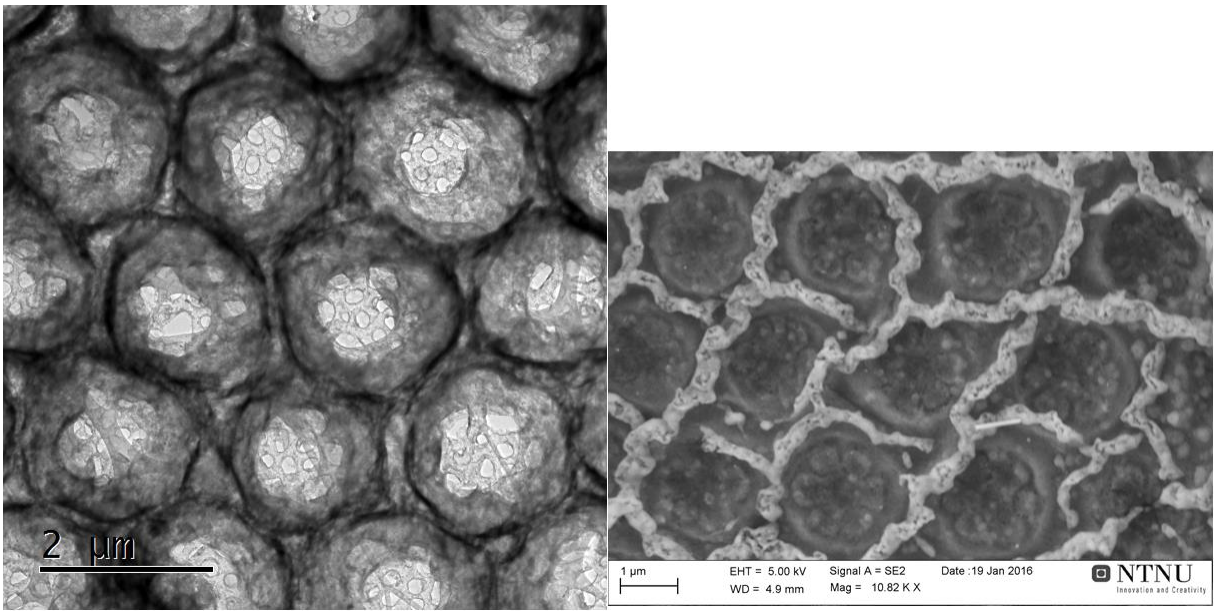

FIGURE 91 STEM/SEM COMPARISON. BOTH IMAGES SHOW THE SAME FEATURES AT THE SAME SCALE. ONE CAPTURED BY STEM (LEFT) AND ONE CAPTURED BY SEM (RIGHT).

Figure 91 shows the areola and cribrum of the frustules imaged by STEM and SEM. Though that is shown in the two images is not directly comparable, the cribrum on the right having undergone significantly more coarsening than the noes on the left, they do illustrate the difference between the two imaging techniques. In the SEM image, what is imaged is the surface of the sample, while in the TEM image, we are not able to see the surface of the cribrum, but instead see through it.

This means that a TEM image would be able to see possible inclusions of differing materials, as that would have differing crystal structure from the surrounding materials. This can be relevant for looking at samples of processed frustules, as it is possible that the conversion from SiO_2 to SiC has only happened at some part of the frustule. It could be possible to see, either SiC inclusions in SiO_2 or the reverse, through the frustule material. That, though, is easier to do using dark field imaging.

For the purpose of seeing how well the structure of the frustules is preserved, this is done much easier using SEM.

As for the second question, the images from High-Resolution Scanning Electron Microscopy could be useful for our purposes in a few different ways. By counting how many lines are across a certain distance we can find the distance between the atomic planes. This can be used to identify which

material that single, fortunately-oriented crystal by cross-referencing with a crystallography database. This, though, is essentially doing the same thing as what is done in the diffraction images; using the diffraction nodes to find plane distances, and then finding material.

A different piece of information that may be gleaned from the high resolution images is grain size of the material. Using Fourier transformation of HRSTEM images, we were able to more clearly see the grains and get an estimate of their size.

The grain size of the frustules post-processing, may not be particularly relevant for the current goals of this thesis, but the fact that we are able to find it during our TEM investigation shows the flexibility of the instrument. It may not be relevant now, but can prove to be valuable knowledge during a more thorough study of reacted frustules.

From this we can say that the use of STEM and HRSTEM to look at frustules is useful in only a few cases. STEM appears to be inferior to the use of SEM. HRSTEM appears to be useful only for specific studies relating to finding grain size in the frustules.

5.3.2 On the utility of TEM diffraction.

As was stated during the discussion on conversion, the sample used for TEM diffraction is left over from an earlier project. It may have undergone a slightly different process, and the results gained from that project was not reproduced in the results we gained in this thesis. From this we can conclude that the sample is not representative for the other samples used in this thesis. That means that the TEM investigation conducted here is not useful for telling us anything about the first point of the stated goals of this thesis, whether or not the conversion into silicon carbide was possible. That, though, was not its intention. What the TEM investigation done here can tell us something about is the other stated goal; whether conducting a TEM investigation may be a useful tool for future research into the conversion of diatom frustules from silica into silicon carbide.

For diffraction to be a useful tool for further investigation, a much more thorough investigation must be conducted. Just checking the measured nodes up against the compounds already found in a XRD investigation does not tell us anything new, only confirm that the results we have are possible.

It can be argued that using TEM diffraction gives us the same information as XRD since both methods uses the diffraction caused by the distances between crystallographic planes. In less amorphous samples the TEM would have the advantage in that it also gains information on the angles between the planes that are detected in order to identify diffraction nodes. Given that we are unable to do that when investigating frustules, TEM diffraction loses some of its utility.

What we can do when using TEM diffraction, that we are not able to do with an XRD is to get diffraction data on a limited area of the sample. When XRD is used, we get a diffraction pattern for an entire powder sample. When TEM diffraction is used we are able to decide which parts of the frustules to get a diffraction pattern from. The diffraction patterns that was gathered during the TEM investigation was gathered from different points of the sample fragment, looking at different features, and therefore getting different diffraction nodes. This is where the usefulness of TEM diffraction lies when investing frustules.

For TEM diffraction to be a useful tool, considerable expertise is required. Though the amorphous and nano-crystaline nature of the frustules makes it harder to properly identify the diffractions found, it could prove useful for investigating which parts of the frustules consists of which compounds.

5.3.3 On the utility of dark field imaging

Looking at the dark field images gathered of the sample we can see that this is potentially a powerful tool to use when attempting to find, not only whether a conversion into SiC has taken place, but where it has taken place. Using the same methods as was done with the diffraction images gathered, we can identify different materials' diffractions and look for them in the sample.

There are some limitations, though. As we see in the diffraction image used to focus the aperture, the diffractions detected there often come in the form of circles (DF3) or double nodes (DF2). This is because of the amorphous and polycrystalline nature of the sample. This creates diffuse diffraction results that is the circles in the diffraction image. This means that by focusing the aperture on just a part one of those circles will indeed highlight the crystals making that diffraction, but only those oriented that particular way. This means that while it highlights the relevant part of the sample, it does so with only a small part of the whole.

A counter argument to this is that as the sample is highly amorphous and polycrystalline, the orientations of the crystals making the circles are random at every point in the sample. This means that only highlighting a small part of what we want is not relevant, as the highlighted features will be distributed in a way that makes it so that we might as well have highlighted all of what we wanted. The overall degree of highlight may be smaller, but, statistically, we see the same.

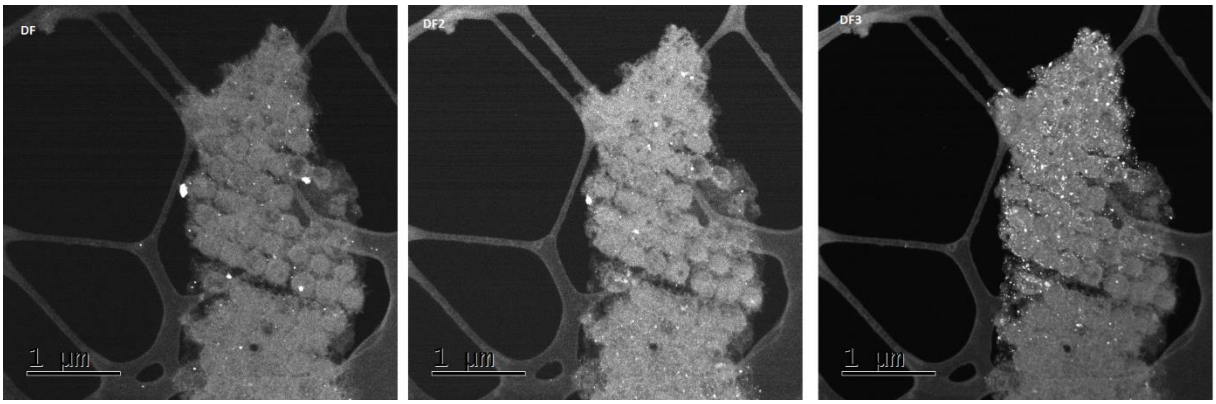

FIGURE 92 SIDE-BY SIDE COMPARISON OF DF IMAGES.

Looking at all three dark field images captured in figure 92, each with the aperture focused on a different part of the diffraction image we can see that different parts of the sample is highlighted.

This would potentially be a very useful tool for the future investigation of converted frustules. In particular, to investigate which parts of the frustule undergoes conversion.

5.3.4 On the utility of penetrating EDS

Penetrating EDS can potentially shed light on one key question regarding conversion of silica frustules into silicon carbide. That is, is the conversion we are have detected a surface phenomenon, or does the conversion go the whole way through the walls of the frustule?

Figures 84, 85, and 86 show the detection of carbon, oxygen, and silicon, respectively, gathered from the area displayed in figure 83. For ease of view, they are gathered in figure 93. From these results we are able to see one crucial thing; the map of the detected carbon has the same shape as the maps of two other elements. Since the EDS is penetrative, we expect to see that the map of detected silicon and oxygen follow the thickness of the sample. In the thicker parts of the sample, the electron beam needs to go through more mass, and will thus detect more of the elements present. Comparing the images in figure 93 we can see that this is the case.

This is seen most clearly in the middle of the lower half of the mapping (circle). In the imaged area (A) we can see this area shows the thin edge of the sample fragment. In (C) and (D) we see nearly no detected silicon or oxygen there. This lack of any detection form the low thickness is reflected in the same area in (B). This means that at this place in the sample, the uptake of carbon is not limited to only the surface of the frustule as previously theorized. Had the carbon only been present on the surface of the sample we would expect to see that the entire surface of the sample fragment would have the same concentration of detected carbon. As it is, we can see a clear difference in density of detected elements between the thick (square) and thin (circle) areas of the sample.

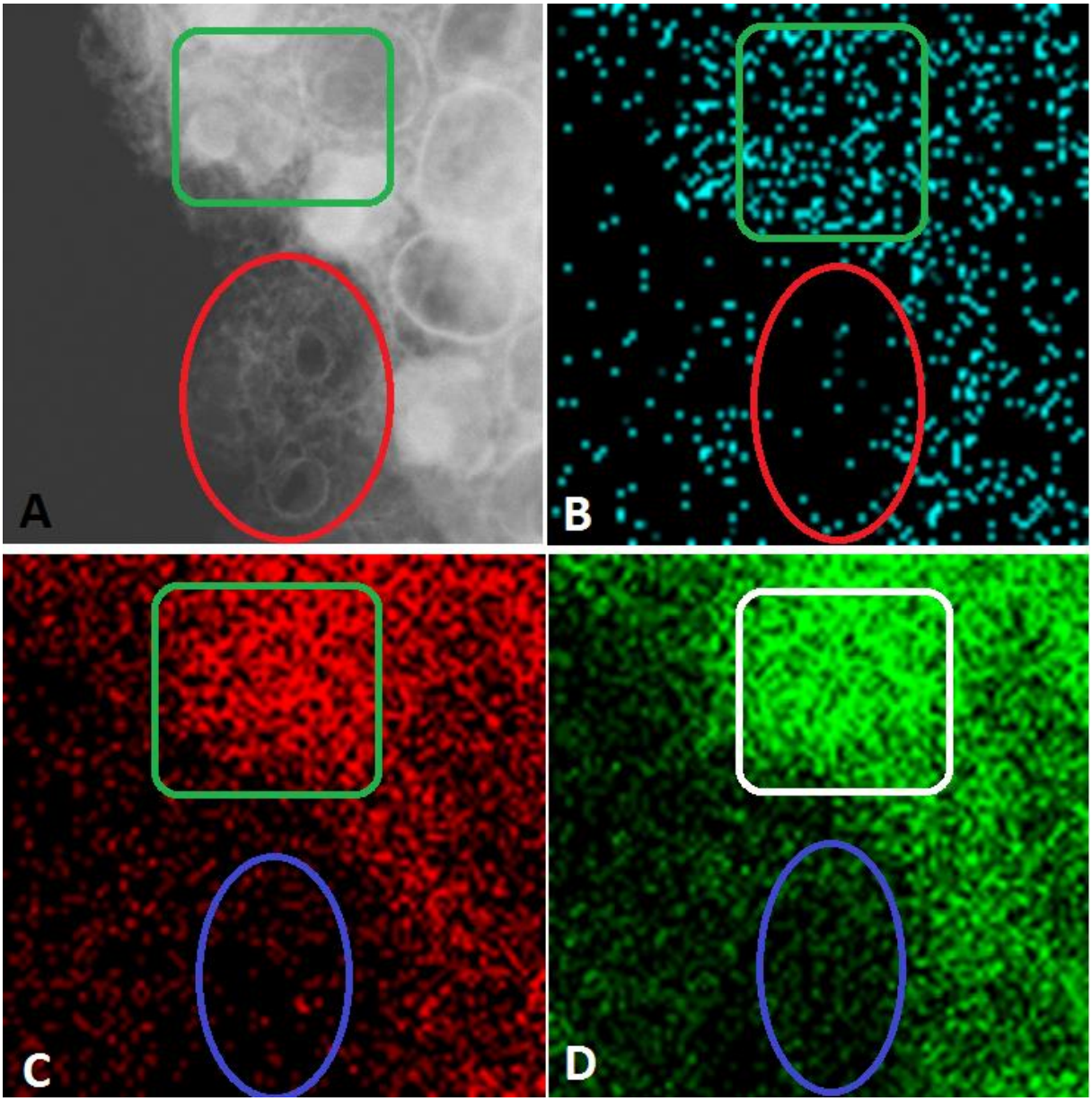

FIGURE 93 COMPARING THE DENSITY OF THE DETECTED CARBON (B) AND THE DETECTED OXYGEN (C) AND SILICON (D) THEY LOOK TO HAVE THE SAME RELATIVE DENSITIES AT DIFFERENT AREAS. THICK (SQUARE) PARTS OF THE SAMPLE HAVE MORE DETECTED CARBON THAN THIN (CIRCLE) PARTS OF THE SAMPLE.

This type of argument could not be done using a regular SEM mounted EDS, as it only detects the surface of a sample, and not through the entirety of the sample. This means that for the purpose of finding out whether the conversion is a surface phenomenon or a penetrating phenomenon, the TEM is a useful tool.

5.4 Miscellaneous

5.4.1 The mismatched peaks in 1-Plain

Looking at the results of the XRD analysis of the 1-Plain sample (figure 94), which, as the name suggests, was not added any carbon in excess of what was left over from the cleaning, the first thing of not is that no match was found for several of the peaks observed. As was described in the experimental section, when the peak matching software was used, the elements chosen as parameters for the search was determined beforehand. In this sample it would seem that there were no compounds matching of the peaks we see at 2Theta=27°, 2Theta=30°, 2Theta=33°, 2Theta=38°, and 2Theta=52° within the given parameters. This can of course mean that our choice for which elements to include in the peak matching search are entirely wrong, though that is not likely, as they have found matches for the peaks in the other XRD results.

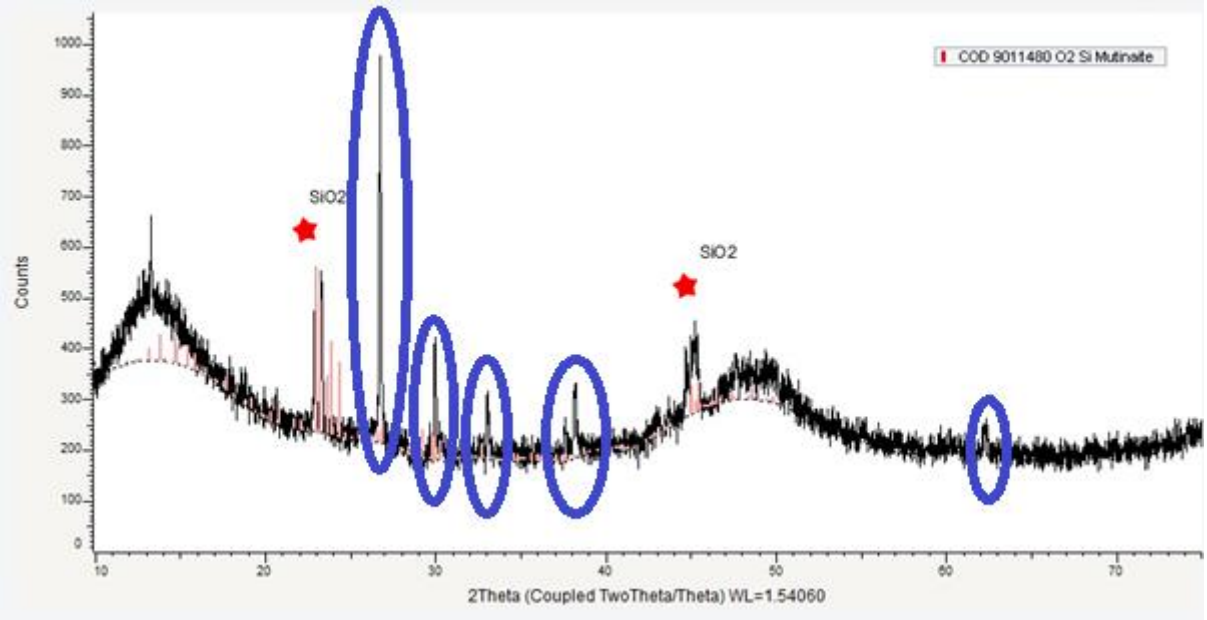

FIGURE 94 XRD DIFFRACTOGRAM OF SAMPLE 1-PLAIN. SEVERAL PEAKS APPEAR TO NOT HAVE BEEN IDENTIFIED BY THE SOFTWARE.

Looking at the other XRD results, the unmatched peak at 2Theta=27° looks like the carbon peak found in several of the other samples. Why it has not been matched here is unknown.

The other unmatched peaks do not readily match any of the other matched peaks in the XRD results from the other samples.

The second thing of note is the low count number, indicating a weak signal from the sample. This comes from a combination of at least two factors. One is the small amount of sample available for analysis. The other is the porous and amorphous nature of the sample. This could be one of the reasons for not finding matches for several of the peaks.[41]

The compound that was found to match, silicon oxide, is what the frustule is made from before the reaction.

Without identifying the unknown peaks, it is impossible to determine what reactions have occurred during the process of this sample.

5.4.2 The lack of silica in 2-Powder and 3-Oil1

The XRD results from sample 2-Powder show only the presence of carbon and a carbon-oxide compound. The results show no sign of the presence of either silica or silicon carbide. This is strange, as we would at least expect to find signs of silica, it being the starting material of the frustules, and something we have found in all the other XRD results with the exception of sample 3-Oil1.

Looking back at how the powder sample was prepared, carbon powder was added in excess to facilitate conversion. It might be that so much carbon was added that when the reacted sample of the frustule-powder mixture was taken for XRD analysis was gathered, the frustules was so diluted in the carbon powder that it could not make a clear silica, or silicon carbide, signal during the diffraction.

If this is the case, then the XRD results from sample 2-Powder must be disregarded in all further analysis, as it does not represent the state of the frustules.

In the 2-Powder sample it is also found a substance tagged as a carbon oxide. If we go to the database entry for “COD 1010305” (COD=Crystallography Open Database) we find that it is a carbon(II) oxide and not connected to any other element. For it to be detected by the XRD, it would not only have to be solid, but crystalline. One usually finds carbon monoxide as a gas. This is either a compound made from the graphite powder, or the result of a mismatched peak. As the main peak it is matched upon is very narrow, and the count number very low, the peak can have come from a random noise effect. This means we can discard this compound from further consideration.

As stated, we see the same lack of any sign of the presence of silica in the XRD results from sample 3-Oil1. It can be that the lack of any silica signal in both these cases are caused by the same phenomena. Since sample 3-Oil1 show signs of silicon carbide, that would mean that the lack of silica in the powder sample is because of some unknown phenomena. The lack of silica in the 3-Oil1 sample could be because all the silica is converted into carbide. This is highly unlikely, though, as this has not happened in any of the other oil-added samples. Additionally, this was the sample where much of the sample material was lost because of a hole in the steel mesh holding the frustules during reaction. Consequently, the signal is weak, and therefore the count number is low, because of the small amount of sample available for analysis. This could cause the silica signal to drown out in the noise. This is also unlikely, as we do see silicon carbide signs, which in all the other XRD results are weaker than the silica signal.

Either way we have an unexplained phenomenon. Either the lack of silica in the samples have the same cause, which we do not know. Or one is caused by mundane experimental errors, and the other is caused by some other thing we do not know. At this point we do not know which is correct.

5.4.3 On the unknown lines in 3-Oil1

In figure 47 and 48 we see lines having formed on the surface of the frustule. At first, they appear similar, but when we put them side by side in figure 95, we see that that may not be the case.

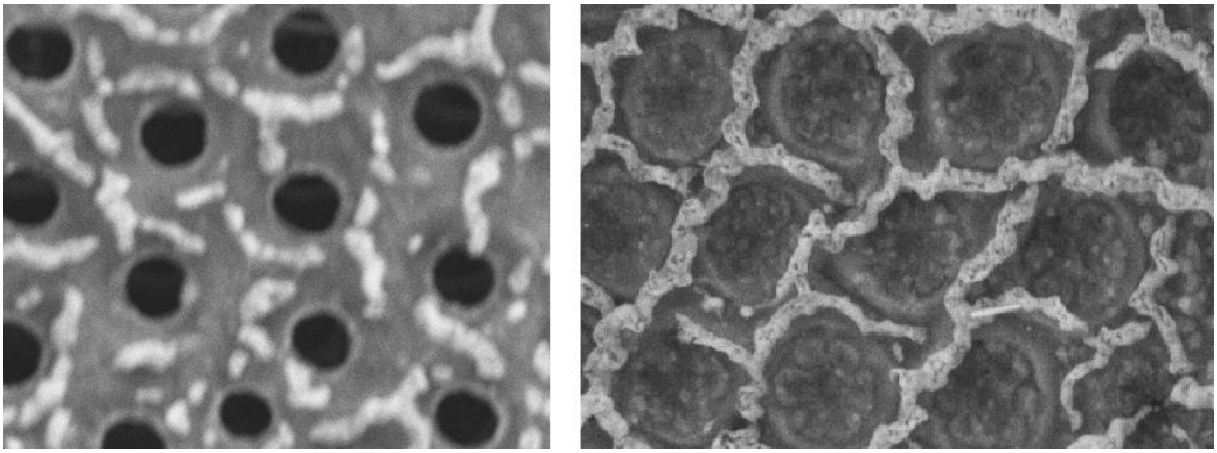

FIGURE 95 SIDE BY SIDE COMPARSION OF UNKNOWN LINES FOND IN SAMPLE 3-OIL1.

The lines on the left is found on the surface of the foramen. They appear to be only sporadic, not connecting in any pattern. The lines on the right is found on the underside of the cribrum, and do appear to consistently connect in a pattern very similar to the areola is shaped.

It is possible that the lines found on the foramen are caused by deposition of organic compounds, like the film observed in sample 4-Oil2 and 5-Oil3, while the lines observed on the underside of the cribrum are the points of contact between the cribrum and areola.

Further study is required to determine the nature of these lines.

5.4.4 The absence of hydrogen compounds

Given that we found the food oil to contain a not insignificant amount of hydrogen, we would have expected that to be reflected in the XRD results of all samples, both frustule and glass, that contained carbon added as oil. We do not see that in any of them.

The reason for this is that hydrogen was not added to the elements included in the search for the matching of peaks. This is because the fact that the oil we used contained hydrogen was found after the XRD analysis was completed. This is, of course, an error in experimental procedure, and should not have happened.

Given that we know of this error; does it influence our results in any way?

When we see look at the XRD results from all the samples containing oil, none of them have any peaks that remain unexplained. All the peaks are accounted for by compounds that are perfectly reasonable for the compounds we know was present, even when we include hydrogen.

Thus, it looks like the error has had no effect on the results gathered.

6 Conclusion

In this thesis, we attempted to answer three things:

1. Is metallothermic reduction using magnesium gas and added carbon a possible process for converting nanostructured silica frustules into silicon carbide?
2. To what degree does the process preserve the nano-stucture of the frustules?
3. Is TEM a useful tool to investigate whether, and to what degree, silica frustules have been converted into silicon carbide?

To answer these questions, we prepared several samples of frustules and glass replacements, cleaned using a simple method of washing with ethanol. Carbon was added to create six different types of samples. One with only frustules and one with glass replacements with no added carbon. One with frustules and one with glass replacements with carbon added in the form of nanographite powder. One with frustules and one with glass replacements with carbon added in the form of food oil (Rapeseed). The different samples were heat treaded in a closed reactor with an internal inert atmosphere at 800^{o}C for 60 min. After the heat treatment, the samples were cleaned using a water-ethanol-HCl solution and distilled water.

The samples were investigated using two main methods. The samples containing frustules were investigated using XRD and SEM. The samples containing glass replacements were only investigated using XRD.

In addition, a sample containing frustules with no added carbon, that had undergone the same heat treatment as the other samples, and showed clear signs of the presence of silicon carbide in an XRD analysis, was investigated using a transmission electron microscope (TEM). During the TEM investigation several techniques were used, including Scanning Tunnelling Electron Microscopy (STEM), diffraction imaging, dark field imaging and penetrative EDS mapping.

Based on the results gathered from this, and the discussion there upon the following conclusions can be drawn:

6.1 Conversion and reaction

- Metallothermic reduction using magnesium gas **is** a possible process for converting silica frustules when carbon is added in the form of food oil.
- **No** conversion into SiC happens in the samples with no added carbon.
- **No** conversion into SiC happens in the samples with carbon added in the form of nanographite powder.
- The conversion reaction is highly dependent on surface area between the silica and the carbon.
- The use of silica glass is **not** a viable replacement for frustules when investigating this reaction.
- In the absence of carbon, the magnesium will react with silica and create Magnesium-silicon and magnesium-oxide compounds.
- The magnesium gas will not react with carbon powder to form compounds that survive the post-reaction washing.
- When the surface area of the silica is low, elemental silicon will be formed instead of silicon carbide when oil is added.
- The reaction will likely not cause any changes in the nano-sized grain structure of the frustules.

6.2 Preservation

- Wear and tear during storage and process causes destruction of whole frustules, breaking them into smaller flakes.
- In the absence of carbon, the cribrum and cribellum of the frustules are worn away. Especially at the edges of the frustule discs.
- When carbon is added, both as powder and as oil, a film is formed covering the surface of the frustules.
- The film that is formed when carbon is added to the frustules protects the structures of the frustules hidden underneath from coarsening and degradation.

6.3 Usefulness of TEM

- STEM is not a better tool to use than SEM for looking at preservation of frustules sructures.
- HRSTEM may be useful for studies here we want to look at the grain size of the frustules.
- Diffraction imaging is a useful tool to characterize the frustules locally, but requires a more thorough analysis of the results.
- The nano-crystalline nature of the frustules somewhat lessens the usefulness of diffraction imaging when it is used for characterization.
- Dark field imaging is a tool that may be very useful for looking at which parts of a frustule has undergone conversion.
- Penetrating EDS is a useful tool for determining whether the conversion happens throughout the frustule material, or is merely a surface phenomenon.

7 Future Work

The results and conclusions found in this thesis opens up several areas for new research.

Given that we have found that using the process described in this thesis to do create conversion into silicon carbide, this process should be investigated further. How much conversion do we get, and how may we get more? What actually happens within the reactor during heat treatment? What are the reaction mechanics? By further studying the conversion process we will gain a greater understanding of which factors are important for the degree of conversion and preservation of the nanostructure. This knowledge can then be leveraged to, ideally, perform a complete conversion of the frustules while perfectly preserving the architecture.

Several of the phenomena detected here should be investigated further. What is the nature of the protective film we found in the samples that were added oil? Does it hinder or further the conversion process? What are the lines we found? What is the fuzzy growth? Further study using SEM and EDS may illuminate these questions.

Given our conclusion that TEM might be a powerful tool when investigating frustules, the obvious next step is a more through TEM analysis of the frustules. A more complete TEM investigation may uncover what formation the created SiC has, and where in the frustules it is found.

Considering one of our initial motivations for converting frustules was to coat them with graphene and create a supercapacitor, now that we have proven that we are able to do a conversion, coating with graphene may be attempted.

8 References

1. Austin WEN, James R, London GSo. Biogeochemical controls on palaeoceanographic environmental proxies: Geological Society; 2008.
2. Fuhrmann T, Landwehr S, El Rharbi-Kucki M, Sumper M. Diatoms as living photonic crystals. Appl Phys B. 2004;78(3-4):257-60.
3. Norimatsu W, Kusunoki M. Epitaxial graphene on SiC{0001}: advances and perspectives. Physical Chemistry Chemical Physics. 2014;16(8):3501-11.
4. Li F, Xing Y, Huang M, Li KL, Yu TT, Zhang YX, et al. MnO 2 nanostructures with three-dimensional (3D) morphology replicated from diatoms for high-performance supercapacitors. Journal of Materials Chemistry A. 2015;3(15):7855-61.
5. Alper JP, Kim MS, Vincent M, Hsia B, Radmilovic V, Carraro C, et al. Silicon carbide nanowires as highly robust electrodes for micro-supercapacitors. Journal of Power Sources. 2013;230:298-302.
6. Tsai W-Y, Gao P-C, Daffos B, Taberna P-L, Pérez CR, Gogotsi Y, et al. Ordered mesoporous silicon carbide-derived carbon for high-power supercapacitors. Electrochemistry Communications. 2013;34:109-12.
7. Wang Y, Shi Z, Huang Y, Ma Y, Wang C, Chen M, et al. Supercapacitor devices based on graphene materials. The Journal of Physical Chemistry C. 2009;113(30):13103-7.
8. Bao Z, Weatherspoon MR, Shian S, Cai Y, Graham PD, Allan SM, et al. Chemical reduction of three-dimensional silica micro-assemblies into microporous silicon replicas. Nature. 2007;446(7132):172-5.
9. Petrack J, Epple M, Jost S, Boenigk J. Magnesiothermic conversion of the silica-mineralizing golden algae Mallomonas caudata and Synura petersenii to elemental silicon with high geometric precision. Beilstein J Nanotechnol. 2014;5:554-60.
10. Krishnarao RV, Mahajan YR, Kumar TJ. Conversion of raw rice husks to SiC by pyrolysis in nitrogen atmosphere. Journal of the European Ceramic Society. 1998;18(2):147-52.
11. Amirthan G, Balasubramanian M. Helium gas permeability of SiC tubes produced using cotton fabric. Ceramics International. 2014.
12. Fujimoto H, Nishihara H, Kyotani T, Hisa M. Carbon tubules containing nanocrystalline SiC produced by the graphitization of sugar cane bagasse. Carbon. 2014;68:814-7.
13. Simonenko E, Simonenko N, Zharkov M, Shembel N, Simonov-Emel'yanov I, Sevastyanov V, et al. Preparation of high-porous SiC ceramics from polymeric composites based on diatomite powder. Journal of Materials Science. 2015;50(2):733-44.
14. Shi Y, Zhang F, Hu Y-S, Sun X, Zhang Y, Lee HI, et al. Low-temperature pseudomorphic transformation of ordered hierarchical macro-mesoporous SiO2/C nanocomposite to SiC via magnesiothermic reduction. Journal of the American Chemical Society. 2010;132(16):5552-3.
15. Ødegård IA, Romann J, Fossdal A, Røyset A, Tranell G. Synthesis and properties of silicon/magnesium silicon nitride diatom frustule replicas. Journal of Materials Chemistry A. 2014;2(39):16410-5.
16. Barker HA. Photosynthesis in diatoms. Archiv Mikrobiol. 1935;6(1-5):141-56.
17. Dolatabadi JEN, de la Guardia M. Applications of diatoms and silica nanotechnology in biosensing, drug and gene delivery, and formation of complex metal nanostructures. TrAC Trends in Analytical Chemistry. 2011;30(9):1538-48.
18. Parkinson J, Gordon R. Beyond micromachining: the potential of diatoms. Trends in Biotechnology. 1999;17(5):190-6.
19. Struyf E, Conley DJ. Silica: an essential nutrient in wetland biogeochemistry. Frontiers in Ecology and the Environment. 2008;7(2):88-94.

20. UBC Department of Earth OaAS. Phyto'pedia - The Phytoplankton Encyclopaedia Project 2015. Available from: http://www.eos.ubc.ca/research/phytoplankton/diatoms/centric/coscinodiscus/c_centralis.html.
21. Dorval Courchesne Nm-M, Steiner III SA, Cantú VJ, Hammond PT, Belcher AM. Biotemplated Silica and Silicon Materials as Building Blocks for Micro-to Nanostructures. Chemistry of Materials. 2015;27(15):5361-70.
22. Romann J, Valmalette J-C, Chauton MS, Tranell G, Einarsrud M-A, Vadstein O. Wavelength and orientation dependent capture of light by diatom frustule nanostructures. Scientific Reports. 2015;5:17403.
23. De Stefano L, Lamberti A, Rotiroti L, De Stefano M. Interfacing the nanostructured biosilica microshells of the marine diatom Coscinodiscus wailesii with biological matter. Acta Biomaterialia. 2008;4(1):126-30.
24. Tsai W, Hsien K, Yang J. Silica adsorbent prepared from spent diatomaceous earth and its application to removal of dye from aqueous solution. Journal of colloid and interface science. 2004;275(2):428-33.
25. Vrieling EG, Beelen TPM, van Santen RA, Gieskes WWC. Diatom silicon biomineralization as an inspirational source of new approaches to silica production. Journal of Biotechnology. 1999;70(1–3):39-51.
26. Nassif N, Livage J. From diatoms to silica-based biohybrids. Chemical Society Reviews. 2011;40(2):849-59.
27. Srinivasarao M. Nano-optics in the biological world: beetles, butterflies, birds, and moths. Chemical reviews. 1999;99(7):1935-62.
28. Vukusic P, Sambles JR. Photonic structures in biology. Nature. 2003;424(6950):852-5.
29. De Stefano L, Rea I, Rendina I, De Stefano M, Moretti L. Lensless light focusing with the centric marine diatom Coscinodiscus walesii. Optics express. 2007;15(26):18082-8.
30. Romann J, Valmalette J-C, Røyset A, Einarsrud M-A. Optical properties of single diatom frustules revealed by confocal microspectroscopy. Optics letters. 2015;40(5):740-3.
31. Weimer AW, Nilsen KJ, Cochran GA, Roach RP. Kinetics of carbothermal reduction synthesis of beta silicon carbide. AIChE Journal. 1993;39(3):493-503.
32. Weimer AW. Carbide, nitride and boride materials synthesis and processing: Springer; 1997.
33. Munro R. Material properties of a sintered α-SiC. Journal of Physical and Chemical Reference Data. 1997;26(5):1195-203.
34. Richerson DW. Modern Ceramic Engineering. 3 ed: Taylor & Francis; 2006.
35. Activation Energy. Available from: http://chemed.chem.purdue.edu/genchem/topicreview/bp/ch22/activate.html.
36. GREGORS TEK. X-RAYS INTERACTING WITH ATOMS IN A CRYSTAL.
37. Jan Ketil Solberg VH. Innføring i Transmisjon Elektronmikroskoi. NTNU, University of Stavanger2014.
38. GRETANA. DIFRACCIONELECTRONESMET.
39. EtherDais. http://etherdaispbworkscom/ [Internet]2010. [cited 2016]. Available from: http://etherdais.pbworks.com/.
40. Sæterli R. Personal communication during TEM investigation. In: Sørensen S, editor. 2015.
41. West AR. Basic Solid State Chemistry. 2nd ed: John Wiley & Sons Ltd.; 1999.
42. http://biology.clc.uc.edu/. Fatty acid. http://biology.clc.uc.edu/.
43. Billaud F, Dominguez V, Broutin P, Busson C. Production of hydrocarbons by pyrolysis of methyl esters from rapeseed oil. Journal of the American Oil Chemists' Society. 1995;72(10):1149-54.
44. Zhenyi C, Xing J, Shuyuan L, Li L. Thermodynamics calculation of the pyrolysis of vegetable oils. Energy Sources. 2004;26(9):849-56.
45. Bao Z, Weatherspoon MR, Shian S, Cai Y, Graham PD, Allan SM, et al. Chemical reduction of three-dimensional silica micro-assemblies into microporous silicon replicas. Nature. 2007;446(7132):172-5.